Meteorology

The meteorology subsystem measures the barometric pressure, temperature, relative humidity, wind speed, and wind direction and provides this information to the computer.

Safety

The safety subsystem includes the aircraft detection assembly, the instrumentation safety and health monitoring assembly and the interlock and human safety assemblies. These are designed to increase the safe operation of the system while also ensuring that the equipment does not experience harmful conditions. A picture of the ATSC-developed aircraft detection assembly is illustrated in Figure 4.

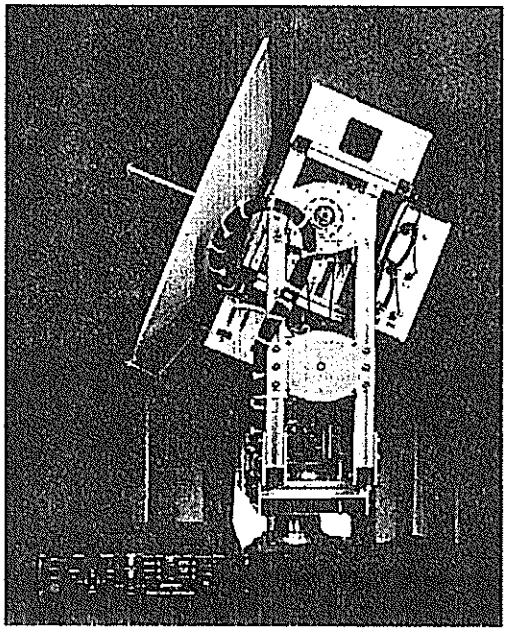

Figure 4: Aircraft Detection Assembly, protective weather enclosure not shown

Control and Processing

The control and processing subsystem consists of five powerful RISC-processor computers. Three real-time VME-based processors, and two HP UNIX workstations make up the subsystem. A drawing depicting the MLRO computing and control configuration is illustrated in the MLRO software paper within these proceedings.

Transmit / Receive Optics

The transmit/Receive optics subsystem contains a large number of assemblies. This subsystem couples the light between the laser, detectors, and telescope. The subsystem has been designed to allow for automated and semi-automated alignments and beam adjustments.

Transmit / Receive Electronics

It features a three GHz microchannel plate photomultiplier tube detector, coupled to an improved Oxford (Tennelec) discriminator for signal detection. These signals are input to the ATSC-developed event timer to determine time interval measurement. Amplitude

information is captured by an ATSC-developed amplitude measurement device, and gating is performed using an ATSC-developed range-gate generator. The subsystem has been designed to employ all of the best techniques developed over the past ten years to yield a highly-precise measurement of range. Some of the assemblies are discussed in more detail in another paper within these proceedings.

Development Process and Status

The MLRO subsystem development phase is nearing its completion. Subsystem development incorporates a number of grouped-functions as illustrated in Figure 5.

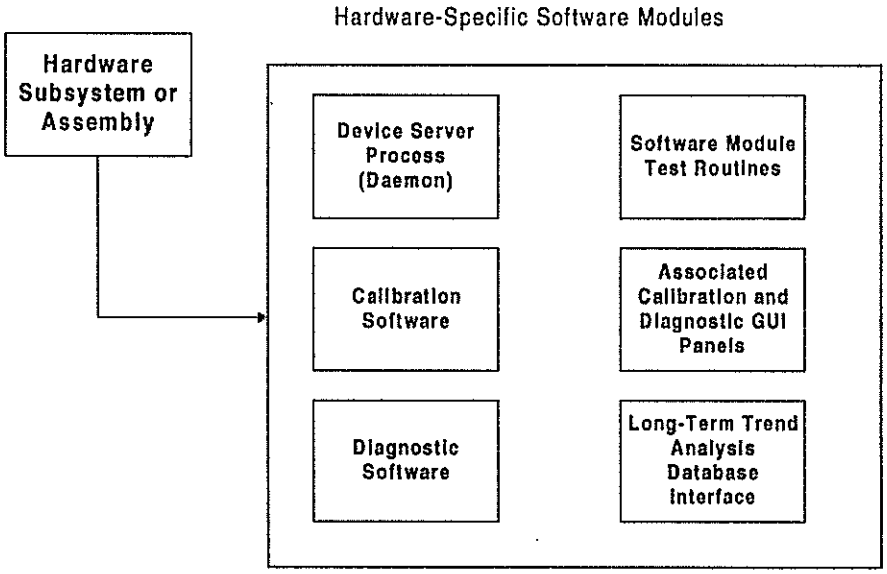

Figure 5: MLRO Subsystem Development

As a subsystem is developed its real-time daemon (device control software), calibration software, diagnostic software, associated GUI applications, and software test routines (to test the software) are developed. Additionally, the parameters which will be included in the system long-term trend analysis application are identified. This trend analysis will be useful to the ASI in monitoring, not only system performance, but also subsystem, assembly, and module-level performance.

Most of the primary subsystem development projects are complete. There are some exceptions to this but, the MLRO is now in the system integration phase. Due to facility-related problems, the MLRO has not yet conducted ranging activities, but the satellite returns are expected by March 1 1997.

Quality and Engineering Improvement Measures

ATSC and the ASI have taken steps to ensure a high-quality system. These include a very detailed and extensive design and design review process, the use of modern engineering modeling and manufacturing tools to improve the electronics, optical, and mechanical design of the system. The establishment and adherence to a modern software development model to ensure that the code is maintainable and upgradable, and extensive testing

throughout the development process was used to ensure that the specifications are met or exceeded.

As an example, the T/R optics subsystem was designed using a ray-tracing application which is used by both ATSC and the ASI. This allowed us to exchange and analyze critical design information on the optical properties. The mechanics of the subsystem were completely designed using the three-dimensional solid modeling package "ProEngineer". This allowed us to check for tolerances, clearances and to manage the quality-control of the manufacturing process very closely. The cabling and wiring diagrams have been developed using the "ProCabling" module which can verify cable stress factors as well as mass and thermal properties.

Our goal has been to produce a system with commercial-quality properties that would compete with the quality of a product produced by a company like Hewlett-Packard, while maintaining a close working relationship between the ASI and ATSC to allow for customization of the products.

Summary

The MLRO system has been designed and is being developed to offer the highest performance possible with a maximum upgrade flexibility and un-paralleled manufacturing and documentation quality. This project is scheduled to be complete in early 1998.

X WINDOW BASED GRAPHICAL USER INTERFACE FOR A LASER RANGING CONTROL SYSTEM

Jacek W. Offierski

Delft University of Technology
Faculty of Geodetic Engineering
Satellite Geodesy Group
Thijsseweg 11
2629 JA DELFT
The Netherlands

and

Marcel J. Heijink

Delft University of Technology
Central Electronic and Engineering Division
Mekelweg 6
2628 CD DELFT
The Netherlands

Abstract

This paper is a short description of the software structure of the **T**ransportable **I**ntegrate **G**eodetic **O**bservatory (**TIGO**) which has been developed in collaboration with TNO Institute of Applied Physics (TPD-TNO) for the Institute for Applied Geodesy (IfAG) in Germany. The modern **G**raphical **U**ser **I**nterface (**GUI**), that is used in this implementation, offers a wide range of flexibility and a user friendly environment. Only GUI's based on Window systems can offer such a wide range of user-friendly and user-intuitive functionality. The applied GUI has the potential to minimize training time for new observers and was implemented on the X Window system (UNIX) using the OSF/Motif widget library. The described configuration provides also remote access capability. Its high level structure and modular construction are sufficiently flexible for future enhancements and replacement of any software module.

Introduction

In all modern measurement techniques, development - which is the engine of scientific progress - requires continues upgrading of each appliance. In Satellite **R**anging Systems (**SLR**) the main trends in instrumentation are accuracy, efficiency and working costs. The application of new

software techniques is an important factor in this trend.. However, software elements like satellite prediction, result data screening, etc., are subject to improvement and contain some problems to solve. Particularly, the software that is responsible for the overall co-ordination of sub-tasks, must follow modern trends in software design.

Basic trends in this kind of software, are the application of parallelism and a user-friendly interface. In general, we can divide the software into a part that has a close relationship with the hardware, the `Real Time Control Systems` (**RTCS**) [Offierski, 1994], and a part that has a close relationship with the observer, the `Off-line System` (**OLS**). Parallelism plays a crucial role in both software parts.

There is no reason to involve the observer directly by tasks such as prediction calculation, ranging data screening (inside possible capabilities) or receiving and sending data. All routine tasks can be efficiently handled by the **OLS** in a transparent way according to assigned goals and priorities, set by experienced users. The main task of the observer is focusing at support of the **RTCS** and taking the strategic decisions.

Another trend should be the possibility for remote login on the **SLR** instrument (e.g. from home), with the aid of an accessible network, on every place on Earth. The described **OLS** implementation tries to reach all these goals.

Fig.1.Structure of the off-line system consisting of a number of parallel tasks

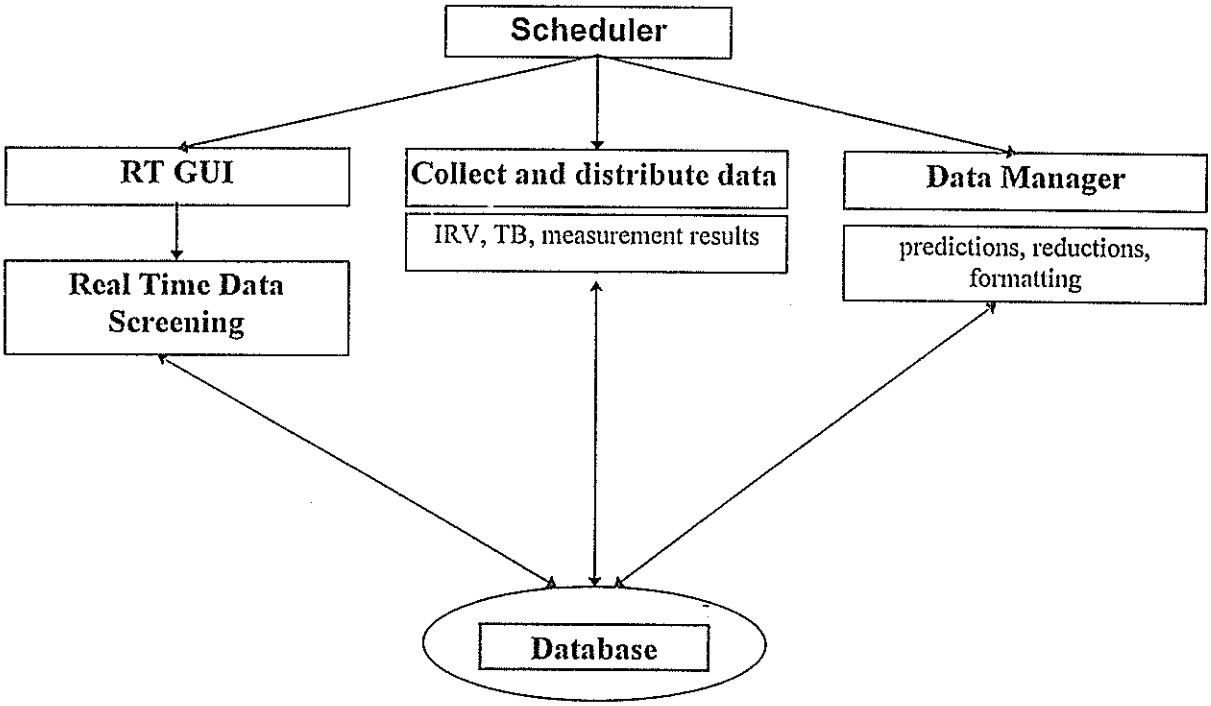

Scheduler

On the top of each parallel working task there is one general process (daemon) which takes control of all data streams from and to the component. It can start (or kill) a selected task with a requested priority level. Tasks can be executed at determined time moments, periodically or as the results of an event. A typical task that must happen in determined time is satellite tracking. `Scheduler` does not perform this task itself but calls the `Real Time Graphic User Interface` (**RT-GUI**) which is responsible for this. An example of a periodical task is the calculation of long-term predictions for satellites (Alerts). Other periodical tasks for this system are levelling and calibration of the 'calibration system'. Typical events that can trigger tasks are user interference (e.g. all tasks that belong to positioning like Star observation), incoming data (IRV or TB), readiness of result data to send or the necessity to make pre- and post- calibration.

Summarising this task:

- Execute tasks at determined time moments (ranging),
- Periodically execute tasks (for example levelling, calibration or collect data),
- Execute tasks on events (user interference, pre- and post- calibration, auto screening).

Collect and distribute data

This task is activated whenever an operation on data must be performed (incoming data available or data ready to send). The arriving data is uploaded to an external accessible FTP input directory. Any modification of the contents of this input directory starts this task. The first step of this task is checking the data for errors, then the data is reformatted to an internal format by independent programs. Independent reformatting has the advantage of being able to add different formats in the future. Finally, the reformatted data is stored in the database.

Also run-time changes in the **OLS** parameters, made by experienced users, can wake up this task. If the **OLS** itself has data to send, the data is put on a selected output directory. The FTP daemon will then automatically send the results to Data Centres.

Summarising this task:

- Error checking,
- Reformatting and storage in the Database,
- Sending results.

Database Management Task (DMT)

All the data that is managed by the **SLR** resides in a number of physical system databases. The system **DMT** are all typical relational databases. Each database contains a number of fields containing system information as well as information associated with the forms of the GUI.

Individual fields and forms can be replaced or changed by the user. It is even possible to completely redefine each database. The consequences of a new form definition or the replacement or introduction of new fields are just re-indexing. All operations on a database are subject to a recovery mechanism. The user has access to all data in a database. However, some of the data cannot be modified, e.g. observation results. Only special prepared programs are allowed to make modifications to such data. A single program, the **DTM** program, is used to maintain, configure and manipulate all system databases.

Currently defined databases include:

1. Satellite database,
2. Site database,
3. Time Bias (TB) database,
4. IRV database,
5. Ranging results database,
6. Calibration results database
7. Star observation results database
8. Ground markers result database.

This list can be extend.

Summarising this task:

- Application of conventional database technology,
- Expandable user defined databases,
- User defined forms.

Real Time Graphic User Interface (RT-GUI)

The main task for **RT-GUI** is to communicate with the **RTCS** in a near synchronous way. Communication is establish with the TCP/IP protocol. The communication between the **RT-GUI** and **RTCS** uses a point-to-point binary data protocol, which makes intrusions from outside almost impossible. The **RTCS** has its own IP identification number which gives the possibility to

communicate with it from different computers. The communication can be traced for maintenance purposes.

The second important function of **RT-GUI** is the visualisation of **RTCS** status information in a form that enables the observer to take the proper decisions (for example correction on wavelengths, position, etc.).

The next function that makes this task the most important task, is the User Interaction that enables the user to carry out his decision's. This interactive process is essential for successfully making measurements.

The **RT-GUI** task can run in two modes: either automatic or manual. During automatic mode, the **RT-GUI** task takes all decisions itself according to pre-determined decision algorithms. In this mode, the only allowed user interference is switching to manual mode. It is also possible to connect external programs with the **RT-GUI** in a modular way to expand on the decision algorithm. This provides an opportunity, together with Real Time Data Screening (**RTDS**), to build a completely automatic system.

Summarising this task:

- Communication with the **RTCS**,
- Visualisation of the **RTCS** status,
- Interaction with the observer,
- Automatic tracking procedure.

Real Time Data Screening (RTDS)

At in current systems, only weak screening algorithms are used. The screening algorithm implemented in the **OLS** software offers the observer almost automatic data screening. Searching for a predicted signal pattern gives a high success / failure rate in the automatic distinction of signal from noise. The used algorithm is sensitive for non-random noise characteristics. The algorithm can communicate directly with the **RT-GUI** and is able to compensate the Time Bias. The results of the data screening can be visualised in different graphical representations (e.g. histogram) and be used by the observer for interpretation.

One of the basic functions of the **RTDS** is interactive graphical data selection. This task has also the ability to connect an external program module. This connection capability is made for future developments in data filtering algorithms.

Summarising this task:

- Near automatic signal from noise separation,
- TB determination for direct use,
- Accuracy calculation for system tuning,
- Interactive graphical data selection.

Data Manager

Almost every **SLR OLS** module contains a number of standard tasks. The described system implements those tasks as a collection of independent and separated programs. There are just a few programs needed to cover all required tasks:

1. Calculate Satellite and Stars predictions. These predictions are necessary to exploit the system.
2. Reduce astronomical measurement results for the position or mount model determination.
3. Formatting to Merit-II format (which is the selected format for external data exchange). Conversion between internal format and the Merit-II format.
4. Generation of Normal Points (NP) from the Merit-II format [Seeber, 1993].The algorithm is based on the 'Herstmonceux' recommendations [Kolenkiewicz, 1986].
5. The calibration results data management module offers the possibility to graphically represent the system calibrations. Long term drifts or accidental jumps in the calibration data can very easily be spotted.
6. For all satellite passes at the actual measure site, the long term visualisation of observation results can be displayed.

Conclusions

- The UNIX pre-emptive multitasking, multi-user and multithreading operating system seems to be the best choice for the modern **OLS** software for a **SLR** system.
- The modular construction of the **OLS** software gives extreme flexibility to include different modules in the future or replace current modules by improved ones.
- The X Window system provides the possibility to fully operate and control the SLR system from a remote site.

List of abbreviations

DMT	Database Management Task,
IRV	Inter Range Vectors,
FTP	File Transfer Protocol,
GUI	Graphical User Interface,
NP	Normal Points,
OLS	Off-line System software,
OSF/Motif	Standard widget set,
RTCS	Real Time Control System,
RTDS	Real Time Data Screening,
RT-GUI	Real Time Graphical User Interface,
SLR	Satellite Laser Ranging system,
TB	Time Bias,
TCP/IP	Transport Control Protocol / Internet Protocol,
TIGO	Transportable Integrate Geodetic Observatory,
UNIX	an Operating System,

References

1. Kolenkiewicz, R., P.J. Dunn, R.J. Eanes and R. Jonson, 'Comparison of LAGEOS satellite laser ranging normal points'. *Sixth international workshop on laser ranging instrumentation,* Antibes - Juan les Pins, 1986.
2. Offierski J., 'Parallel aspects of Laser Ranging Control'. *Ninth International Workshop on Laser Ranging Instrumentation*, Canberra - Australian Publishing Service, 1996.
3. Seeber, G., *Satellite Geodes; foundations, methods, and applications.* Berlin: De Gruyter, 1993.
4. E. Vermaat, J.W.Offierski, 'TIGO-SLR Control System'. *Ninth International Workshop on Laser Ranging Instrumentation*, Canberra - Australian Publishing Service, 1996.

Real-Time Correction of SLR Range Measurements for the Return Amplitude Induced Bias of the Multi-Channel Plate PMT/TC-454 DSD Discriminator Receive System

O'Gara, D.J., Zane, R., Maberry, M.T.
University of Hawai`i, Institute for Astronomy
LURE Observatory at Haleakala
PO Box 209
Maui, Hawai`i, USA
E-Mail: ogara@lure.ifa.hawaii.edu

Abstract: The receive system used at LURE introduces a recoverable bias (0-35mm) into the range measurement. This bias can be estimated by fitting a set of calibration residuals and their associated receive energy measurements to a straight line model. This model is updated on a daily basis by analyzing scheduled calibration runs taken during the previous 24 hours of operation. Range measurements (calibration and satellite) are then corrected for this bias real time by the ranging system software.

Introduction

By analyzing the effects of return energy on the range measurements to a calibration cube at LURE, it was shown that the range varied linearly with the received energy (commonly called time walk). A high energy return generally produces a range measurement that is early when compared to a low energy return. Figure 1 illustrates this by plotting the un-corrected range measurement residuals of a calibration (nanoseconds) against the relative received energy (REM).

In the LURE ranging system, this bias is attributable to the Multi-Channel Plate photo multiplier tube /TC-454 DSD discriminator receive subsystem. (See "Increasing System Sensitivity at LURE Observatory", Zane,et.al., these proceedings). The variation of this time walk was shown to be small over periods of months (Measurements made over a months time showed a slope of -57 femtoseconds/REM with a standard deviation of ~5 femtoseconds/REM). It was decided that a method to correct for the bias during data collection should be implemented.

Method

The amplitude dependent range bias can be determined by investigating the effect of return energy on the range measured during calibration. By subjecting sets of calibration range measurements to a least squares fit analysis (as in Figure 1.) it was shown that the

range was biased as a function of the REM. By removing this bias from all range measurements, the effect of the system time walk can be minimized. Figure 2 is the same data as in figure 1, but with the calculated time walk removed from the measurements.

On a daily basis, each calibration file that was taken the previous day is subjected to a linear least squares fit analysis. The independent variable is taken to be the relative receive energy

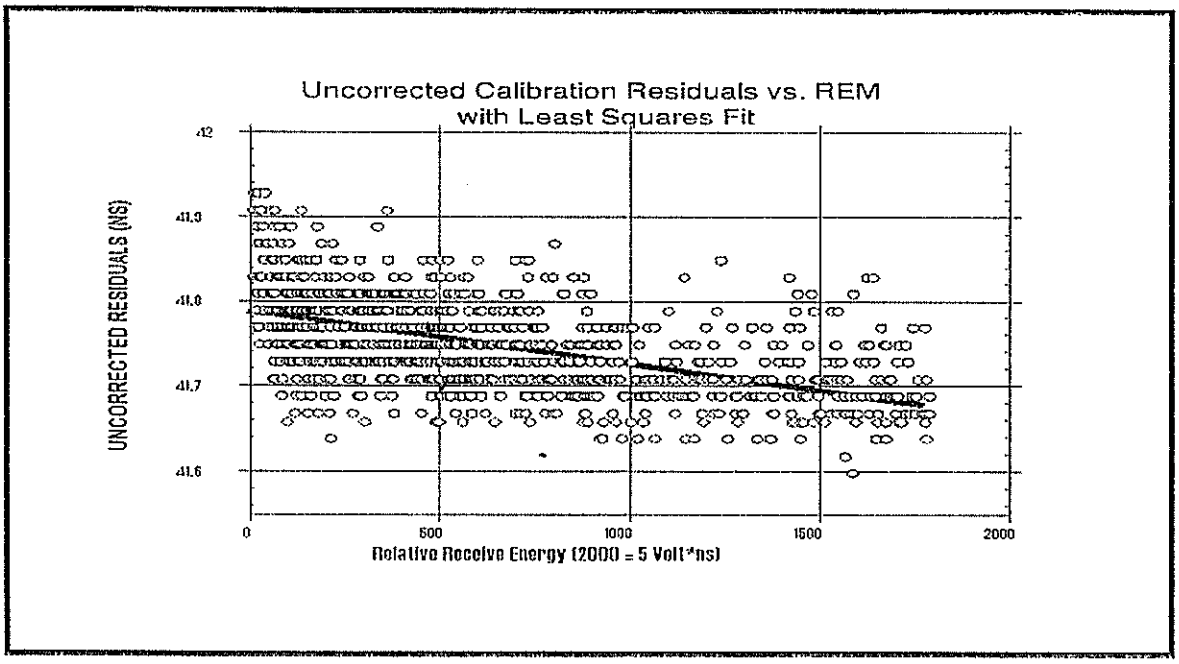

Figure 1.

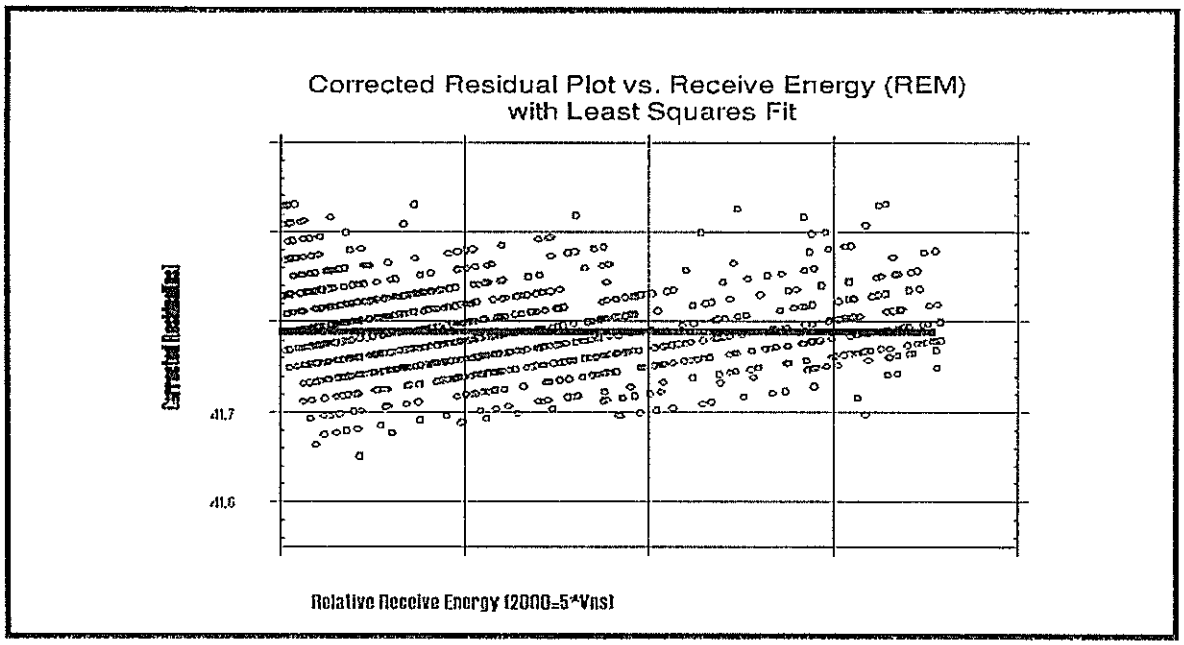

Figure 2.

(REM) number, with the calibration range residual (Observed Range - Calculated Range) being taken as the dependent variable. A FORTRAN program was written that takes as input raw calibrations files, and produce as output the model parameters and the update to the bias correction.

The resulting slope of each straight line fit is first divided by a damping value. This number is then added to the bias correction that is kept in a system data base file. A damping value is divided into the individual slope values to allow daily updates to the bias correction without a single "outlier" causing an abrupt change. Since all data is taken using the best known bias correction, the slope of subsequent calibrations will be the deviation from this correction. Thus, to update the system bias correction, simply add in the slope as determined by analysis of the individual calibrations.

This bias correction is used to correct range measurements in real time. The real time ranging system at LURE will read in the bias correction from a system data base file at start up. During operations, the raw target range is corrected before it is recorded to disk, using the expression:

Corrected Range = Raw Range - (Relative Receive Energy * Bias Correction)

This correction is done to both satellite data and calibration data.

The bias correction can be initialized to zero, or an initial bias correction can be determined by taking a calibration and entering the slope of this calibration as a starting value. At LURE, the initial bias was determined from a month long experiment. This experiment involved analysis of all calibrations (with bias included in the range measurements) taken during that period. An average bias from this experiment was used as a starting correction bias.

Conclusions

The time walk bias is a function of the returned energy. The targets that return the highest average energy benefit the most from this procedure. For example, the average correction for LAGEOS is approximately 2.5 mm, while for TOPEX/Poseidon, it is about 7.0 mm.

The process of maintaining the bias correction at LURE is entirely automated and requires no action by the operators. The analysis process is started automatically by the controller computer at 0:00 UT every day. The least squares fit analysis parameters and the bias correction used for each UT day are stored on disk. These data can be monitored for anomalies and are archived as a part of system history.

This process is currently implemented at LURE on a DEC PDP/11 running RSX-11/M OS.

COMBINED DIGITAL TRACKING SYSTEM

K.Hamal, I.Prochazka

Czech Technical University, Brehova 7
115 19 Prague 1, Czech Republic
fax +42 2 85762252, prochazk@mbox.cesnet.cz

The Combined Digital Tracking System for SLR consists of two CCD based subsystems. The Coude CCD is coupled to the main beam path via the dichroic. The Field of View (FOV) limited by the vignetting to 1 arcminute allows fully automated star tracking for the mount flexure model construction with arcsecond resolution and satellite tracking, as well. The wide FOV subsystem consists of the 8 inch or 11 inch telescope, variable focal reducing optics, laser blocking filter and CCD. The FOV is 3 - 12 arcminutes. The camera control electronics and the software package enables automatic guiding (lock on target), if desirable.

The Peltier cooled CCD has 164x192 pixels, 8 bits. The image integrating time up to 12 sec facilitates a considerably high sensitivity. The newly developed software package permits to operate under Windows NT or Windows 95 up to 4 CCD cameras on a single PC among other real time applications simultaneously. Due to an efficient video data compression plus image processing the transmitted data volume is reduced down to kilobits per frame.

The resolution of the Coude CCD at Tokyo 1.5 meter telescope is 1.5 arcseconds per pixel and at the Keystones telescopes 2 seconds of arc. The wide FOV subsystem allows to track all satellites up to 20 ooo km range proved at Helwan SLR rather polluted atmosphere.

10th Intenational Workshop on Laser Ranging Instrumentation, Shanghai, China, November '96

OBJECTIVES

Combined Digital Tracking system

- VISUAL GUIDING / all laser satellites
- Satellite image / laser beam / paralax
- MOUNT FLEX AUTOMATION / remote control
- Image data processing: low data flow rate
- WINDOWS NT platform
- Multiple camera control/image on one PC
- Calibration pier

K.Hamal,B.Greene, Shanghai '96

Combined Digital Tracking Subsystem (CDT)

- The CDT subsystem is dedicated for the coaxial (transmiter/reciver setup in Coude) SLR station
- The CDT consists of two CCD sensors, one subsidiary telescope, one focussing optics, PC+ software.
- The wide FOV subsidiary telescope/CCD is providing:
  - visual guiding/tracking of satellites (low, satellites, Lageos, Etalon, Glonass, GPS) on the displayed laser beam
- The narrow FOV CCD in Coude is providing :
  - star tracking for mount flex, autotrack option
  - telescope optics alignment tool

K.Hamal,I.Prochazka,Keystone, Nov. 27,'95

WIDE FOV SUBSYSTEM

Combined Digital Tracking system

Telescope	C8, D=200mm, f/D=10
Focal reducer	adjustable 2-4 x
CCD camera	ST-4, 2.5 x 2.5 mm 192x164, 14x16um
FOV (reducer 3x)	12 x 12 arcminutes 17 arcmin diagonal
Resolution	5 arcsec / pixel
Capability up to 10 sec.integration	up to Etalon, GPS in good conditions

I.Prochazka,K.Hamal, Keystone,November '95

WIDE FIELD OF VIEW TELESCOPE

Digital Guiding & Ranging Subsystem

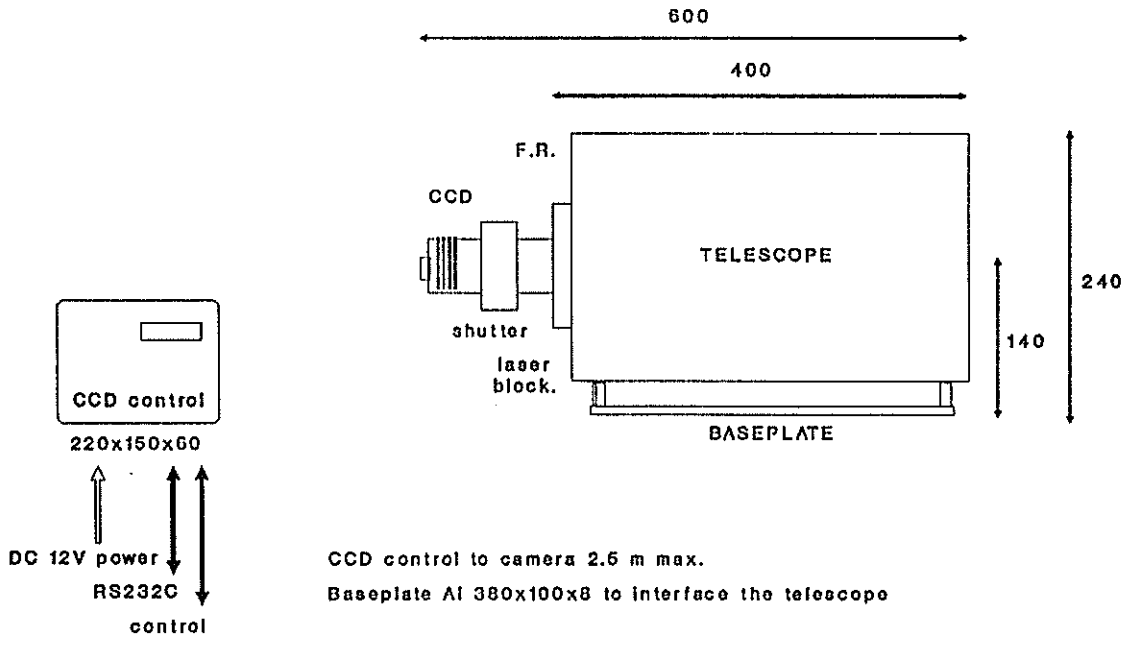

CCD control to camera 2.6 m max.

Baseplate Al 380x100x8 to interface the telescope

Hamal,Prochazka, Shanghai '96

NARROW FOV SUBSYSTEM
Combined Digital Tracking system

Coupling to main T/R telescope	via dichroic directing 600-1000 nm to CCD
CCD camera	ST-4, 2.5 x 2.5 mm 192x164, 14x16 um
Field of view	1 arcmin limited by vigneting
Camera optics	f = 56 mm Dmin = 37 mm f/D = 1.5
Pixel size (KSP)	2.0 arcsec / pixel
Tracking resolution	< 1 arcsec

I.Prochazka,K.Hamal,Keystone,Dec.6,'95

CCD in Coude block scheme
Combined Digital Tracking System

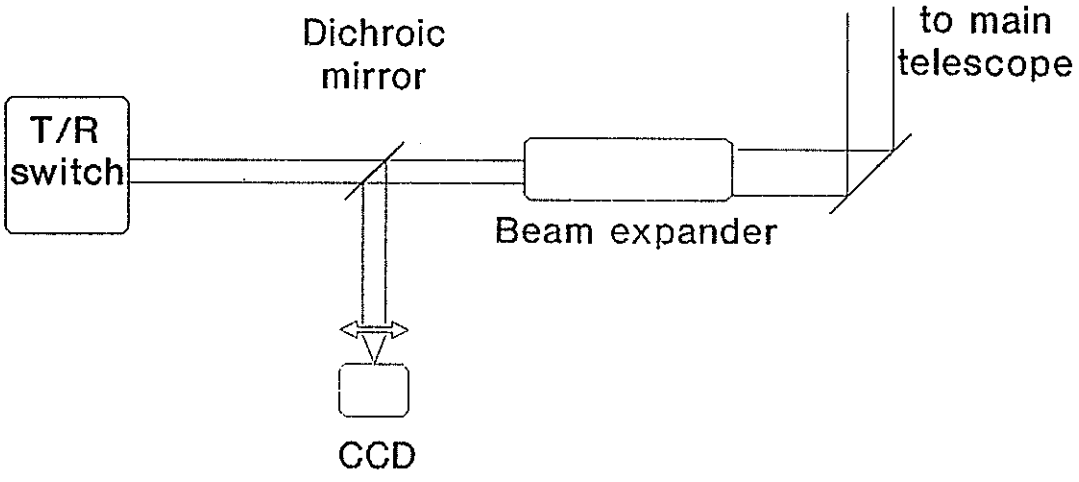

K.Hamal,I.Prochazka, Shanghai '96

HELWAN 2 SATELLITE LASER STATION
Visual guiding on CCD star tracker

LAgeos 47 deg medium sky ret.rate 50%

Contrast
Background:155
Range : 3

Unsmoothed
Unzoomed

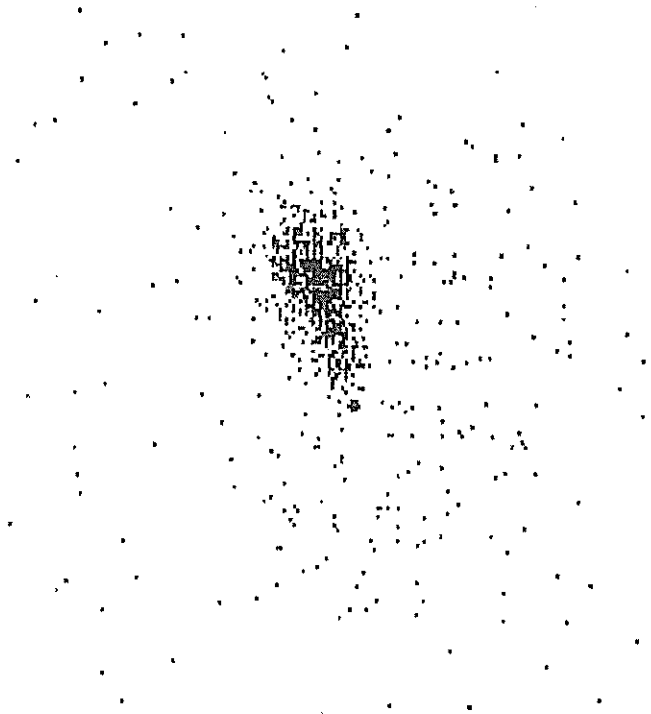

etalon 2 37 deg laser beam 99% dichr

Contrast
Background:170
Range : 15

Unsmoothed
Unzoomed

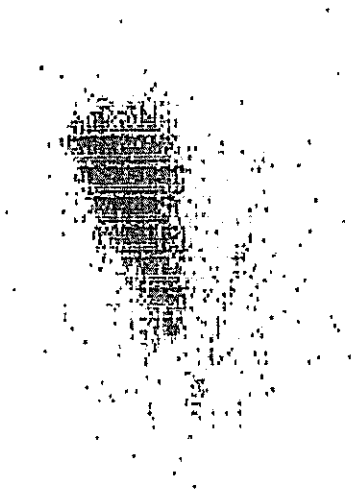

Helwan, September ;95

SATELLITE TRACKING IN GRAZ
Digital tracking system

TOPEX

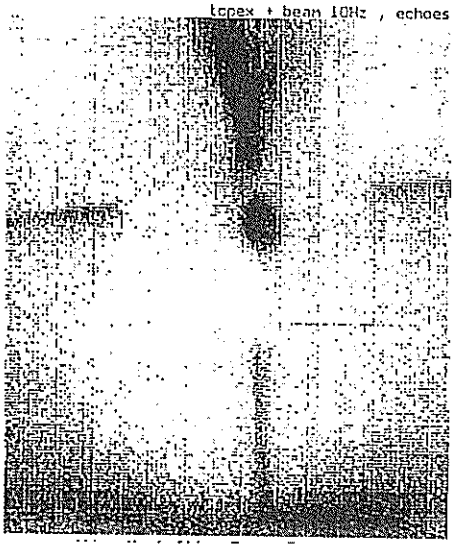

GPS

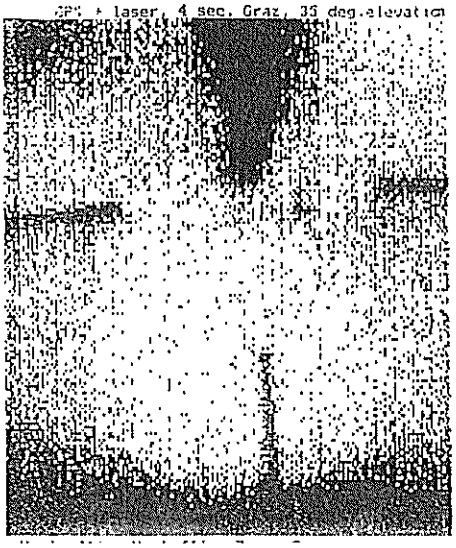

10th Workshop, Shanghai '96

SATELLITE TRACKING IN HELWAN
Digital tracking system

LAGEOS

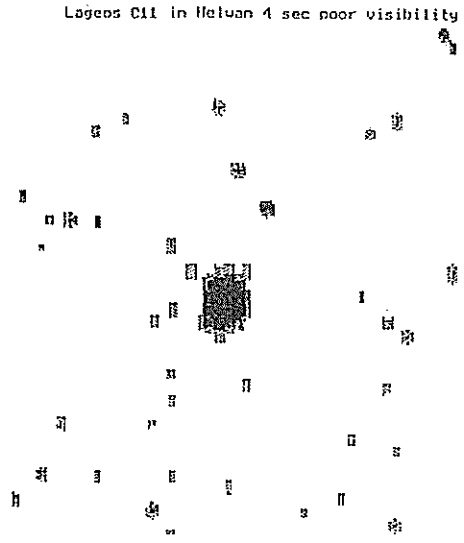

ETALON

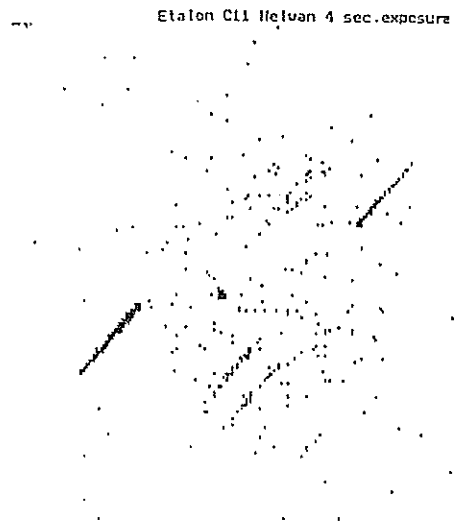

10th Workshop, Shanghai '96

LAGEOS tracked on C8 wide FOV camera, 6 seconds exposure, zoomed, gain level settings 0,55

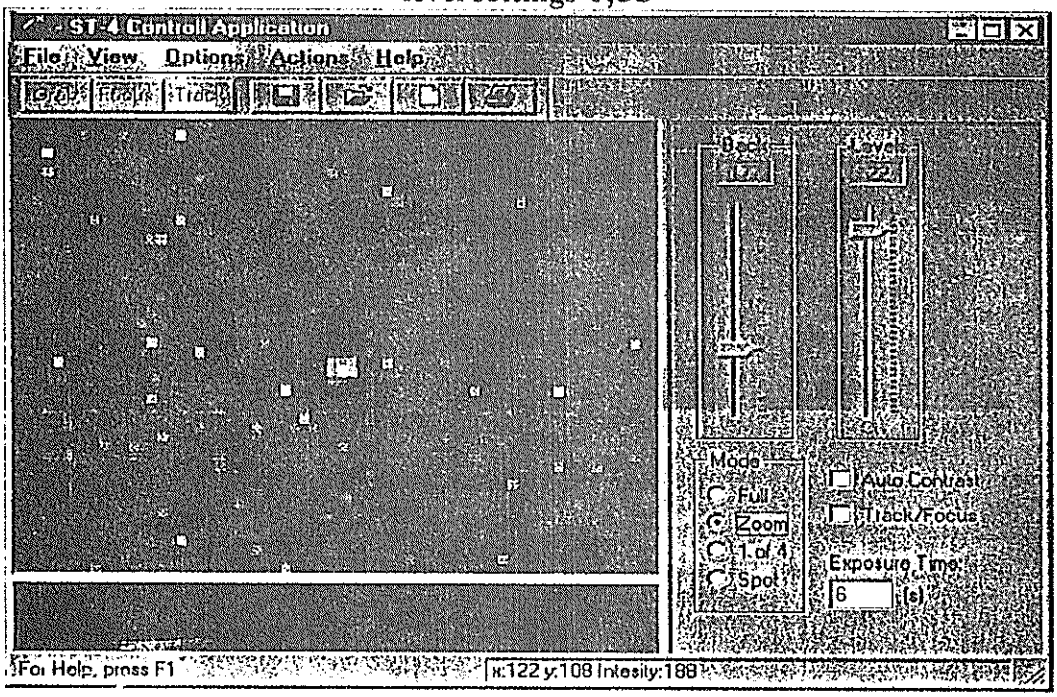

Laser beam on the LAGEOS C8, settings as above

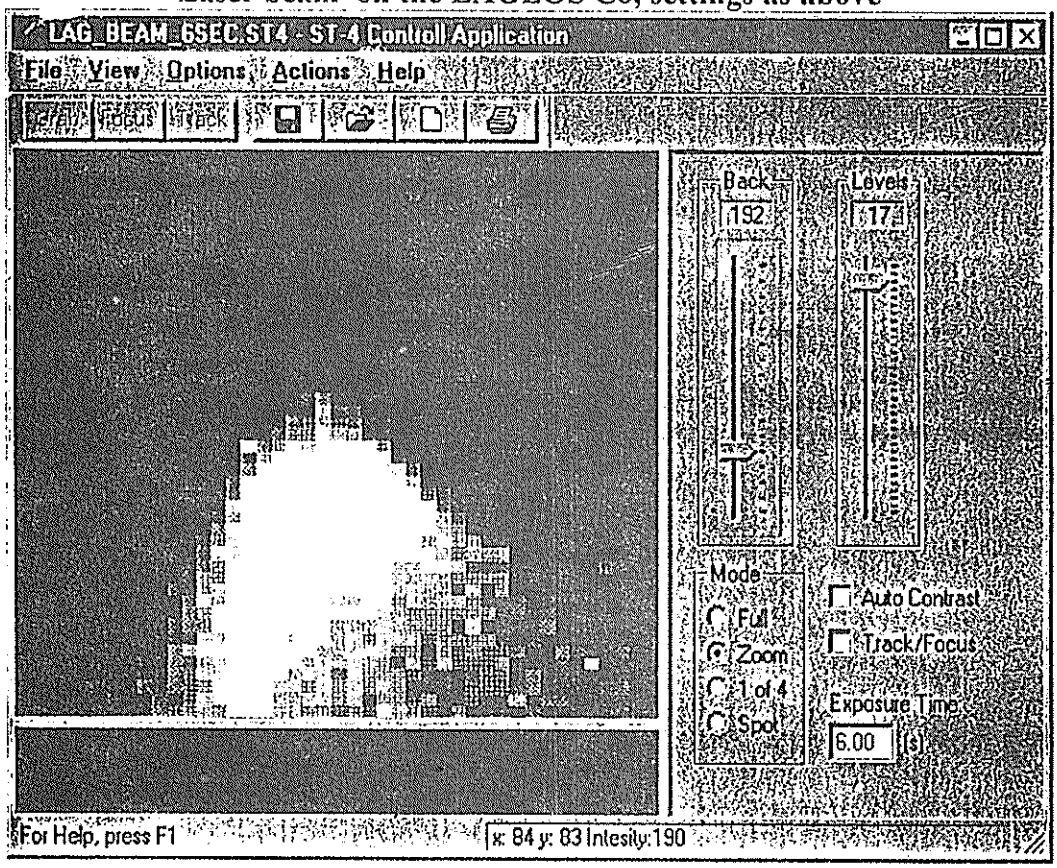

The Coude camera star image

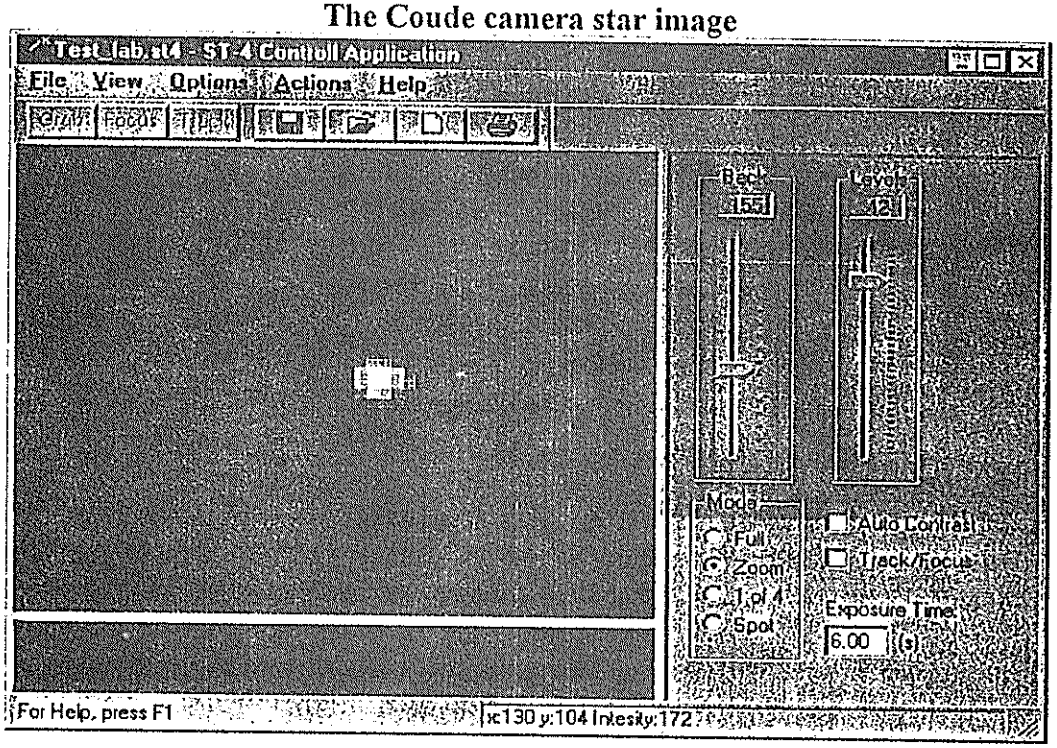

The Coude camera, star image demonstrating the secondary mirror alignment.
The main telescope was slightly defocussed,
in optimum alignment, the ring is symmetrically illuminated.

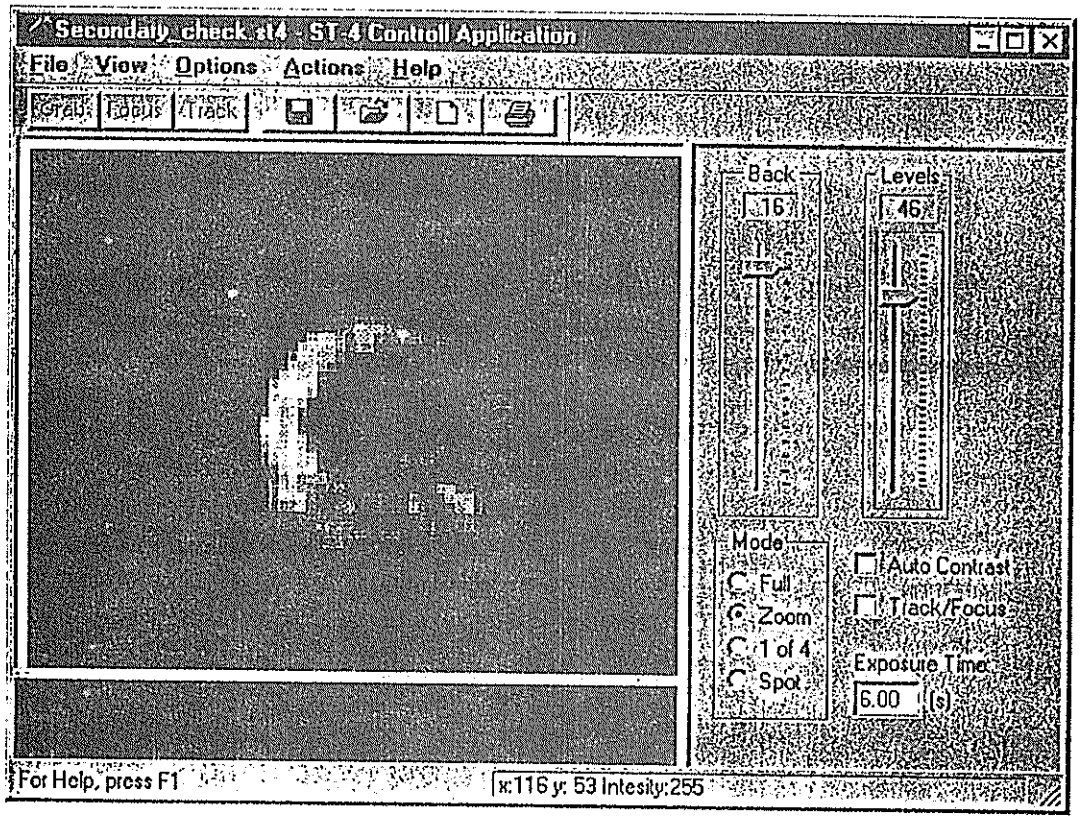

AUTOMATION OF THE BOROWIEC SLR

S.SCHILLAK, J.BARTOSZAK, E.BUTKIEWICZ

SPACE RESEARCH CENTRE
OF POLISH ACADEMY OF SCIENCES
BOROWIEC ASTROGEODYNAMICAL OBSERVATORY
62-035 KÓRNIK, POLAND
tel: +48-61-170-187
fax: +48-61-170-219
e-mail: sch@cbk.poznan.pl

ABSTRACT. The need for automation of the SLR systems arises fro two main reasons: faster pre- and post-observation operations induced by increasing number of laser satellites and assurance of single operator or full automatic operation because of prolonged observational activity and higher operational costs. The achievement of those two goals is the subject of intense effort at the Borowiec SLR station. The paper gives an exemple of satellite pass starting from the calculation of predictions and ending with sending the normal points to EDC. The process of automation will begin with automatic calculation of predictions for one day (or night) for all satellites at a step of 1 second (IRA program). The next stage will be a replacement of two men crew by a single operator. Then a CCD camera will work as an eye of an observer, small engines will be applied for remote control of the position of the beam, neutral filters and diaphragm, sensors will be used for read out of meteorological data. The third stage will be automation of analysis of the results after the pass (AOP program). At present we are at the stage when the operator's task is to choose the calibration set, eliminate the noise points by using a mouse and finally, accept the results before they are sent. The time of data processing has been significantly shortened and amounts now to about two minutes from the end of observation to sending the results as normal points.

The automation of SLR systems is necessary for obtaining a large number of results of observations and essential reduction of the cost of their obtaining. At present a large number of stations work with a single operator, however, still many stations, especially those equipped in separate transmitting and receiving systems need two person staff. In the second case the number of observers is increased or the number of observation days is limited. This is the case in Borowiec station whose construction, coming from the early 80s, poses serious problems as far as introduction of single man operation is concerned. In 1996 The Borowiec station entered the APO project aiming at introduction of a single person crew and reduction of the operator tasks. The main aim of the project whose realisation was planned for 3 years, was minimisation of the tasks to be performed by the operator during an observation. This process includes automation of the preparation of predictions, the hardware and software related to observation in the real time, results processing, their check and sending to EDC.

1. Prediction

The work on automation of ephemeries preparation has been already completed and includes:

- automatic read out of IRV data from the e-mail and attachment of these new data to the IRV string of each satellite,

- prior to the first observation automatic calculation of ephemeries for all satellites predicted in the observation program at Borowiec for a given night at a step of 1 second, and saving the data in the catalogue of ephemeris (IRA program); the operation does not require operator's intervention and takes only several seconds.

2. Observation of a satellite and calibration.

The main objective related to automation of hardware was installation of a CCD camera on a tracking telescope and little engines controlling the movement of the output prism of the Coude system. This solution permits correction of the position of the laser beam relative to the centre of the field of view by the operator at the controlling computer. The next task will be construction and installation of a packet for remote control of the neutral filters and diaphragm for calibration purposes and release and hold of the shutter. The following tasks will be installation of the meteorological data sensors and an automatic radar system for protection against the aircrafts.

The aim of the automation of the controlling software is elimination of all possible actions which require operator's intervention. A block diagram of the program controlling satellite tracking is given in Fig. 1. The exclamation marks are used to indicate the tasks requiring operator's intervention. These tasks and the ways of their elimination are listed below.

Pre-observation process:

- ephemeris; choice of the ephemeris from the list for a given night, made by the operator;
the program should be supplemented with automatic elimination of the overlapping satellite passes taking into account their priority (in the IRA program) then, for a given satellite, the program may start automatically,
- pass parameters; a change of pass parameters for a given satellite, mainly the filter and diaphragm for calibration, and introduction of time bias;
the filter and the diaphragm can be set automatically during calibration on the basis of the amplitude of the return signal or the percentage of good measurements for a given satellite, time bias should be introduced automatically during the ephemeris calculation (in the IRA program) and its corrections should be made during the observation,
- meteo; read out of the pressure, humidity and temperature;
the intended introduction of sensors will eliminate this problem,
- pre-pass calibration; the program requires the operator to decide about pointing the telescope to the target and beginning of the calibration, when the filter level and diaphragm are incorrect, the calibration process is terminated and begun again once the filter and diaphragm are correct;
setting of the telescope and beginning of the calibration can be conducted automatically at a certain time (a number of seconds) before the observation start; the filter and diaphragm could be selected automatically on the basis of the amplitude of the return signal or a percentage of good measurements for a given satellite,
- read keyboard; change of parameters directly before the observation starts;
in practice very rarely conducted mainly to introduce the time bias.

Observation:

- Fig. 2 presents the view of the controlling computer screen during an observation; the upper part presents the gate window with the O-C values in meters, on the right hand side there are the input points, the middle of the bottom part shows the deviation of the telescope position from the ephemeris position (a black square) which can be moved during an observation at an arbitrary step, the large circle has a diameter of 2.5 arcmin, the small one - 30 arcsec, the left hand bottom part shows the data which can be changed via keyboard during an observation; laser switch on/off, model of the telescope delay, gate window, step at which the telescope position is changed, time bias, corrections of the cross, azimuth and altitude; the right hand bottom part displays the results, that is the current number of the ephemeris point (with a step

STR - SATELLITE TRACKING PROGRAM BOROWIEC SLR STATION

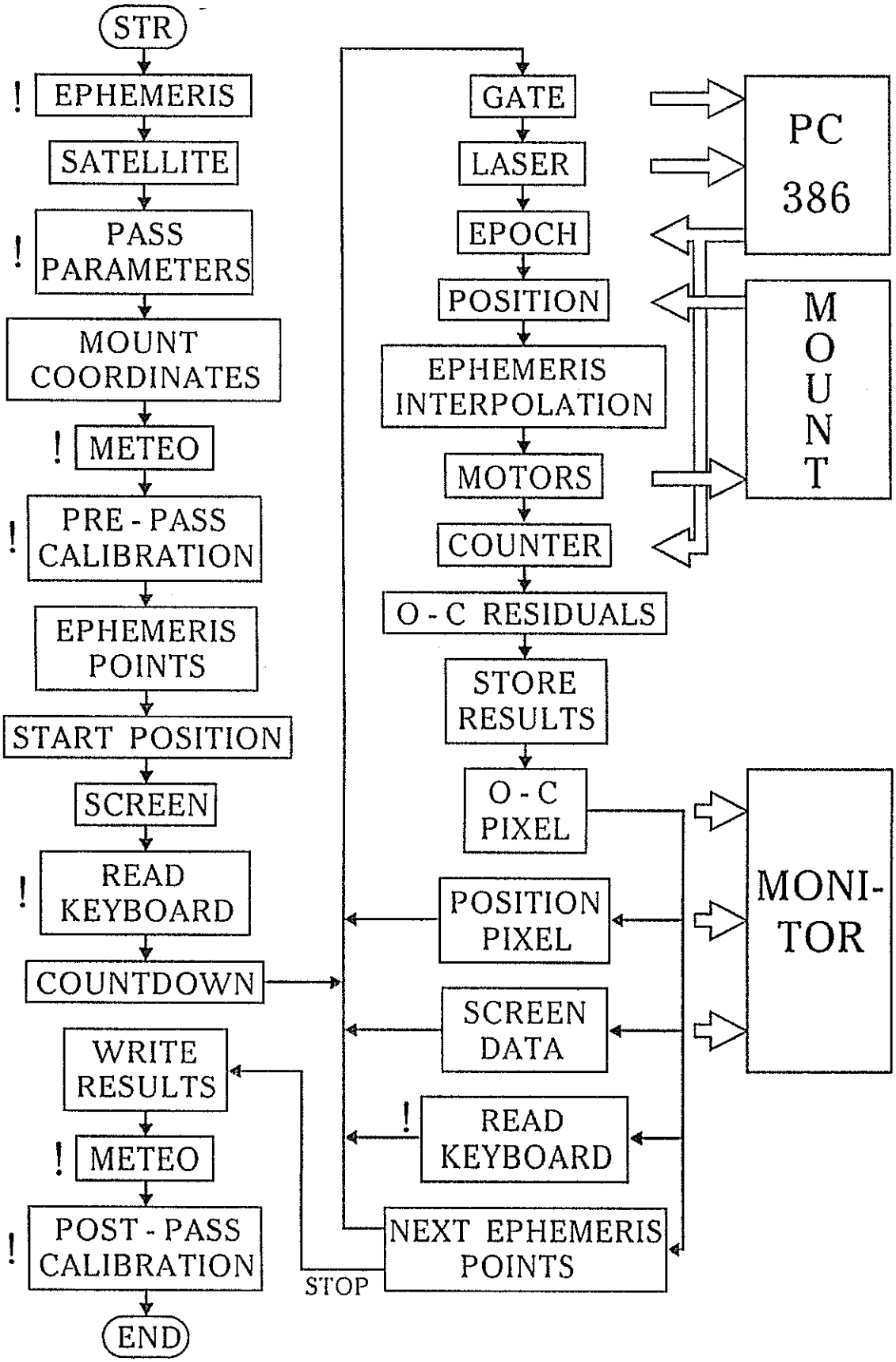

Fig. 1

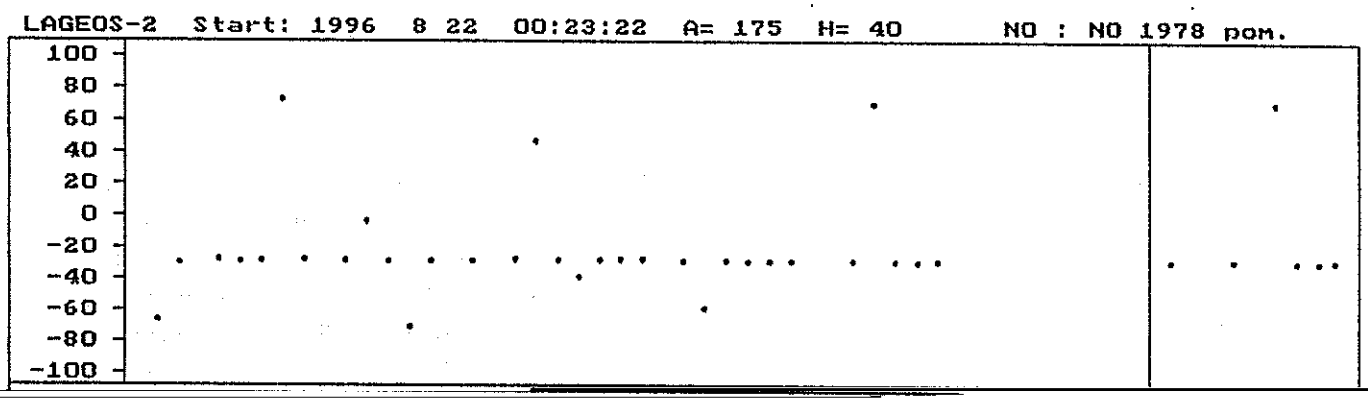
LAGEOS-2 Start: 1996 8 22 00:23:22 A= 175 H= 40 NO : NO 1978 pom.
100
80
60
40
20
0
-20
-40
-60
-80
-100

position will be automatically corrected by the servo engines driving the output prism, preliminary tests have confirmed the possibility of applying this solution.
Post-observation process:
- meteo; the solution proposed is the same as in the pre-observation process,
- post-pass calibration; the choice of the filter and diaphragm should be adjusted to the average amplitude of the return signals or the percentage of good measurements during the satellite pass, if there are significant differences between the results pre- and post-pass calibrations in the mean, RMS or the level of sensitivity, the calibration performed before the observation should not be taken into account (this is a consequence of specific weather conditions in Borowiec where frequent fogs prevent from a correct choice of the filter and diaphragm for the pre-pass calibration, at present this is left up to the operator's decision), the other problems will be solved as indicated for the pre-pass calibration.

3. Results processing.

The processing of results including their control and formatting is carried out by the AOP program which ensures fast and almost fully automatic performance of all necessary operations: elimination of noise pulses, determination of range bias and time bias, polynomial smoothing, rejection of points according to the 2.5 sigma criterion, presentation of the distribution of deviations with determination of RMS, skewness and kurtosis, generation of normal points and assessment of their precision, graphic presentation of residuals (Fig, 3), analysis of the results of calibrations, saving the results in the inner catalogue of Borowiec, formatting of the results in the normal points quick-look format and their sending. The time the program takes to perform all these tasks from the end of the observation to sending of the results to EDC for about 1000 points is of about 2 minutes. At any time after processing the basic information about a given observation can be retrieved and printed: log sheet, distribution of deviations, graphic presentation of residuals (Fig. 3), results and assessment of the precision of normal points. A block diagram of the AOP program is shown in Fig. 4, where the exclamation mark indicates the tasks which require operator's intervention. These tasks and the proposed ways of elimination of operator's actions are listed below:
- calibration data, the choice of a calibration for a given pass;
automatic choice can be carried out on the basis of the mean amplitude of the return signal or the percentage of good results,
- noise points elimination; at present performed by using a mouse;
this process can be carried out by the point by point analysis according to one of the geometrical or filtration methods,
- store results; at present a decision on acceptance of results is made by operator;
an additional program is necessary to control basic data on the results of observations and calibrations,
- e-mail to EDC; operator's decision on sending data to EUROLAS DATA CENTER;
requires automation of the process of data sending by e-mail, the decision on sending the results will be made as indicated above.

Realisation of the above presented tasks will permit almost full automation of the Borowiec SLR. Unfortunately, complete elimination of operator's involvement is impossible mainly because of the need to set the system on and off, control its work and response to highly unstable weather in Borowiec (decision to open or close the roof, to carry an observation out or break it).

Acknowledgements.
This work was supported within the grant Z/137/t12/96/07 of the Committee for Scientific Research.

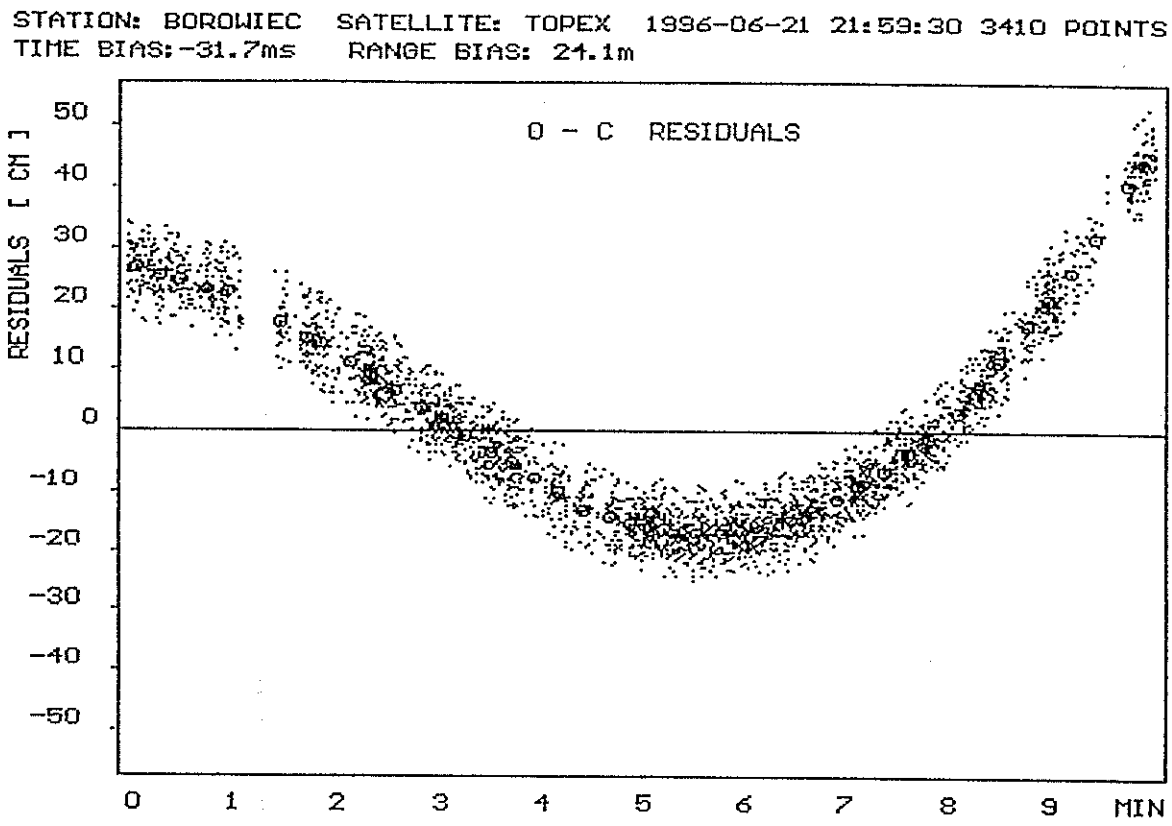
STATION: BOROWIEC SATELLITE: TOPEX 1996-06-21 21:59:30 3410 POINTS
TIME BIAS:-31.7ms RANGE BIAS: 24.1m
O - C RESIDUALS
RESIDUALS [CM]
50
40
30
20
10
0
-10
-20
-30
-40
-50
0 1 2 3 4 5 6 7 8 9 MIN

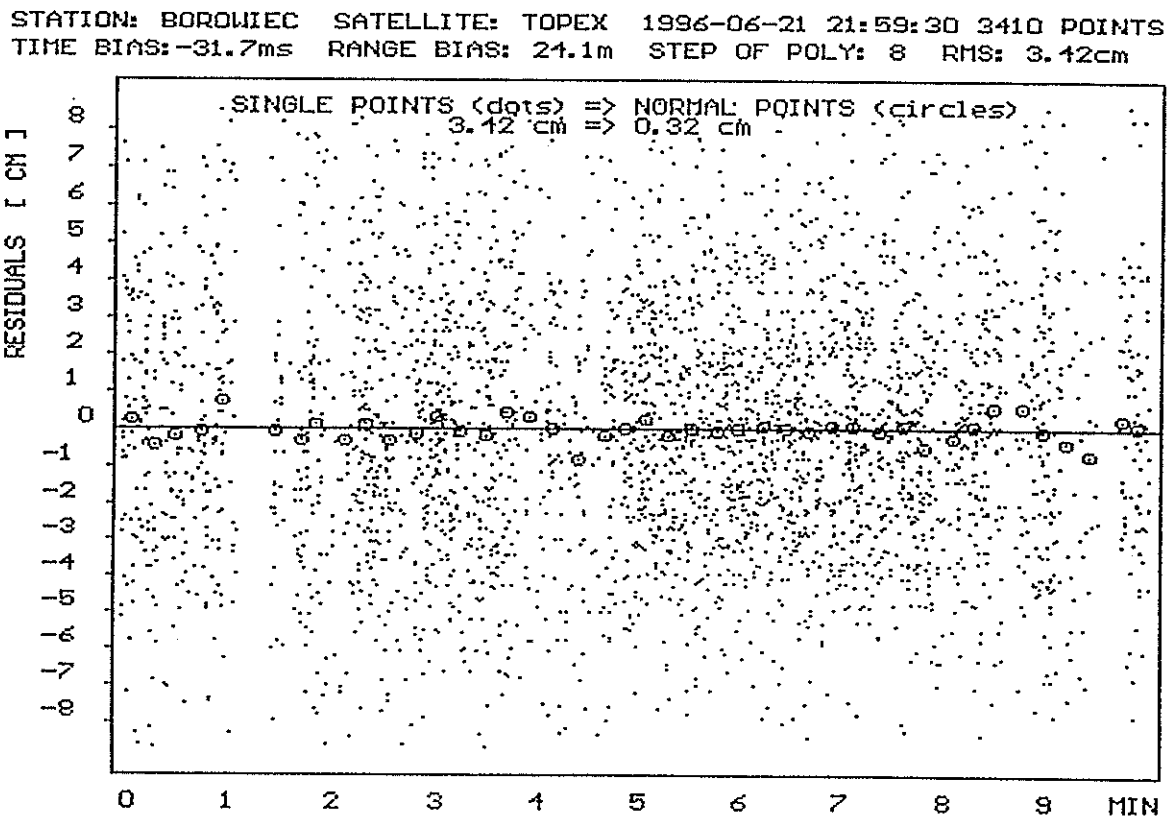
STATION: BOROWIEC SATELLITE: TOPEX 1996-06-21 21:59:30 3410 POINTS
TIME BIAS:-31.7ms RANGE BIAS: 24.1m STEP OF POLY: 8 RMS: 3.42cm
SINGLE POINTS (dots) => NORMAL POINTS (circles)
3.42 cm => 0.32 cm
RESIDUALS [CM]
8
7
6
5
4
3
2
1
0
-1
-2
-3
-4
-5
-6
-7
-8
0 1 2 3 4 5 6 7 8 9 MIN

Fig. 3

AOP
POST - PASS DATA HANDLING PROGRAM
BOROWIEC SLR STATION

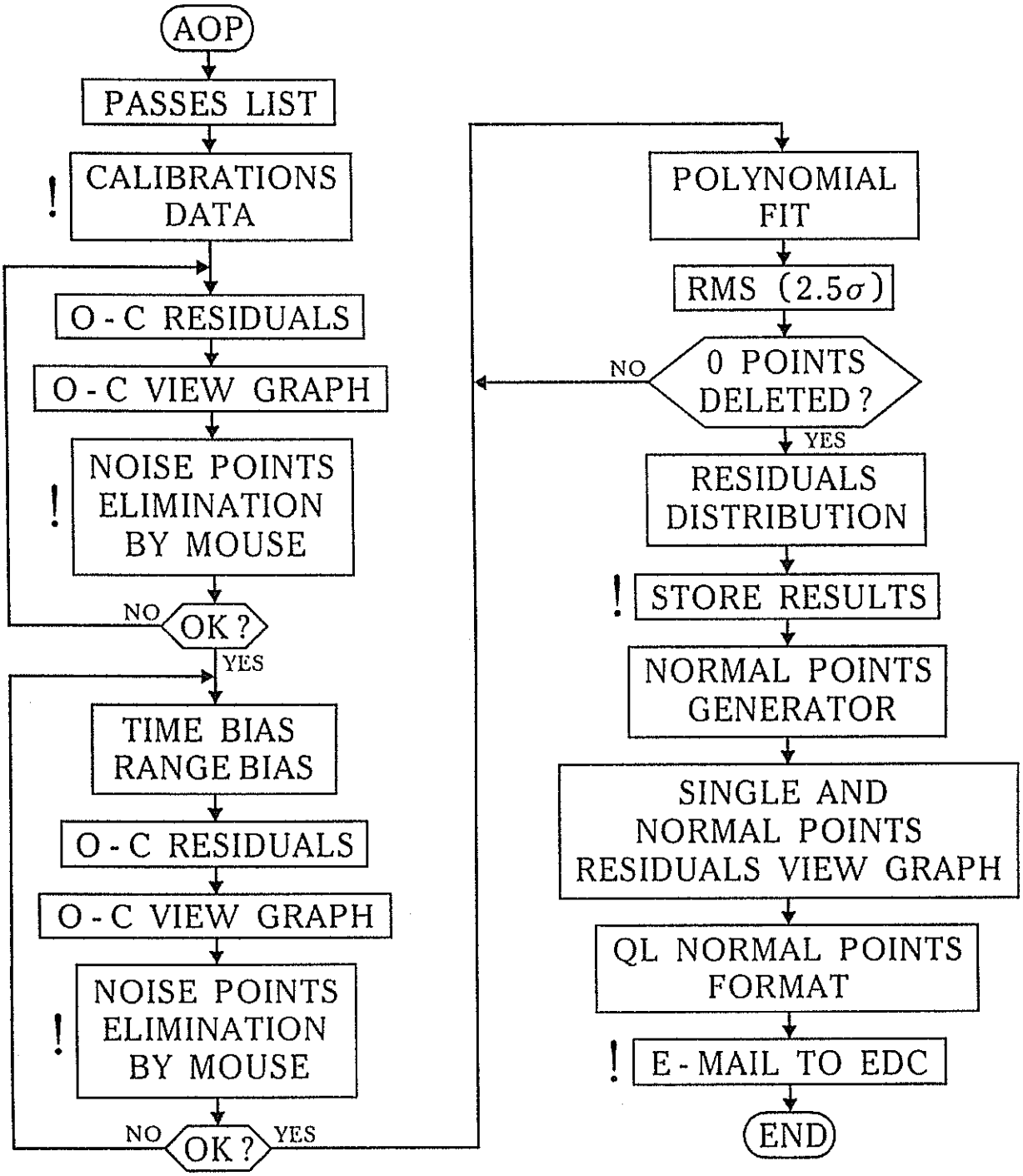

Fig. 4

UPGRADING THE NASA SATELLITE LASER RANGING NETWORK FOR THE 21ST CENTURY and THE SINGLE OPERATOR AUTOMATION PROJECT

Presented in the System Automation and Operational Software Session of the Tenth International Workshop on Laser Ranging Instrumentation
November 11-15, 1996

John Bosworth, David Carter, John Degnan, Jan McGarry
NASA Goddard Space Flight Center
Greenbelt, Maryland 20771 USA

Winfield Decker
AlliedSignal Technical Services Corporation (ATSC)
Lanham, Maryland 20706 USA

The NASA Satellite Laser Ranging (SLR) Network has been preparing for the 21st century by upgrading and planning the redistribution of its systems. NASA intends to relocate two of its MOBLAS systems to Tahiti, French Polynesia and South Africa, respectively. The purpose of the redistribution of the NASA MOBLAS systems is to improve the geographical distribution of the global SLR network. The upgrading program for the MOBLAS systems included several automation projects. The objectives of these projects were to improve productivity and make the MOBLAS systems more cost efficient while enhancing the quality as we approach the 21st Century. The automation program included the Mount Observer Automation (MOA), MOBLAS Upgrade Project (MUP), the High Sensitivity Laser Receiver (HSLR), and the Single Operator Automation Project (SOAP). The MOA, MUP, and HSLR have been discussed at previous conferences, therefore, the details of SOAP will be presented.

Introduction

The NASA SLR Network consist of five MOBLAS systems, two University systems, and a Transportable Laser Ranging System (TLRS). These systems are located across the United States in Maryland, Texas, California, and Hawaii. NASA also have systems located in Arequipa, Peru and Yarragadee, Australia. In order to provide better geographical coverage particularly in the southern hemisphere, NASA intends to relocate MOBLAS-8 (Quincy, California) and MOBLAS-6 (Greenbelt, Maryland) to Tahiti, French Polynesia and South Africa, respectively. The MOBLAS transfer to Tahiti is a joint effort among NASA, CNES, and the French University of the Pacific (UFP). The SLR site will be located on the campus of UFP. GPS, DORIS, and PRARE systems will also be located at the site. The MOBLAS system is scheduled to be transferred to Tahiti during July/August 1997. The discussions concerning the transfer of a MOBLAS to South Africa is in preliminary stages.

Over the past few years, NASA has been involved with an upgrading program for the MOBLAS systems. The program consist of four major upgrades: the Mount Observer Automation (MOA), MOBLAS Upgrade Project (MUP), High Sensitivity Laser Receiver (HSLR), and the Single Operator Automation Project (SOAP). The purpose of the MOA was to eliminate the necessity of a mount observer by replacing the observer with a radar and several automated processes. The purpose of the MUP was to enable future automation by the centralization of ranging and processing functions, upgrading of the computer platform, standardization of the hardware and software, and upgrading of the software and troubleshooting infrastructure. The purpose of the HSLR was to enhance the detection capabilities of the NASA MOBLAS systems on low optical link satellites such as GPS, GLONASS, and Etalon.

Single Operator Automation Project (SOAP)

SOAP was conceived to enable the NASA MOBLAS stations to operate effectively and safely with one operator per tracking shift. A single operator per shift will enable an increased level of satellite tracking support by making more effective utilization of personnel resources. SOAP builds on the other automation projects (i.e. Data system automation, MOA, and MUP), and is the culmination of a series of engineering projects designed to automate the functions of the mount observer and streamline processes for the console operator.

The MOBLAS systems currently operate with two crew member per 9-hour tracking shift. For SOAP to be implemented, detailed examinations on the engineering, maintenance, personnel, and safety issues, as well as operating procedures had to occur. Methods were developed to address the engineering and safety constraints associated with current operations. This was accomplished through field HP380 software enhancements, modifications to field operating procedures, additional operator training, and operator certification (see Figure 1). A strong emphasis was placed on crew safety especially with the remote locations of some of the NASA sites. With these modifications, SOAP will be able to provide 24 hour per day, seven days per week operations using 4 operators. This will double the temporal coverage over the previous two shift operations.

The final design approval for SOAP took place in June 1996. The installation and testing of the prototype occurred at MOBLAS-7 in July 1996. The installation of SOAP at MOBLAS-4 is scheduled to be completed in November 1996. The MOBLAS-8 installation will occur in January 1997, followed by the installation in MOBLAS-5 and MOBLAS-6 which are expected to be completed in the first quarter of 1997. The development, testing, and installation will occur on a parallel schedule for HOLLAS and MLRS.

Summary

NASA's upgrading program for the MOBLAS systems will be completely implemented in 1997. The benefits of these automation projects are that it reduces the cost of operations, increases the data volume, and enhances the safety of the MOBLAS operations. The MOBLAS-8 system will be transferred to Tahiti by August 1997 and detailed discussions will begin concerning transferring a system to South Africa. This will lead NASA into building and deploying "SLR2000"[1] systems in the 21st century.

References

[1] 1. Degnan, John, Jan McGarry, Thomas Zagwodzki, Paul Titterton, Harold Sweeney, et al, "SLR2000: An Inexpensive, Fully Automated, Satellite Laser Ranging System," in this Proceedings.

SINGLE OPERATOR AUTOMATION PROJECT (SOAP)

- HARDWARE / SOFTWARE ENHANCEMENTS
  - IMPROVED AUTOMATION OF STATION DATA REPORTING FUNCTIONS
  - INTERNET CAMERAS TO ALLOW VISUAL CONTACT BETWEEN STATIONS

- MODIFICATIONS TO FIELD OPERATING PROCEDURES
  - EMPOWERED EACH OPERATOR TO DECIDE THAT UNSAFE TRAVEL CONDITIONS WILL CANCEL OPERATIONS
  - PROHIBITED SPECIFIC TYPES OF MAINTENANCE UNLESS AT LEAST 2 PEOPLE ARE PRESENT (HIGH VOLTAGE)
  - PROVIDED CELLULAR TELEPHONE FOR EMERGENCY USE
  - ESTABLISHED COMMUNICATION SYSTEM TO MAINTAIN CONTACT WITH OPERATORS ON PRE-DETERMINED SCHEDULE

- OPERATOR TRAINING AND CERTIFICATION
  - ALL OPERTORS TRAINED FOR HIGHER LEVEL CERTIFICATION
  - FORMAL TRAINING IMPLEMENTED PRIOR TO START OF OPERATIONS
  - TYPES OF MAINTENANCE THAT CAN BE PERFORMED BY INDIVIDUALS SPECIFICALLY DEFINED

Figure 1

Automated Quality Control of NASA SLR Data

Van S. Husson
AlliedSignal Technical Services Corporation
NASA SLR Program
7515 Mission Dr.
Lanham, Md 20706

1.1.1 Introduction

This is an update to a paper that was previously published [*Husson et al.*, 1994] in the proceeding of the previous SLR workshop held in Canberra, Australia. The purpose of Automated Quality Control (AQC) is to quickly identify any data problems so that the cause can be identified and corrected as soon as possible to prevent more bad data from being taken. Therefore, AQC results needs to be readily available to the people who can take corrective action. In the current NASA network, this place is still at the system where we still have operators. The operators are the first line of defense in identifying data problems using information provided by AQC coupled with other routine evaluations of the sub-systems.

1.1.2 History

In the early and mid 1980's, the NASA SLR network hardware was upgraded and standardized with 200 picosecond pulsed non-mode locked Quantel lasers, Micro-Channel Plate Photo-Multiplier Tubes (MCPPMT), cascaded Tennelec discriminators, and stable short range calibration targets [*Husson*, 1992]. Before and after these system upgrades, extensive testing of the different sub-systems were performed in the laboratory. Collocation testing (see Figure 1) were used as a verification test of the complete system. These hardware upgrades coupled with improvements in NASA/ATSC data analysis and processing techniques improved the NASA SLR data precision and accuracy from the 10cm level in 1980 to the sub-cm level by the mid to late 1980's.

AlliedSignal Technical Services (ATSC), formerly Bendix Field Engineering Corporation, has been responsible for NASA SLR Network data processing, analysis, and quality control since the late 1970's. All through the 1980's, ATSC had 4-6 people at it's central facility who's primary responsibility was to perform these data related functions. Full-rate data was primarily used for system performance evaluation. The biggest problem with full-rate data analysis was the delay (up to 1 month) between the time the data was taken to when it was analyzed. Data problems could and did go undetected for a month. Most of this delay (2-3 weeks) was caused by the full-rate data shipment process. Full-rate data was stored on 9-track magnetic tapes and was forwarded only once per week to the central facility via regular postal mail. After the data was received at central facility, another week was needed for the data processing and data evaluation.

By the late 1980's, weekly long-arc analysis reports of quicklook data, produced by both the University of Texas and the University of Delft, were distributed to the global SLR community. Quicklook data was sampled full-rate data sent immediately after the data was taken. Quicklook data was not quality controlled at that time and because of that quicklook data quality was inferior to full-rate data quality. In the late 1980's, 5-10 cm problems were detectable in the Texas and Delft analysis and ATSC became reliant upon these reports as a redundant gross level quality control check. By the end of the 1980's, sampled data was being replaced with normal point data.

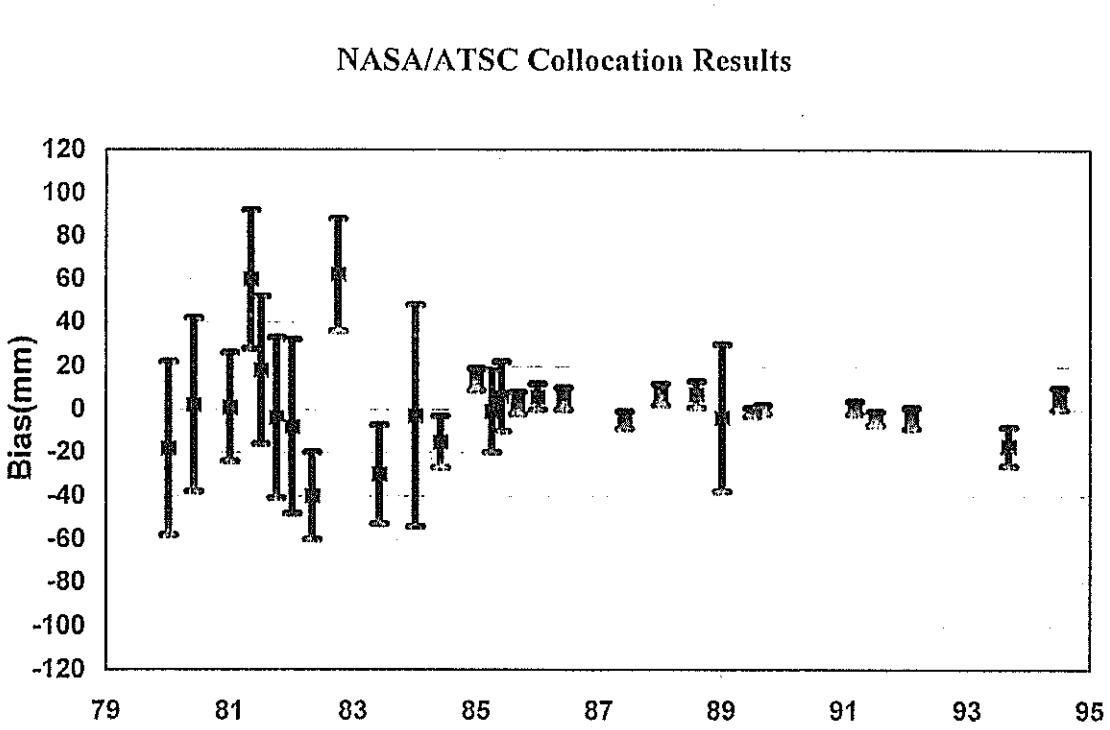

Figure 1. Collocation Results

By the early 1990's, we were faced with a huge technical challenge. NASA only had funds to support a single person quality control operation, NASA SLR data quality was to be maintained, management of full-rate data was to be phased out, and at the same time new SLR satellite missions had to be supported that would cause a dramatic (4-5 fold) increase in NASA SLR data quantity. AQC was mandatory to our survival.

1.1.3 Pre-requisites

The pre-requisites for development of AQC is a comprehensive understanding of system performance at the sub-system and overall system level [*Pearlman*, 1984].

1.1.4 Requirements

One initial requirement of AQC was to identify 95% of the NASA SLR data problems. NASA was willing to take some risk and could accept a 5% data loss. Problem data that was repairable in the past would now either have to be thrown away or if possible be documented (i.e. provide range bias, time bias, or barometric offset information) [*Husson*, 1992]. It took about 2 years to develop a quality control algorithm, benchmark it's effectiveness, automate it, and migrate it from the central facility to the field systems.

1.1.5 Algorithm Development and Benchmarking

Over 50 years of ATSC data analysis experience was used to develop the first LAGEOS quality control model. The algorithm was based on LAGEOS only, because LAGEOS was the primary target, had a very stable orbit, and the only satellite who's data was analyzed on a routine basis. The Center for Space Research (CSR) Weekly LAGEOS Reports and collocation analysis results

were used in determining the final quality of the data. Problem data was defined as any data having a known systematic error above the 1-2 centimeter (cm) level. This was and still is the smallest error detectable using LAGEOS long arc analysis techniques. Other satellites were eventually added to the algorithm.

Five years of NASA SLR LAGEOS-1 and LAGEOS-2 (1988 - 1993) data, consisting of a total of 11,167 passes, were used to benchmark this model. During the algorithm development and benchmarking, it was discovered that the basic pass-by-pass processing statistics (i.e. satellite RMS, calibration RMS, and calibration shift), that are computed in the generation of normal points, would become the critical performance statistics. These statistics already existed in the CSTG normal point format. This fact was critical to the success and ease of implementation of the algorithm, because full-rate data was being phased out and quicklook data was being transitioned from sampled data to normal point data. Another interesting discovery was that there should be two levels of quality control, a gross level and a fine level. Data should be verified first at the gross level, if it passed at the gross level, then it should be verified at the fine level. Below are the 2 levels in the algorithm:

1.1.5.1 Gross Level

```
If LAGEOS RMS > 5 cm or
      if combined calib. RMS > 5 cm or
            if (calib. shift > 5 cm and combined calib. RMS < 5 cm) Then
                  DATA IS BAD
```

Note: calib. is an abbreviation for calibration

All data that did not pass the gross level was bad and should be edited. However, certain NASA SLR system problems (i.e. excessive laser multi-pulsing), which would cause the data to flunk the gross level check, were and are repairable by manual intervention in the full-rate data and normal point generation process.

1.1.5.2 Fine Level

```
Else

If LAGEOS RMS > 1 cm or
      if combined calib. RMS > 0.8 cm or
            if (calib. shift > 0.5 cm and combined calib. RMS < 0.8 cm)
Then
                  DATA IS OK, BUT SHOULD BE CLOSELY MONITORED
End if
```

Data that passed the gross level check, but failed the fine check was still very usable data (i.e. accurate), but it's precision was slightly degraded. If degraded precision continued for an extended period of time (i.e. a few days), then a investigation should be initiated into the potential source of the problem.

1.1.5.3 Benchmark Results

The exact same algorithm could be used for each NASA SLR system, due to many of the standardized components in our network.

The AQC is still not a replacement for other sub-system performance checks done routinely as part of normal NASA SLR system operations. These other sub-system performance evaluations include daily monitoring of station time through use of GPS receivers to the 1 microsecond level; daily monitoring of barometric performance by comparing dual station barometers to the 1 millibar level; monthly monitoring of the timing frequency to one part in 10^{-12}; monthly multi-target ranging closure to the sub-cm level; and periodic checks of the station key processing parameters. If these sub-systems checks reveal a problem, data precision would usually not be effected, but data accuracy would be adversely effected. The good news is if thorough station performance records are maintained, the data can be corrected.

The benchmark results revealed that 15 percent of the total benchmark dataset had significant problems, but only 5 percent would be detectable by the AQC algorithm. The other ten percent of the data, had errors that would not manifest itself in either an abnormal satellite RMS, calibration shift, or calibration RMS. But, these problems, which effect accuracy and not precision are detectable through the sub-system tests mentioned above.

There are some other interesting benchmark discoveries. The root cause of the problem can be narrowed based on the values of the quality control statistics. For instance, if the satellite RMS or calibration RMS > 1-2 times nominal values, then the problem is usually in the receive electronics (i.e. MCPPMT, discriminators, time interval unit). If the satellite RMS or calibration RMS is between 20-40 cm, then the problem is usually laser related. If the satellite RMS or calibration RMS > 40 cm and if the pass was daytime, then low signal to background noise ratio is the cause.

1.1.6 Conclusions

Global SLR data quality control needs to be migrated to the stations as much as possible. To be successful in doing this, a complete understanding of the performance of every sub-system, including the system as a whole is required. We have demonstrated that AQC can be done and be effective, but many years of hard work were involved in getting to where we are today.
Standardization within the NASA SLR network was a key to the AQC success.
AQC needs to be readily accessible to the people that maintain the system. With recent advancements in computer networking technology (i.e. INTERNET), AQC can be done in near real time virtually anywhere (i.e. a centralized facility or in the field).

The AQC algorithm needs to be closely monitored for it's effectiveness, especially after any system hardware, software, or procedural changes or after tracking of a new satellite. AQC has been very crucial in maintaining NASA SLR data integrity in the 1990's and is a requirement of SLR2000.

1.1.7 Current Status

The AQC algorithm originally was used to flag data, not to edit data. We have since realized this is a severe weakness and on January 28, 1997, we now edit any NASA SLR data that flunks the gross level check as part of our automated global normal point data management operation.

1.1.8 Acknowledgments

I would like to thank Dr. John Degnan, NASA, and Dr. Michael Pearlman, Smithsonian Astrophysical Observatory (SAO), for challenging us to develop a quality control algorithm. Without their push and moral support, this paper would not have been possible. I would also like to thank Richard Eanes and Rick Pastor from CSR for incorporating the normal point processing statistics into their weekly LAGEOS analysis report. This has been in an invaluable aid in quickly identifying the root cause of problem data not only in the NASA SLR network, but the global SLR network. And lastly, I would like to thank two other ATSC colleagues, Michael Heinick and David Edge, that are no longer with our organization, who both were significant innovators in SLR data analysis techniques.

1.1.9 References

Husson V, "Historical MOBLAS System Characterization", Proceedings of the Eighth International Workshop on Laser Ranging Implementation, Annapolis, Md, May 1992.

Husson V, Horvath J, and Su G, "NASA Automated Quality Control", Proceedings of the Ninth International Workshop on Laser Ranging Implementation, Canberra, Australia, Nov 1994.

Pearlman M, "Laser System Characterization", Smithsonian Astrophysical Observatory, Proceedings of the Fifth International Workshop on Laser Ranging

Automated and Remotely Operated SLR Systems

Christopher Moore, Jeff Cotter, Iztok Fras, Ben Greene, Adrian Loeff, Tim May

Electro Optic Systems Pty Limited (EOS) Queanbeyan NSW Australia 2620

Abstract

The Keystone SLR Project aims to continuously measure and monitor the geodetic positions of the invariant points of a number of sites around Tokyo to provide local crustal deformation information and to provide accurate predictions of the trajectories of selected satellites. The SLR systems at each site are required to provide highly reliable routine observations and be controlled by automatic processes supported by relatively unskilled operators from a central site. These requirements place a high demand on the hardware and software systems being developed for Keystone. This paper presents on overview of the software systems being developed to support this program.

1. INTRODUCTION AND BACKGROUND

The Keystone system requires hardware and software systems for four fixed SLR observation stations, located at Koganei, Kashima, Miura, and Tateyama, all within 200 km of Tokyo, and one mobile SLR facility which can be deployed much further afield. All of these stations are to be controlled from a central station. Figures 1 and 2 illustrates the software related facilities of the central network control station and a typical remote station respectively. The fixed stations are to be connected by a 128 KBytes per second wide area network and all stations connected by the low bandwidth public switching telephone network.

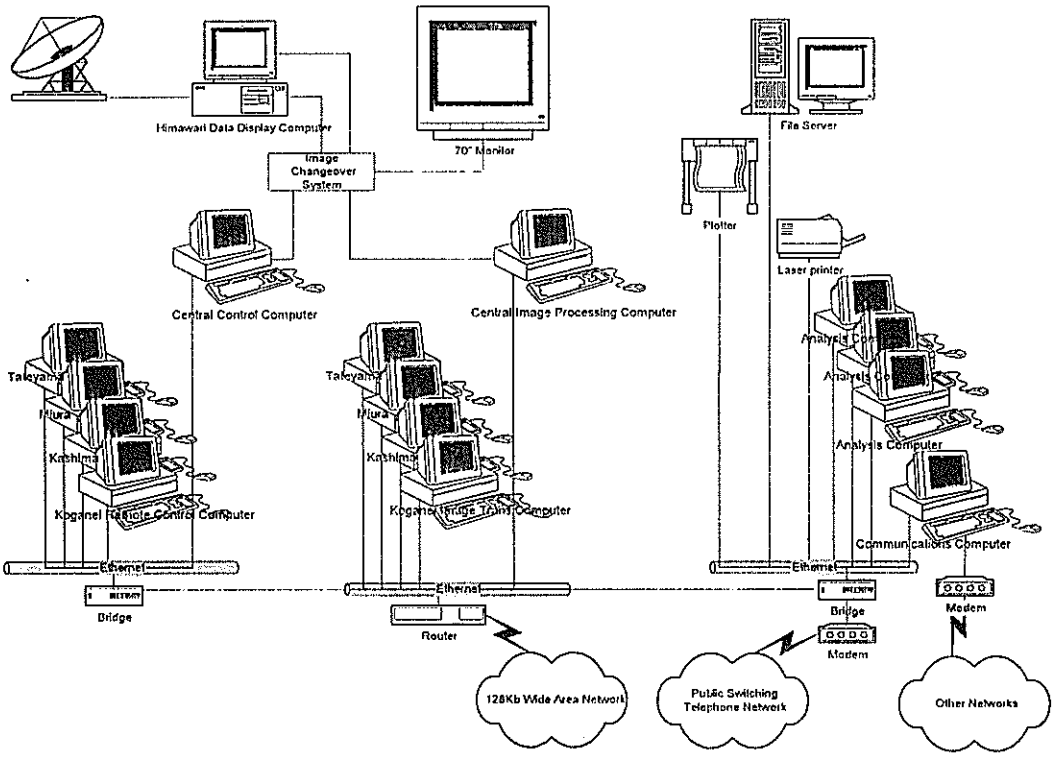

Figure 1 - Schematic of the Central Control facility

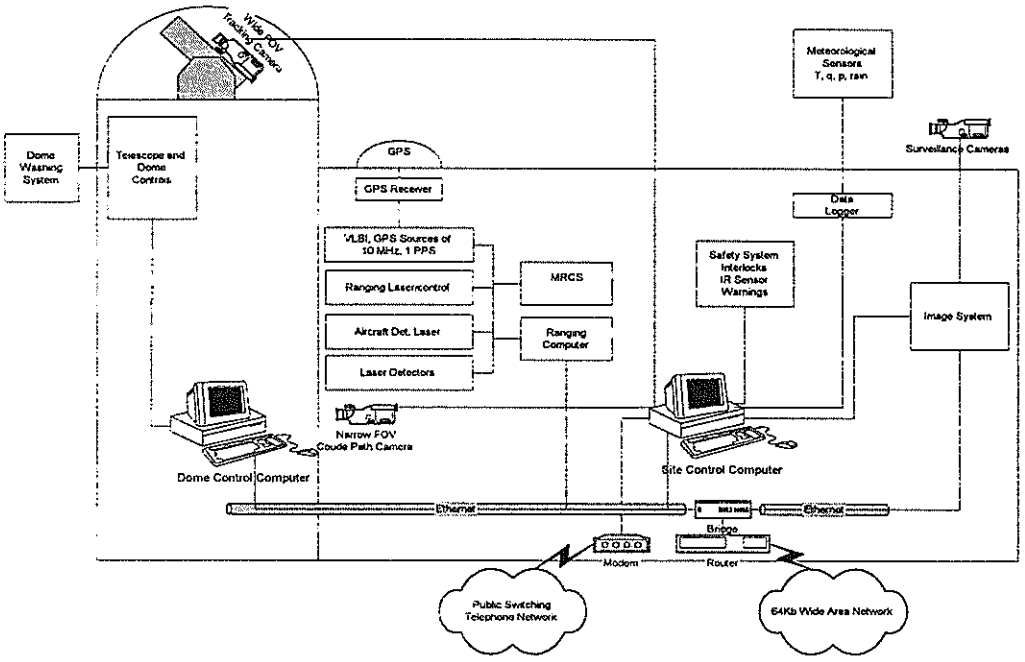

Figure 2 - Schematic of a Remote Station

The system supports three modes of control. One mode of operation will consist of control and monitoring of all network sites under the control of a single operator at the central station. The second mode allows single operators at the central station to be allocated to specific remote sites and undertake control of those sites separately from one another. The third mode allows operators at each station to control local operations independently from the central station.

All of the major software functions are being developed to support the requirement that the network of Keystone stations be operated automatically and remotely. These functions include:

- mission planning, i.e. the development of mission schedules and trajectory predictions;
- laser, dome and telescope systems control during SLR operations;
- performance of system testing and calibration; and
- data collection, analysis and archival.

2. SYSTEM ARCHITECTURE

The Keystone system is based on standard commercial Pentium PCs running under Windows NT. The central control facility computing resources, illustrated in Figure 1, consist of three groups of computers. One group provides a central control computer, and a number of remote site computers for the operational control and data monitoring of one or more sites. Another group provides for surveillance monitoring while the third group consists of computers dedicated to data analysis and data management and archiving.

Computing resources for each remote station consists of three computers as illustrated in Figure 2. The ranging computer, which is a dedicated VXI rack mounted Pentium microprocessor, controls laser and the master ranging control systems (MRCS), The dome control computer is dedicated to the control and monitoring of telescope, dome and associated equipment. The third computer provides general processing for the site, including user displays, data handing, intersite communications, operations scheduling and management of tests and calibration processes. This approach is designed to ensure high real time performance of the laser ranging subsystems yet allow applications to perform sophisticated automated and remote control operations.

Keystone software applications are developed in C++ with graphical user interfaces developed under Microsoft's 32 bit Windows NT. This approach allows the high performance requirements to be met, yet allow development to make use of the wide range of commercially available development products and hence minimise costs.

3. REMOTE CONTROL

To support the management of multiple sites, especially by a single central controller, it is important to use the power and flexibility of Windows style graphical user interfaces (GUIs). Figure 3 illustrates a "hierarchy" of related windows GUIs that are being developed for the Keystone project. It illustrates that from a top level "program manager" layer, an SLR application can be executed that allows control and monitoring of one or more remote stations, and other SLR applications can be launched, e.g. mission planning and engineering diagnostic tools.

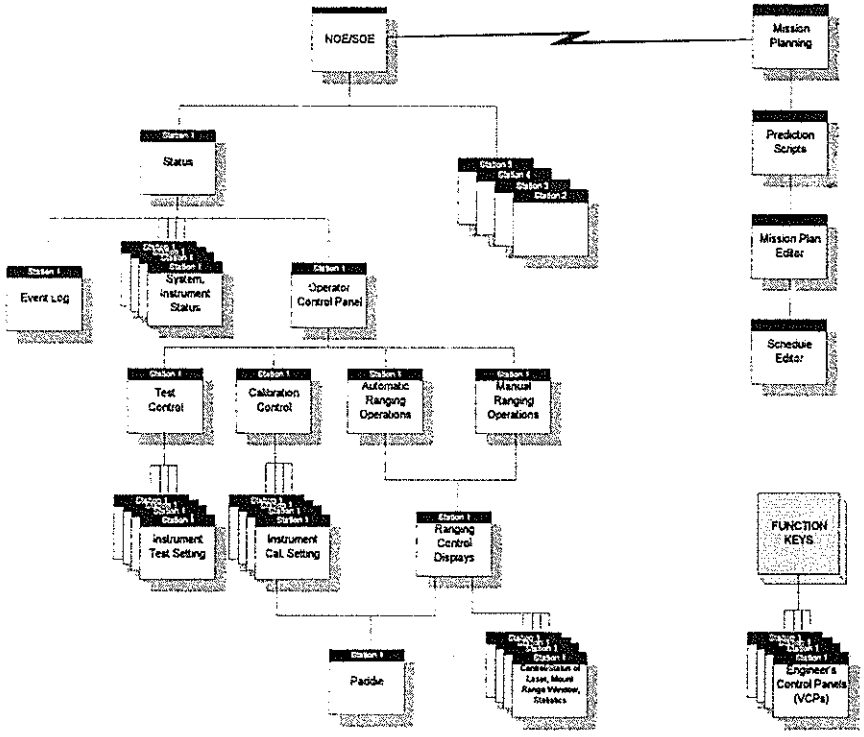

Figure 3 - Overview of KSP Operations Screens

To provide both local and remote management of a site, the general approach taken has been to provide upper level GUIs that allow site selection and monitoring - a function that is available to both local and remote operators, and to provide control screens at lower levels in the hierarchy for one operator authorised to have control. Note that the GUIs presented in this paper are schematics of conceptual displays only; and any data shown do not represent actual nor representative data.

3.1 STATUS MONITORING

Figure 4 illustrates the top level screen in which the status of all network sites is displayed in forms suitable for unskilled operators, but which can be expanded to suit the needs of more skilled operators. For example, it is possible for a network station to observe whatever operations are being performed by a selected remote site. If any problem or fault is reported by a remote station, more detailed status information can be readily accessed for that station. Such a display is illustrated in Figure 5.

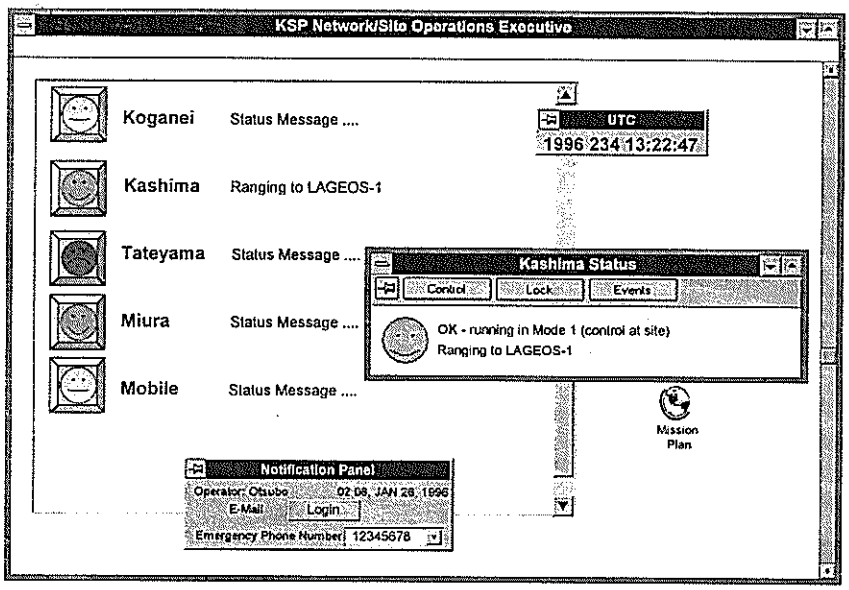

Figure 4 - Schematic of Top Level Operations Main Window

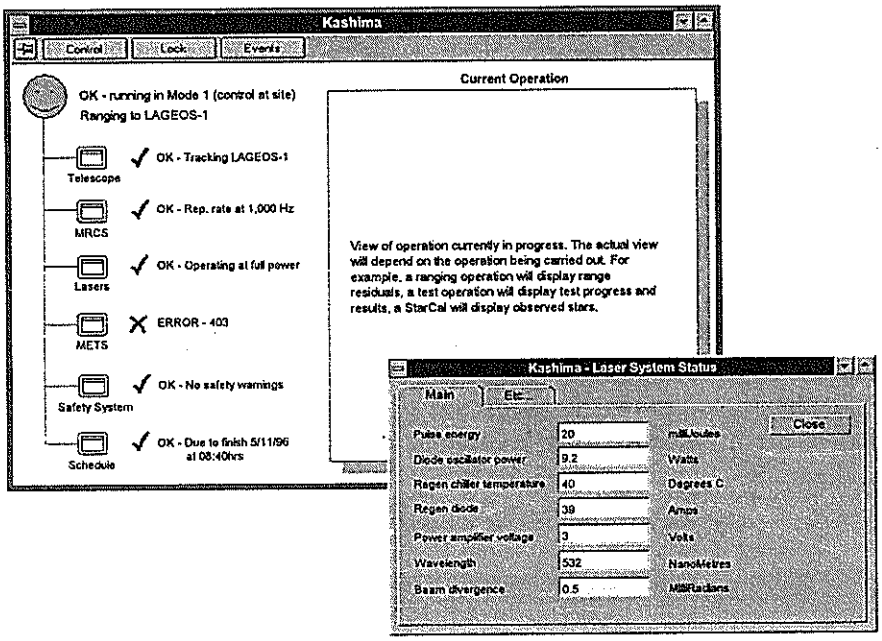

Figure 5 - Schematic of the detailed status screen

To allow local and remote control of sites, the software is designed to support all manual controls necessary for SLR operations once an operator gains the appropriate authorisation. Manual operations include the ability to conduct system and subsystem tests and calibrations, and the ability to manually select a satellite and initiate ranging operations. GUIs for such manual operations are illustrated in Figure 6 for the manual control testing and Figure 7 for ranging operations.

4. AUTOMATED OPERATIONS

The key characteristic of the Keystone system will be its ability to perform automatic SLR operations and maintain a reliable observation program with a minimum of operator attendance.

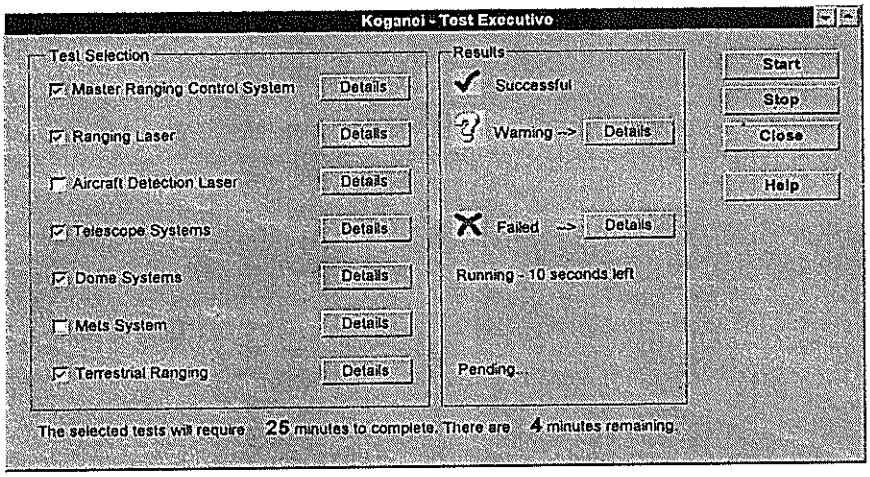

Figure 6 - Schematic of Test Control Screen

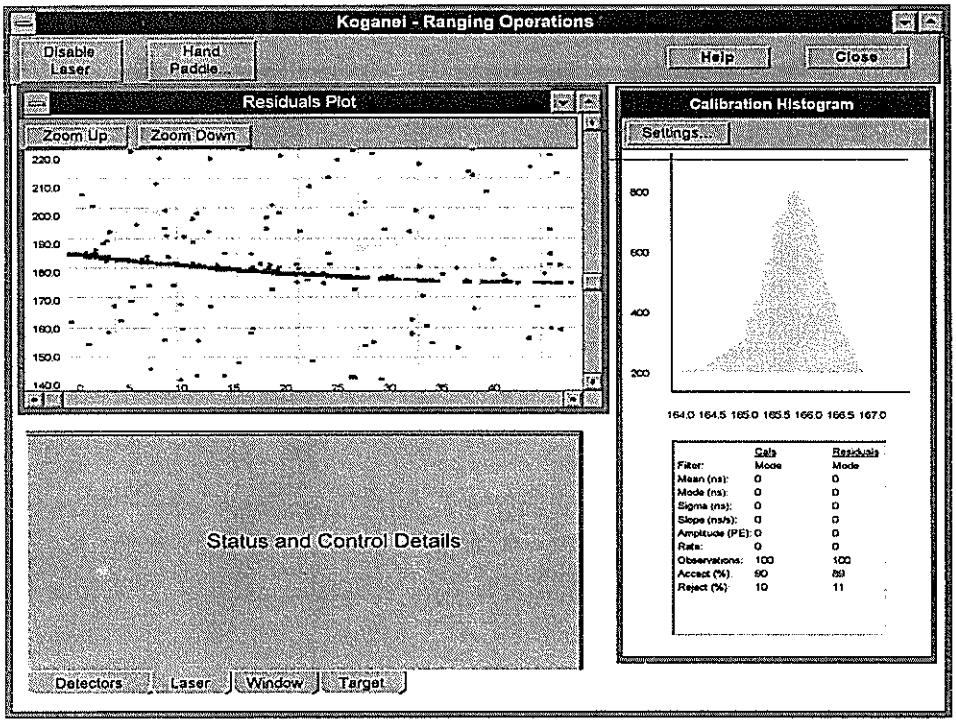

Figure 7 - Schematic of Ranging Operation Screen

Software related functions that support automated operations include:

- Automated and manual development of operating schedules
- Automated distribution of operating schedules to network sites
- Automatic performance of scheduled operations
- Automatic tracking
- Automated observation data management
- Automated data exchange between Keystone and external agencies.

Routine development of detailed operating schedules can be generated using a mission planning system, in which the tracking of selected satellites can be scheduled together with routine and automated calibration and test activities. This mission planning system will include an editor, illustrated in Figure 8, allowing selection of satellites for prioritised and dedicated SLR, or for selecting a number of satellites for interleaved observations.

To ensure as a high level of observation effectiveness, the system will support automatic acquisition and tracking, in which the software will have the ability to perform search patterns and adjust and optimise window widths and offsets, firing rates and laser power.

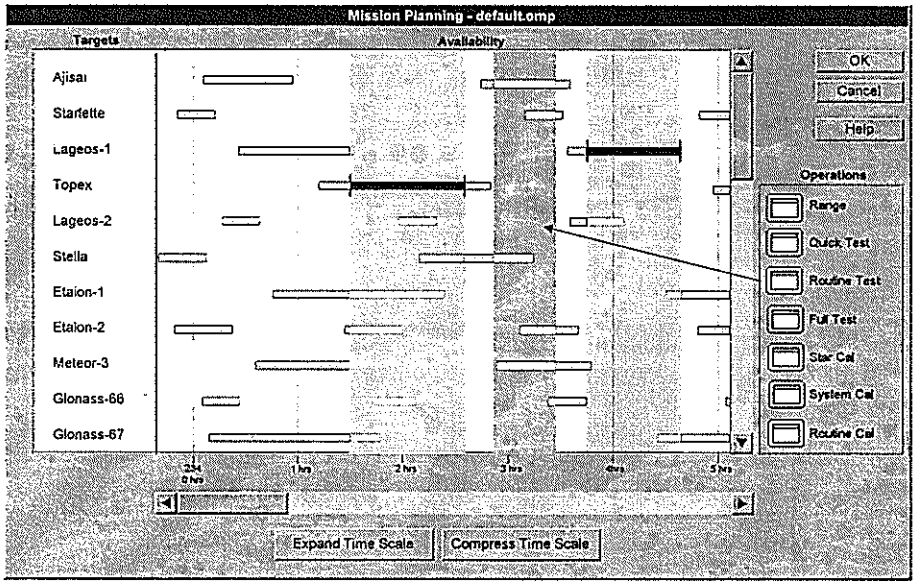

Figure 8 - Schematic of Mission Plan Editor

5. CONCLUSIONS

Software functionality needed to support the automated and remote operational requirements of the Keystone SLR Project has been summarised in this paper. Samples of the types of graphical user interfaces needed for this project have been presented. The ability to support, over a network containing multiple SLR stations:

- operator control at each local site
- operator control of one or more remote sites
- automated or unattended operation of one or more sites

places high demands on all systems, not least the software. The capability of current computing technologies, including advanced networking, file management, security and flexible graphical user interfaces executing on powerful processors, has made it possible to develop such a sophisticated system at a reasonable cost.

Development of software for the Keystone system will take remote and automatic operations of SLR stations to a new level of performance. This and other systems being developed by other groups suggest that this is just the first step in the evolution of advanced SLR software systems.

A method to improve the accuracy of low orbit satellite prediction[1]

Lin Qinchang[2] Yang Fumin[3] Tan Detong[3]
Tang Wenfang[3] Zhang Zhongping[3] Deng Youjun[2]

[2] (Guangzhou Satellite Station, Chinese Academy of Sciences,
Guangzhou 510640, China)
[3] (Shanghai Observatory, Chinese Academy of Sciences,
Shanghai 200030, China)

Abstract

In this method, the orbit elements a 、 i 、Ω、 $\xi = e \sin \omega$ 、 $\eta = e \cos \omega$ and $\lambda = M + \omega$ derived from IRV data are taken as basic variables in numerical integration. By these elements the polynomial's degree of the interpolation can be decreased. The change of x-coordinate axis to Mean Equinox decreases the influence of the error of the predicted UT1-UTC. The usage of up date SLR data can improve the orbit elements of satellites. The order and degree of the Earth's spherical harmonic perturbation are extended to 20 × 20. The solar and lunar coordinates are improved to about 2', that can further improve the solar and lunar perturbations. The light pressure perturbation, the air drag perturbation, and the influences from the coordinate system and the polar motion transformation are also taken into account. The improved satellite prediction procedure would be available to the laser satellite observation at the daylight.

All computation programs are carried out at microcomputer 486/66 in Shanghai Observatory SLR station.

1. The necessary to improve the accuracy and fast computation of low orbit laser satellite prediction

Although the predicted accuracy of low orbit laser satellite prediction higher and higher, it is still very difficult to realize low orbit satellite laser ranging at the daylight. The succeeded echo ratio of SLR is no too high, even at night. One of the reason is that the accuracy of the low orbit laser satellite prediction is limited, at least, because following factors:

1) The error of the predicted values of UT1-UTC, polar motion of the Earth, $F_{10.7}$, K_p et al.

2) The error to compute various perturbations at satellite prediction.

3) The dynamic systematic errors of the tracking telescope of the SLR instrument.

We have investigated the dynamic systematic errors of the tracking telescope of the SLR instrument and detected the dynamic systematic errors of the tracking telescope of the SLR instrument at Shanghai Observatory. It is more urgent to improve the accuracy of the low orbit laser satellite prediction. Because if the precision of the low orbit laser satellite prediction is low, at least, following three situations often occur.

1) It increase the time to research the satellite and labor strength of the observers, and decrease the arc which could be laser range.

2) The regularity of the differences between observed and predicted values time-bias and ranging-bias is no enough good. These values have larger error. If it is used to improve the satellite prediction for following

[1] Project supported by the National Natural Science Foundation of China and the Natural Science Foundation of Guangdong Province.

several passes, it would derive the error of satellite prediction. These values are no sufficiently used.

3) It increased the trouble to separate the signal and noise after satellite laser ranging.

For the laser satellites are launched more and more, the number of the laser satellites moved around the Earth are reached about 20. There are about 40 passes opportunity to SLR. But only microcomputers would be used to most SLR stations. Therefore, it is necessary both to improve the precision and fast computation of low orbit laser satellite prediction.

2. To decrease the influence of the error of the predicted UT1-UTC to the laser satellite prediction

In order to decrease the influence of the error of the predicted UT1-UTC to laser satellite prediction, following rectangular coordinate system is adopted in our software system: the mass-center of the Earth is taken as the origin of the coordinate system; x axis is directed to the Mean Equinox; y axis also is located within the mean equator of the Earth and directed longitude 90° measured eastward from the Mean Equinox; and z axis is directed the Mean North Polar of the Earth. This system is independent with UT1-UTC. Until to predict the satellite before observation, the most new predicted value of the UT1-UTC would be substituted following equation to compute the local sidereal time S of the station, thus, the influence of the error of the predicted value of UT1-UTC to satellite prediction would be decrease to least. Let

$$\begin{aligned} S = {} & 1.7533685592333+(628.33197068884+(0.000000677071394 \\ & -0.000000000045087672343T)T)T+0.000072921158553066t \\ & +(UT1-UTC)+\lambda+(x_p E+y_p D)C/B. \end{aligned} \tag{1}$$

Where, T is the Julian Century Number counted from 1.5 Jun. 2000 to UTC 0^h of the date to compute the satellite positions (36525 days as the time unit); t is the time counted from UTC 0^h of that day (second as the time unit); λ is the geocentric longitude of the station measured eastward from the meridian of Greenwich, x_p and y_p are two components of the polar motion of the Earth, and

$$\begin{aligned} B &= \cos\phi', \\ C &= \sin\phi', \\ D &= \cos\lambda, \\ E &= \sin\lambda. \end{aligned} \tag{2}$$

Where, ϕ' is the geocentric latitude of the station. Therefore, in this coordinate system, the error of the prediction value of UT1-UTC is no any influence upon satellite coordinates, and the influence on the compute the predicted station position would be decrease to least.

3. The computations of various perturbations on the satellites

In many SLR stations, among the computations of various perturbations on the satellites, only lower order and degree of the Earth's spherical harmonic and solar and lunar perturbations by coarse solar and lunar coordinates are computed. To improve the accuracy of predicted positions of the satellite, we computed following various perturbations.

1) The spherical harmonic perturbation of the Earth.

A method researched by us not only overflow in operation no occurs, moreover, even when the order and degree of the Earth's spherical harmonic are extended to 100 × 100 or more, but also the computing speed is higher than those of Cunningham's method and any other existing methods. When the order and degree of the Earth's spherical harmonic are extended to 20 × 20 by us, it is enough to satisfy the prediction to the low orbit laser satellite at the daylight.

2) Solar and lunar perturbations.

The accuracy to compute the solar and lunar coordinates is directly influence computing accuracy of the solar and lunar perturbations. Only microcomputers would be used to the satellite prediction in most stations. Although lunar ephemeris LE200 has high accuracy, but it is very difficult to be used to this kind of microcomputers. If several developments of triangle function is used to computed solar and lunar coordinates, we are afraid that the computed accuracy is no enough. We adopted following method to compute solar and lunar perturbations. Tens terms of developments of triangle function was used to computed solar and lunar coordinates, and the operation of triangular functions are transformed arithmetic operation as possible as. Thus, the operation speed is very high, and the accuracy to compute the solar and lunar coordinates are improve to about 2'. The accuracy to compute the solar and lunar perturbations would be improved.

3) The light pressure perturbation.

4) The air drag perturbation.

The computation of air drag perturbation on the low orbit laser satellite are not considered in many stations. Here not only the computation of air drag perturbation, but also the computation of air drag perturbation on the orbit plane of low orbit laser satellite derived by the rotation of the Earth are computed.

5) The coordinate system perturbation.

6) The polar motion perturbation.

4. The numerical integration

Many people adopted three rectangular coordinates and their three one-order variables as the basic variables to numerical integration. However, considered following factors, we adopt orbit elements as the basic variables.

1) Within same the duration of the period, the variance of the satellite's orbit elements is much slower than the compounds of their coordinates and velocity. If the orbit elements are adopted as basic variables to numerical integration, using lower degree of the polynomial, it can get higher accurate interpolated values during the interpolations. Therefore, it decreases the machine time used to interpolation.

2) Using the values of satellite's coordinate and velocity to numerical integration, if the initial coordinates just is in the most north (or south) of the orbit, the error of the start coordinates would bring bigger error to extrapolated orbit plane of the satellite. In the time, it increases the difficult to SLR at the daylight.

Adopting orbit elements a 、 i 、 Ω 、 $\xi = e \sin \omega$ 、 $\eta = e \cos \omega$ and $\lambda = M + \omega$ as the basic variables to numerical integration, we use 4 degree Runge-Kutta method to numerical integration. It can be satisfy the demand for both to predicted accuracy for satellite laser ranging and to save the machine time at the same time. During numerical integration, further, we adopted the multi-step method and predicted-rectify method.

5. Interpolation

Adopted upper measure, we use 5 degree and 6 terms polynomial to interpolate the orbit elements which accuracy satisfied the demand. Interpolating is one part of a subroutine, and only several lines of the program. It

not has to be programmed to a special software, and decreases the trouble to operation.

6. The fast computation of the visual topocentric coordinate of the satellites

Following all computations are included in our software:

1) The transformation from the equatorial coordinate system of the satellite to the topocentric coordinate system of the station.

2) The computation to correct the rotation of the Earth UT1-UTC and the polar motion.

3) The correction of dynamic systematic errors of the tracking telescope of the SLR.

4) The correction of time delay of SLR system.

5) The satellite mass-center correction.

6) The corrections of azimuth, altitude and ranging derived by the atmosphere refraction, using the data of temperature, pressure et al. of the ground near station.

7) The correction of the satellite's position, using correction time-bias.

8) The primary selecting. To each SLR station, the time would be laser ranging is only tens minutes to every low orbit satellite for one day and night. To decrease the machine time to compute the topocentric coordinate of the satellites which is not have to compute, this software system would automatically select out the time when the satellite just arrives to the highest point of its visual arc. If the satellite's altitude on the ground is still lower the minimum predicted altitude at the time, this software would make that the predicted time will jump to the next time when the satellite just arrives to next the highest point of its visual arc. The stridden time interval may be 1 pass or several passes. Thus, the machine time to compute the visual topocentric coordinate of the satellites which is not have to be decrease minimum.

However, the used formulae are short. The method has be programmed to a software system and it need much less machine time.

7. Data procession and filter

The method of data procession adopted by us is included the filter. Because the data of SLR at daylight is including more noise, the filter method of this software system can separate the signal from the noise which is occupied 90 % of total data.

8. Initial orbit elements

In this software system, the method to determine initial orbit elements has two ways.

1) According the orbit elements which are before 1 month or 1 year, they be extrapolated to given time.

2) According three coordinate components and three velocity components in IRV data which are corresponded given time, the orbit elements a 、 e 、 i 、 M 、 ω and Ω are derived.

9. The orbit improvement

The method for orbit improvement of this software system can derive the corrected values which are any

combination of a 、 e 、 i 、 M 、 ω 、 Ω 、 $\ddot{M}$ and $\dddot{M}$, using SLR data

10. Application

Among the software system, the filter is programmed to a signal software, others are programmed to another software. Used filter software, the signal are separated from the observed data. Later software also has some filter function and has several computed schemes. If the computed schemes need be changed, it is only replace a figure in a datum file. Operating the microcomputer just once, it would carry out all computation, including initial orbit elements, data procession and filter, the computations of various perturbations on the satellites, the numerical integration, the orbit improvement, interpolation and the fast computation of the visual topocentric coordinate of the satellites.

Although the software system would improve the predicted accuracy of laser satellite, the operation speed is very fast. Using microcomputer 486/66 in SLR station Shanghai Observatory, it is only 10 second of machine time to perform 1 day numerical integration for low orbit laser satellite, and much less that 1 second of machine time to other auxiliary computation.

RGO Predictions and Time Bias Functions

Roger Wood

Satellite Laser Ranger Group
Herstmonceux Castle, Hailsham
East Sussex, BN27 1RP, UK

Abstract *The RGO's Space Geodesy Group in Cambridge computes Inter-Range Vectors (IRVs) for 8 satellites widely observed by the SLR network. The SLR Group at Herstmonceux produces time bias functions (TBFs) with respect to the RGC predictions for these satellites; and also for a further 9 satellites with respect to IRVs produced by other groups. IRVs and TBFs are publicly available at the RGO's web site, by anonymous FTP from Cambridge or, on request, by email from Herstmonceux. This paper describes what is available for which satellites, how the data are produced, the frequency with which they are updated and how to access them.*

Introduction

The requirement for good predicted orbits is self-evident. The additional benefits of having the very best estimate of time bias trends with respect to a particular orbit are threefold: ease of satellite acquisition; improved tracking of the satellite without offsetting; and better noise elimination by using a narrow range gate. The RGO group aims to provide high accuracy IRVs which give good predictions for several weeks supplemented by TBFs based on the most recent data and made available to all stations as quickly as possible.

RGO Predictions

Satellites: The satellites treated fall into two groups according to the origin of the basic data for computing orbits:

A Ajisai, Glonass 63, Glonass 67, Starlette, Stella and Topex;

B GPS 35 and GPS 36.

Basic data:

A normal point data from the worldwide SLR network retrieved from the CDDIS data bank;

B broadcast elements from the GPS satellites themselves using the data from the GPS Rogue receiver at Herstmonceux.

Method: For each satellite the basic data for an interval of 2 to 3 weeks are used to generate a precise orbit. This precise orbit is then projected forward for a period of 4 to 6 weeks and used to form daily IRVs.

Updating: New sets of IRVs are formed at roughly monthly intervals or sooner if a satellite such as Topex is manoeuvred or (very rarely) if the time bias trends are not smooth enough to be fitted by simple polynomials.

Filenames: Each filename consists of a 3-character satellite identifier and the date of formation, *e.g.* Stella IRVs produced on 1996 November 7 would be stored in file `ste_9611.07`.

Table 1: *Satellite identifiers for RGO predictions*

`aji` Ajisai	g63 Glonass 63	g67 Glonass 67	gpa GPS 35
gpb GPS 36	`ste` Stella	`str` Starlette	`top` Topex

Special notes for GPS IRVs: Using the broadcast data from the GPS satellites has the twin advantages that data are gathered every day, whatever the weather, and continuously over much longer arcs than are generally observed with SLR.

In addition, Andrew Sinclair has recently been developing techniques to utilise the highly accurate orbits produced each day at AIUB using GPS data from all around the world. Every afternoon the AIUB orbit data are FTPd to Cambridge as soon as they are available, converted to IRVs at 6 hourly intervals (rather than the usual daily intervals) for that day and the two following days, and then deposited in the RGO anonymous FTP account for general use. These IRVs are computed afresh every day and can therefore be used with zero time bias, which is why they do not appear in RGO TBF files. They are expected to provide the best possible IRV predictions for SLR with only minimal changes to existing prediction software. The best solution of all would be to use the GPS XYZ data directly in place of the XYZ generated by the IRV integrator.

Table 2: *Identifiers for RGO predictions based on daily Swiss GPS orbits*

`spa` GPS 35	`spb` GPS 36

RGO Time Bias Functions

Satellites: Adeos, Ajisai, ERS–2, Etalon 1 and 2, GFZ–1, Glonass 63 and 67, GPS 35 and 36, Lageos 1 and 2, No ton, Ralph, Starlette, Stella, Topex.

Basic data: Time biases for individual passes are derived from:

- Herstmonceux observations for all satellites;
- observations from all stations for all satellites retrieved as normal points from CDDIS;
- timebias values supplied from GFZ for ERS–2 and GFZ–1;
- for GFZ–1 only, normal points exchanged *immediately* after each successful pass between a few participating stations.

The time biases are referred to the most recent IRV set for the satellite from ATSC, GFZ, NASDA, RGO or Texas, as appropriate.

Method: For each satellite simple polynomials of first, second and third order in time are fitted through the available data and the one which is judged to give the best extrapolation of future trends is chosen for inclusion in the published file of TBFs.

Updating: TBFs are updated continuously as observations are reduced at Herstmonceux, day and night, and as data from other sources become available. Results are deposited in Cambridge every hour and emailed to anyone who requests them twice a day at 0800 and again at 1700 UT.

Filenames: The format is identical to that described above for IRVs but the prefix `tbf` is used to designate time bias functions *e.g.* `tbf_9611.07`.

Table 3: *Satellite identifiers for RGO Time Bias Functions*

`ade`	Adeos	`aji`	Ajisai	`erb`	ERS–2	`eta`	Etalon 1
`etb`	Etalon 2	`gfa`	GFZ–1	`g63`	Glonass 63	`g67`	Glonass 67
`gpa`	GPS 35	`gpb`	GPS 36	`lga`	Lageos 1	`lgb`	Lageos 2
`nor`	Norton	`ral`	Ralph	`ste`	Stella	`str`	Starlette
`top`	Topex						

Contents: TBF files are designed to give a compact, easy to use, one line per satellite summary of TB information for all current satellites. Each line contains:

- the 3-character identifier for the satellite;
- the starting Modified Julian Date (MJD) for the function, T_0;
- four polynomial coefficients, C_0, C_1, C_2, C_3;
- a code indicating the origin of the IRVs to which the TBs are referred;
- the identifier for the IRV set used.

Thus a typical entry is:

```
AJI 50390.00 61.222458 1.588192 -0.214656 0.000000 RGO AJI037
```

At MJD T, and writing $t = T - T_0$, the timebias in milliseconds is computed from

$$C_0 + C_1 t + C_2 t^2 + C_3 t^3$$

Special notes for GPS TBFs: For GPS 35 and 36 only TBFs are computed for IRVs from ATSC as well as RGO. In order to differentiate between the functions alternative TBF identifiers are, somewhat arbitrarily, assigned.

Table 4: *Identifiers for RGO TBFs using ATSC IRVs*

gqa GPS 35	gqb GPS 36

Access and Distribution

World Wide Web: All IRV and TBF data are available on the Royal Greenwich Observatory's Cambridge web site via the Space Geodesy pages.

Web site address: `http://www.ast.cam.ac.uk/RGO`

Anonymous FTP: All IRV and TBF files are also available from the RGO's Cambridge anonymous FTP account.

Address: `ftp.ast.cam.ac.uk` or `131.111.69.186`

Directory: `/pub/slrirv/current`

Filenames: according to the date of deposit—see above for details.

Email: Anyone who would like to be added to the distribution list and receive twice daily updates to the time bias files by email should contact Roger Wood at the address below.

Contacts:

Roger Wood SLR Herstmonceux
Telephone: +44 (1323) 833888
Internet: `slr@gxvf.rgo.ac.uk`

Graham Appleby RGO Cambridge
Telephone: +44 (1223) 374737
Internet: `gma@ast.cam.ac.uk`

Automatic Ranging Software in Graz

G. Kirchner, F. Koidl
Institute for Space Research / Austrian Academy of Sciences
Observatory Lustbühel; A-8042 GRAZ / AUSTRIA

1.0 Introduction

About 2 years ago, we switched from the old HP1000 computer to a PC control system for all real-time ranging operations and calibrations in Graz; the simple PC (486/66mhz) has some standard interface cards added (GPIB, Digital I/O, Analog IN etc.). For this system, we wrote a complete new tracking / ranging software, and implemented fully automatic return detection/identification within the noise, automatic SemiTrain track identification, automatic range gate setting, automatic tracking optimization etc. Except an initial search phase (which will be implemented later, when we have time available), most passes are tracked, controlled and optimized fully automatically, ensuring maximum number of returns, keeping return energy within desired limits, and allowing our untrained students - after 1 night training - to enjoy their coffee during actual tracking ...

2.0 General Methods

For all real-time programs, we use LAHEY 16-Bit Fortran, which is in general much more suitable for real-time applications than 32-Bit versions; we use 32-Bit Versions for post-processing and data handling programs only.

Both main real-time programs used in Graz (Ranging and Calibration) are written as simple sequential programs, running under DOS (or in any DOS window), with a 10-Hz loop; no multi-tasking environment etc. is used. The programs are extremely structured, and very easy to maintain / improve / change. Although these programs handle all real-time operations, control / program / read all instruments, handle SemiTrain and MultiCounter (up to 4 different counters) procedures, and implements fully automatic tracking features, the source code of each program is only about 6000 lines (about 25% of that are comments!), which gives quite reasonably sized EXE-files of about 250 kB, leaving lot of space for future extensions. We have tested that at the moment even the simple 486-PC (66 Mhz) is still running at a small percentage of its capabilities, again leaving enough spare for the future.

To create a real time scale with sufficient resolution and accuracy, we use one of the available internal counters on the general Analog/Digital I/O Card in the PC slot; the counter is synchronized to and driven by an external 1 kHz derivate of our 10 Mhz standard frequency; this counter can be read by the PC within some µs, giving a real time clock with fast access, with the accuracy of our external time source, and with a 1 ms resolution.

3.0 Return Identification

Operating the SPAD at 10 V above break, it delivers noise rates of 400 to more than 2000 kHz, depending on cooling, day/night conditions etc.; besides limiting our maximum useful range gate to about 500 to 1000 ns, it is difficult to find returns of satellites with low return signals, e.g.

GPS etc, within this noise, without any assistance from the software.

To identify returns within the noise, we assume always a well known time bias for the satellite (due to the necessary small range gate, we HAVE to know it anyway; as it can be changed also in real time, it is easy to identify and set the correct satellite time bias down to sub-ms level); this ideally gives a flat, straight line of residuals. Of course we use all possible ways for accurate time bias predictions: All time bias functions arriving via e-mail (from RGO, GFZ-Potsdam, and now the standardized Time Bias Function File), as well as the automatically stored/updated values of our own last observations.

During tracking, any new residual is compared with the last 100 residuals, taking into account also the fixed SemiTrain distance of 8759 ps; if the new residual coincides with more than 3 previous residuals (we use a 250 ps coincidence limit at the moment), the new residual is identified as a valid return, gets a corresponding flag, is plotted in a different color and produces a special beep for easy acoustic identification.

The necessary calculations are simple (a small subroutine with 25 lines) and extremly fast, because they use only simple comparisons and coincidence number counting.

This method, although quite simple, proved to be much faster - especially in low return rate situations - than any trained observer; it also detects returns under conditions were it would be impossible or at least very difficult for observers (low return rate, high noise etc.); for higher return rates, it identifies valid returns within about 0.5 to 1 s (in our 10 Hz system).

There is - mainly during very noisy daylight sessions - a small probability that some noise points are identified as valid returns; but this probability is below 1% in worst case, and never disturbs any of the following procedures which depend on correctly identified satellite returns.

4.0 SemiTrain Track Number Identification

The last residuals are also used to identify the track number of the SemiTrain to which the new residual belongs; this is done by filling the last residuals of valid returns into bins of SemiTrain width, and identifying the bin with the maximum number of residuals; these residuals are than assigned to track #1 of the SemiTrain; as the SemiTrain distance is known, the correct SemiTrain track number can be assigned now easily to all other residuals, including the new one. The identified, valid residuals of different SemiTrain tracks may be plotted in different colors - according to their SemiTrain track number - on the real-time screen.

In addition, as soon as the track #1 of the SemiTrain is known, it is easy to identify also any pre-train returns (identified returns BEFORE track #1), which are due to small leakage of the Nd:YAG laser pulse selector, and may appear for low satellites with strong return signals (indicating too high received energy). This pre-train identification is used in the AutoTrack routines for immediate offset pointing to keep the return energy within the tolerable range for the SPAD Time Walk Compensation Unit [1] (see below).

5.0 Automatic Range Gate Setting and Shifting

As soon as the first track of the SemiTrain is identified, it is easy to use these residuals to control automatically all range gate parameters: The range gate is shifted so that all returns of track #1 always appear between 50 to 70 ns from range gate begin; this ensures that any influence from range gate setting (ringing etc.) has disappeared safely, while the time between range gate begin and returns is minimized (to minimize noise stops before actual returns). The range gate

width is also reduced automatically to about 200 ns, which allows space for roughly the first 15 tracks of the SemiTrain.

This AutoGate is set ON automatically as soon as the first few returns are identified; this is indicated by changing the range gate bar color on the real-time display (into blue, which is the standard color indicator for all our automatic processes).

The range gate follows any slopes of the residuals, regardless if due to incorrect time bias settings, time bias changes by the operator etc., as long as there are any identified residuals. If there are no identified returns for some time (e.g. due to clouds), the range gate parameters are just kept constant, until new returns are identified again.

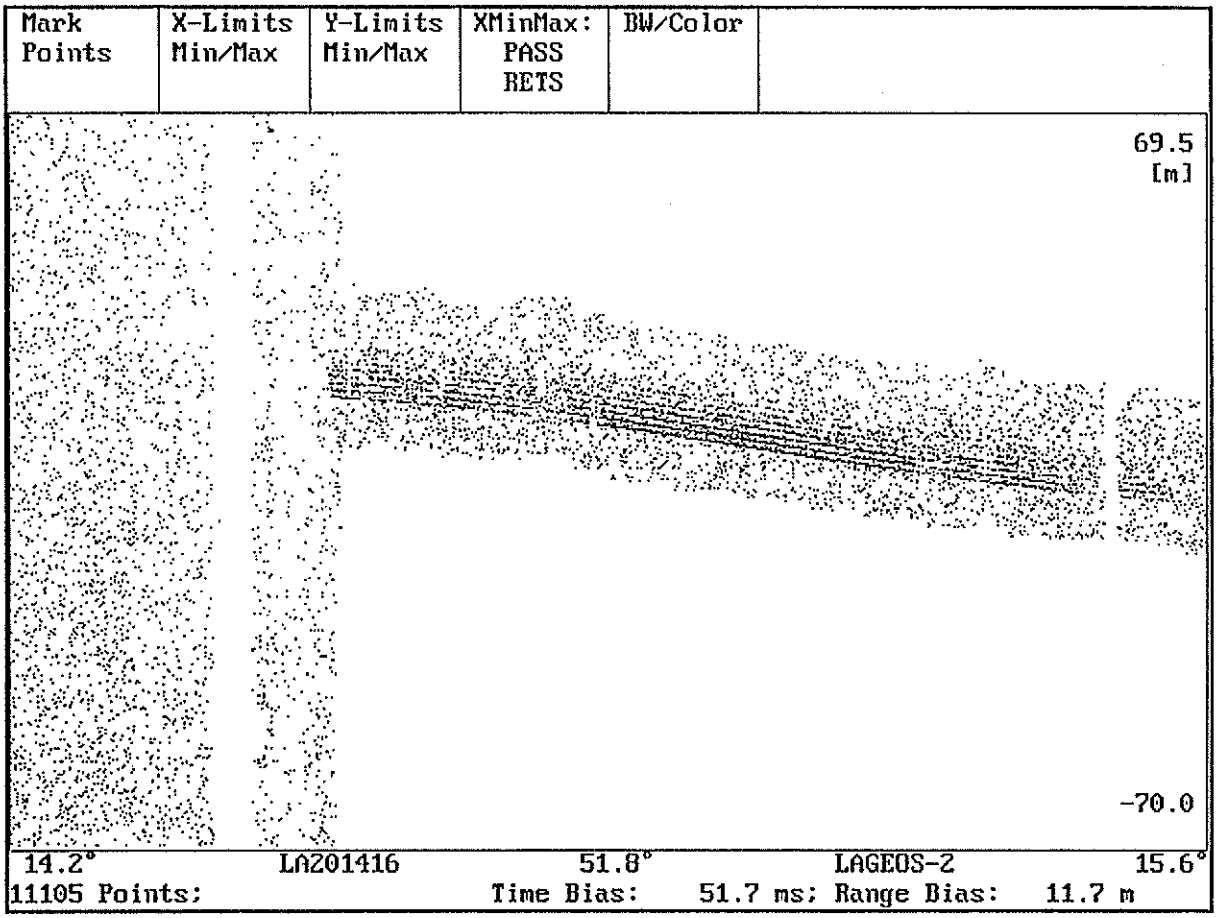

Fig. 1: Lageos-2 Post-Processing: Shows Return AutoDetection, and how AutoGate follows the Identified Residuals

The AutoGate can be switched OFF/ON or overwritten at any time also by manual input of the observers (via keyboard, function keys etc.).

6.0 Automatic Tracking Optimization

6.1 Weighted Return Rate Figure

The AutoTrack routines use these identified return residuals to calculate their own return rate figure, with each identified return weighted according to which SemiTrain track number it is assigned; returns in the first tracks are weighted higher, so that the return rate figure is maximized if as many returns as possible (or all) appear in the first SemiTrain track.

All AutoTrack routines try to maximize this weighted return rate figure; thus the systems optimization goal always is to have one single track only; this is easily reached for all lower satellites, and is achieved for LAGEOS in good weather conditions; but with the few mJ laser in the small Graz station, it will remain a goal for GPS-35 and GPS-36 anyway ...

6.2 Gradient Search for Maximum Return Rate

Usually, any tracking system moves the mount/telescope system according to the predicted satellite orbit; most systems allow the introduction of small offsets (along-track, azimuth/elevation offsets etc.) by operator inputs; the feed-back is usually some type of real-time display showing the returns, their amount, their position etc.

As all this feed-back information is now available to the software, it can be used to optimize any tracking offsets automatically in order to get maximum number of returns. The AutoTrack routines check the identified return rate figure per time unit, and perform a gradient search around the present position, changing slightly all tracking offsets always in those directions where the identified return rate figure increases.

To optimize the search for the various satellites, we assign all satellites to different, random categories according to their tracking requirements. Each category defines its own parameters for the search, like high/low limits for the time span to check for identified returns, high/low limits for azimuth/elevation offset step sizes, high/low limits to stop (no identified returns, or near 100% identified returns) or reassume (sufficient return rate figure again) the gradient search etc. All these parameters are increased or decreased dynamically by the software during actual tracking, according to the actual return rate: Thus the satellite is acquired fast (lower time spans, higher az/el step sizes) at begin, while settling down to optimize slowly and in small steps as soon as return rate figure is approaching higher values.

6.3 Gradient Search: Handling of Various Special Situations

The gradient search is started automatically as soon as there are some returns identified (the same minimum limits are used as for the automatic start of the AutoGate); to indicate this to the observer, the tracking offset indicator on the real time display changes it color into blue.

As soon as the software identifies too many pre-trains (more than the small amount, which is tolerable, indicating a still acceptable return energy for our Time Walk Compensation Circuit [1]), the AutoTrack routines perform immediately a slight offset pointing, increasing the offset until pre-train returns disappear. This ensures that the tolerable return energy levels are not exceeded, independent of - and much faster than - any observer action.

In case of clouds, the return rate figure decreases rapidly, and approaches Zero; this leads quickly to an increase in speed and steps of search in the vicinity, of course now without any success; in such a case, the systems returns to the average offsets of the last identified returns, waiting there for any new identified returns. For low satellites in daylight ranging (where we can observe the clouds with a small, low-cost video camera), the system re-starts already to identify returns (and consequently re-startsAutoGate / AutoTrack), when it is approaching the end or the

edge of the cloud (ranging through thin cloud layers), somewhat before any observer would even start to try getting echoes ...

At the end of each pass (or when the observer exits), all actual parameters, offset values, time bias etc. are stored on disk. If the same pass is re-started, all these actual parameters are used automatically; this ensures fast satellite re-acquisition, allowing efficient switching back and forth between the same passes (interleaved pass ranging). If the next pass of the same satellite is started within 24 hours, some selected parameters (Time Bias etc.) are also used automatically by the system.

As with the AutoGate, also the AutoTrack can be switched ON/OFF by manual observer inputs via keyboard; in addition, when AutoTrack is ON, the observer still has the full set of keyboard commands available for any tracking offsets (most of that is done simply with the keyboard arrow keys), which are just added to the AutoTrack offsets; this allows any desired operator assistance or correction to all AutoTrack features when deired.

7.0 Results and Conclusions

The automatic ranging software, operational in Graz now since almost 2 years - with improvements added according to our experience -, has a lot of advantages:

- It increases significantly the system output, by optimizing all tracking procedures;
- For most satellites, Graz gets the highest data density (returns per Normal Point);
- This is done almost independently of any observer action;
- New observers are able to do the best possible observations after a one-night training;
- Return signal level is kept automatically within required limits;
- The software is easy to change, extremely flexible, and poses no limits on our PC-486/66;
- Any additions can be made easily; e.g. adding or changing counters is done in minutes;
- Future extentions will include automatical initial search (which will use also the - averaged - 'experience' of the last passes, stored on disk), and direct switching from satellite to satellite for interleaved pass ranging (at the moment the telescope goes back to Zero position after each Pass Exit, which takes some additional seconds);
- The only tasks remaining for the observer at the moment are: Rotating the dome, scheduling the passes, starting - if necessary - some initial search, and correcting any Coudé path mispointing by tilting the remotly controlled last Coudé mirror.

With the additions planned, the system should be able to run fully automatically, although unfortunately we will not be allowed to use that really (one person is required always due to aircraft safety regulations).

Reference:

[1] Automatic SPAD Time Walk Compensation. G. Kirchner, F. Koidl; in these Proc.

Data Analysis and Models

Analysis of HTLRS Data at Marine Fiducial Points in Japan

Masayuki Fujita and Arata Sengoku

Hydrographic Department of Japan
5-3-1, Tsukiji, Chuo-ku, Tokyo 104, Japan
e-mail : mfuji@cue.jhd.go.jp

Abstract

The Hydrographic Department of Japan (JHD) has operated a mobile SLR station (HTLRS) since 1988 in the framework of the marine geodetic control project. In 1996, it has completed a first observation cycle at 14 marine fiducial points distributed at major off-lying islands and at some coastal areas in Japan.

The AJISAI data at all the HTLRS sites were analyzed with global data. The used software is GEODYN-II developed by NASA. The reference fixed stations are GSFC (Maryland, USA) and Haleakala (Hawaii, USA), for which the coordinates of the ITRF93 with its velocity field are adopted as a priori values. The rms of the resulted range residuals for the HTLRS data are 5-10cm, which is comparable to those of all the global stations.

The stability of the solutions for the baseline vectors between the HTLRS sites and Simosato, the stationary SLR station in central Japan, was examined by comparing the solution with those obtained under different estimation conditions. As a result, followings are concluded; (1) the estimated baseline vector can be determined within 1cm as far as the coordinates of both the HTLRS sites and Simosato remain as estimated parameters; (2) it can be well determined by a single arc analysis; (3) it can be determined within 1cm when the frequencies of estimations of the empirical acceleration and the drag coefficient are less than 3 days; (4) the estimation does not depend on the frequency of estimation of the solar radiation pressure coefficient; (5) the estimation does not depend on the selection of the atmospheric density model if the drag coefficient is appropriately estimated.

1. Introduction

The Hydrographic Department of Japan has been carrying out Satellite Laser Ranging (SLR) observations aiming at establishing the marine geodetic control network in Japan. In this project, a stationary observation by a fixed type laser ranging station has been continued at Simosato Hydrographic Observatory in Wakayama Prefecture, central Japan, since 1982, while a mobile type station, called HTLRS, has been operated at marine fiducial points since 1988, where 2-3 months campaign observations have been made.

The HTLRS sites were set at 14 sites located in major off-lying islands and some coastal areas as a backbone of the marine geodetic control network. It has completed its first round at all 14 fiducial points with Tyosi in 1996. A significant amount of ranging data of AJISAI were obtained for all the sites, whereas there were limited data acquired for LAGEOS-1,2 etc. at limited sites. The project for second round observations at some of these points has just started in order to monitor the variation of baseline from Simosato.

In this study, we demonstrate the result of analysis for all 14 HTLRS sites by using the software GEODYN-II developed by NASA and discuss the precision of baseline estimation between the HTLRS sites and Simosato.

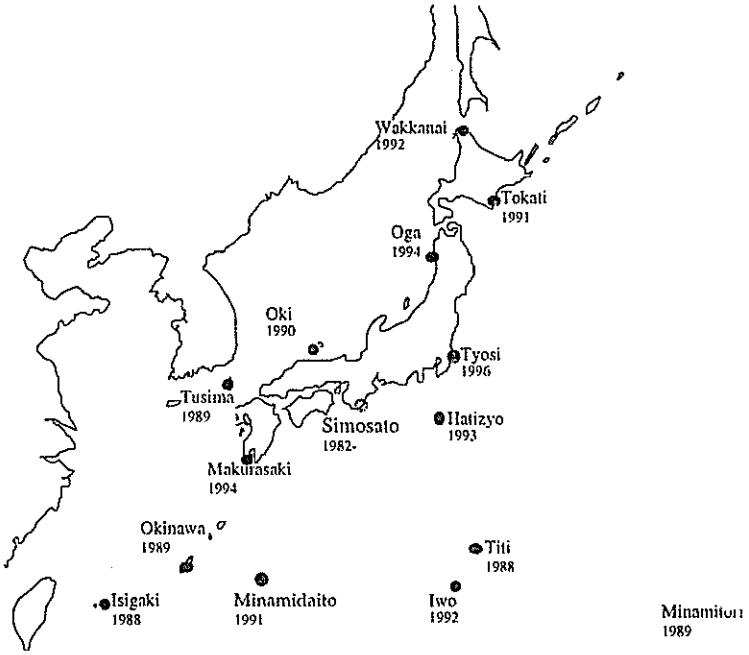

Figure 1. Map showing HTLRS sites

2. Data and analysis

Figure 1 shows the distribution of observation sites for Simosato and the HTLRS sites. The baseline lengths between Simosato and the HTLRS sites are about 360km for Hatizyo at the shortest and about 2020km for Minamitori at the longest.

Used data are global normal points of AJISAI. Table 1 lists the observation period and the number of passes at the HTLRS sites and Simosato. It also gives the abbreviation for each HTLRS site appearing in the later figures.

The software used for these analyses is GEODYN-II (Eddy et al., 1986). A single arc method, in which initial elements of the satellite are solved once at the start epoch, was applied to the analysis. As parameters as to non-gravitational forces on the satellite, we estimated 3-day atmospheric coefficient, 3-day once-per-revolution empirical accelerations in the cross-track and radial components, and 30-day radiation pressure coefficient.

An applied gravitational potential model is the JGM2 (Nerem et al., 1994) and atmospheric density model is MSIS86 (Hedin, 1987). Earth rotation parameters are fixed to the final values

Table 1. Data summary

Site name	(Abbrev.)	Start epoch (yymmdd. 0)	End epoch (yymmdd. 0)	Number of passes HTLRS	Simo
Titi	(TT)	880121	880228	34	98
Isigaki	(IS)	880724	880903	27	28
Minamitori	(MT)	890115	890317	41	49
Okinawa	(ON)	890709	890820	44	43
Tusima	(TS)	891007	891118	50	40
Oki	(OK)	900917	901024	27	26
Minamidaito	(MD)	910113	910204	12	39
Tokati	(TK)	910826	911025	21	54
Iwo	(IW)	920122	920314	25	35
Wakkanai	(WK)	920907	921013	24	26
Hatizyo	(HT)	930203	930311	19	75
Makurasaki	(MK)	940128	940311	11	58
Oga	(OG)	940814	940921	18	60
Tyosi	(TY)	960110	960307	62	80

appearing on IERS Bulletine B. An anisotropic reflection model (Sengoku, 1995) is applied.

The reference stations whose coordinates are fixed are Maryland(NASA/GSFC) and Hawaii(Haleakala Observatory). Applied coordinates as fixed values are ITRF93 with its velocity field (Boucher et al., 1994). Since the ITRF93 coordinates are given at the epoch 1993.0, the station positions are moved to the observation epoch by use of the velocity field.

A priori data sigmas given are 10cm for all stations, which implies that there is no weight difference between the stations.

3. Result

Table 2 shows estimated rectangular coordinates of the HTLRS sites together with their formal errors and residual rms' for the HTLRS sites and all the global stations. Table 3 shows 3 components of baseline vectors between Simosato and the HTLRS sites and baseline lengths with their formal errors. These values are evaluated at the start epoch of each observation.

Residual rms' of the HTLRS data are 5-10cm, which are comparable to those of all the global data. No correlation was found between observation periods and the resulted residuals. The formal errors for the HTLRS coordinates are 2-4cm.

Table 2. Estimated rectangular coordinates of HTLRS sites. Unit is in m.

Site	X		Y		Z		Residual RMS HTLRS	Residual RMS all
TT	-4491072.311	0.020	3481527.911	0.022	2887392.004	0.020	0.046	0.066
IS	-3265753.798	0.021	4810000.840	0.020	2614265.635	0.020	0.052	0.058
MT	-5227190.039	0.018	2551882.337	0.023	2607609.849	0.017	0.120	0.148
ON	-3505323.669	0.019	4532740.991	0.018	2792253.157	0.017	0.076	0.094
TS	-3344473.916	0.016	4087076.263	0.016	3564512.521	0.015	0.106	0.122
OK	-3536204.424	0.019	3749974.186	0.025	3744418.415	0.016	0.052	0.062
MD	-3786331.517	0.024	4320316.193	0.023	2761964.083	0.025	0.052	0.062
TK	-3788457.912	0.014	2820917.951	0.014	4271798.281	0.014	0.090	0.088
IW	-4522801.801	0.012	3622640.405	0.013	2656232.056	0.012	0.092	0.106
WK	-3522929.119	0.010	2779243.479	0.012	4517637.339	0.012	0.086	0.074
HT	-4087880.318	0.017	3451764.241	0.015	3460902.383	0.013	0.048	0.058
MK	-3528449.724	0.026	4162495.219	0.020	3291166.953	0.022	0.080	0.058
OG	-3731492.594	0.018	3164405.340	0.017	4078228.570	0.014	0.054	0.054
TY	-4021278.003	0.014	3273585.521	0.015	3701666.336	0.012	0.072	0.060

Table 3. Estimated baseline vectors and lengths between HTLRS sites and Simosato. Unit is in m.

Site	dx		dy		dz		Baseline	
TT	-668684.107	0.024	-217835.704	0.025	-620181.329	0.024	937665.031	0.024
IS	556634.604	0.025	1110637.339	0.025	-893307.650	0.023	1530148.993	0.025
MT	-1404801.736	0.021	-1147481.190	0.022	-899963.364	0.020	2024874.084	0.021
ON	317064.645	0.019	833377.421	0.019	-715320.022	0.018	1143123.199	0.019
TS	477914.434	0.018	387712.729	0.018	56939.226	0.017	618033.528	0.018
OK	286183.853	0.023	50610.564	0.027	236845.192	0.017	374911.019	0.022
MD	36056.891	0.024	620952.630	0.022	-745609.074	0.025	970986.694	0.028
TK	33930.497	0.015	-878445.590	0.016	764225.078	0.014	1164842.437	0.017
IW	-700413.429	0.013	-76723.168	0.014	-851341.157	0.012	1105100.530	0.014
WK	299459.315	0.014	-920120.075	0.016	1010064.141	0.014	1398758.880	0.018
HT	-265491.958	0.017	-247599.336	0.015	-46670.814	0.013	366018.545	0.017
MK	293938.656	0.027	463131.639	0.021	-216406.249	0.022	589680.010	0.019
OG	90895.741	0.020	-534958.250	0.018	570655.396	0.015	787457.901	0.019
TY	-198889.697	0.016	-425778.026	0.016	194093.246	0.015	508444.911	0.016

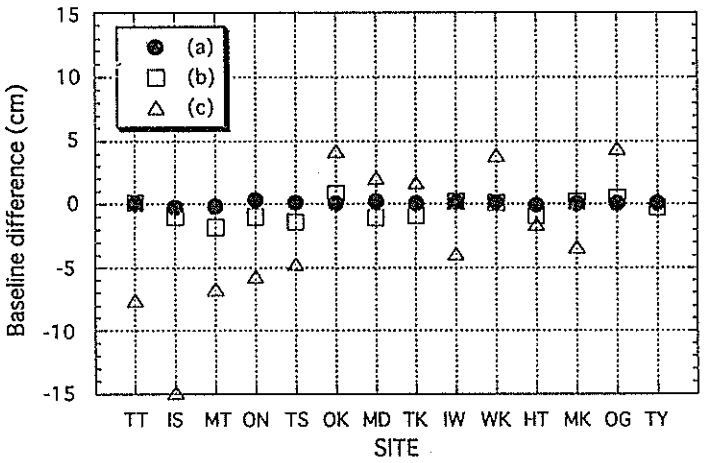

Figure 2. Comparison of estimated baseline lengths between Simosato and the HTLRS sites for the different fixed stations. Plotted are the baseline differences from the reference case.

4. Stability examinations

In the following, we examine the stability of the solutions by comparing with those obtained under different estimation conditions.

A. Different fixed stations

First, we examine differences of estimated baseline solutions depending on the different combination of fixed stations for all the HTLRS sites.

In the above analysis, we selected Maryland and Hawaii as fixed stations (reference case). Here we change the combination of fixed stations for the following 3 cases:

(a) Maryland (GSFC) and Greenwich (RGO),
(b) All but HTLRS sites and Simosato,
(c) All but HTLRS sites.

Figure 2 shows the differences of estimated baseline lengths from those obtained for the reference case. The agreement is especially good for (a) and the difference does not exceed 1-2mm. As clearly shown from these comparison, the baseline estimation is significantly affected by whether Simosato is estimated or not, but not affected so much by whether other global stations are estimated or not.

B. Estimation frequency of arc parameters

Next, we examine the variation of estimated baseline vectors due to the estimation frequency of arc parameters, such as satellite elements and non-gravitational force parameters, for Titi sima and Tyosi results.

Table 4 shows the comparison of the estimated results between single and multi arc (every 3 days) analyses. The values are fractional parts of the estimated baseline vectors and lengths. This shows that the differences between these two conditions are insignificant.

Figure 3 shows the variation of estimated baseline lengths against the frequency of estimation of non-gravitational force parameters, plotted as a difference from the most frequent case for each parameter. As seen from the figure, the differences are within 1cm when the general

Table 4. Comparison between estimated baseline vectors for single and every 3-day arc for Titi and Tyosi. Unit is in m.

Condition		dx	dy	dz	Baseline	Residual	
						HTLRS	ALL
Tit	single*	0.107	0.704	0.329	0.031	0.046	0.066
	3-day	0.110	0.692	0.348	0.042	0.030	0.054
Tyo	single*	0.697	0.026	0.246	0.911	0.072	0.060
	3-day	0.682	0.025	0.253	0.906	0.070	0.060

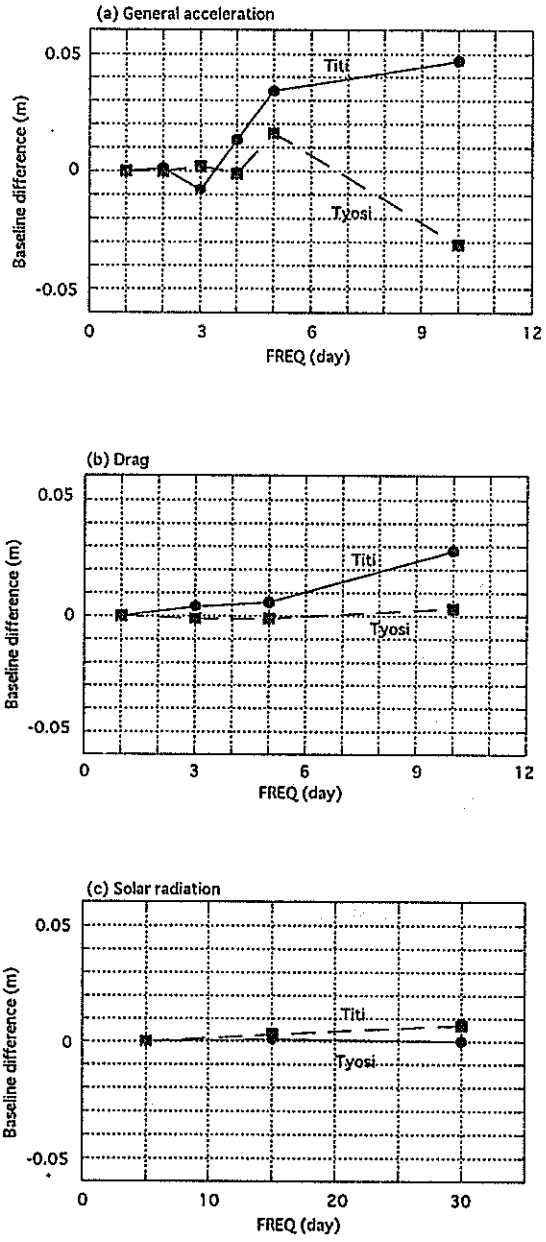

Figure 3. Variation of estimated baseline lengths against the frequency of estimation of non-gravitational force parameters for Titi and Tyosi: (a) general acceleration; (b) drag coefficient; (c) solar radiation pressure coefficient.

Table 5. Comparison between estimated baseline vectors for different atmospheric density models for Titi and Tyosi. Unit is in m.

Condition		dx	dy	dz	Baseline	Residual	
						HTLRS	ALL
Tit	MSIS*	0.107	0.704	0.329	0.031	0.046	0.066
	DTM	0.108	0.696	0.333	0.032	0.042	0.064
	JAC	0.102	0.684	0.336	0.027	0.044	0.066
Tyo	MSIS*	0.697	0.026	0.246	0.911	0.072	0.060
	DTM	0.697	0.026	0.247	0.911	0.072	0.060
	JAC	0.698	0.026	0.246	0.911	0.072	0.060

difference depending on the estimation frequency of the solar radiation pressure coefficient is quite insignificant.

C. Atmospheric density model

Finally, we compare the results for different atmospheric density models: MSIS86, DTM (Barlier et al., 1978), Jacchia71 (Jacchia, 1971). Table 5 shows the comparison of the results from these 3 models in the same way as Table 4. The table shows that the difference between the results for these 3 models is quite insignificant.

5. Conclusions

We analysed AJISAI data at all the HTLRS sites with global data. The rms of the resulted range residuals for the HTLRS data are 5-10cm, which is comparable to those of all the global stations.

The stability of the solutions for the baseline vectors between the HTLRS sites and Simosato was examined by comparing the solution with those obtained under different estimation conditions. As a result, followings are concluded;

(1) the estimated baseline vector can be determined within 1cm as far as the coordinates of both the HTLRS sites and Simosato remain as estimated parameters,
(2) it can be well determined by a single arc analysis,
(3) it can be determined within 1cm when the frequencies of estimations of the empirical acceleration and the drag coefficient are less than 3 days
(4) the estimation does not depend on the frequency of estimation of the solar radiation pressure coefficient,
(5) the estimation does not depend on the selection of the atmospheric density model if the drag coefficient is appropriately estimated.

References

Barlier, F., Berger, C., Falin, J., Kockarts, G., Thuillier, G.: Atmospheric Model Based on Satellite Drag Data, *Ann. Geophys.*, **34**, 9-24, (1978).

Boucher, C., Altamimi, Z., Duhem, L. : Results ans Analysis of the ITRF93, IERS TECHNICAL NOTE, **18**, (1994).

Eddy, W.F., McCarthy, J.J., Pavlis, D.E., Marshall, J.A., Luthke, S.B., Tsaoussi, L.S., Leung, G., Williams, D.A. : GEODYN-II System Operations Manual, Vol.1-5, *Contractor Report, ST Syst.Corp., Lanham, Md.*, (1990)

Hedin, A.E., MSIS-86 Thermospheric Model, *J.Geophys.Res.*, **92**, 4649-4662, (1987).

Jacchia, L.G., Revised Static Models of the Thermosphere and Exosphere with Empirical Temperature Profiles, *Special Report 332, smithsonian Institution Astrophysical Observatory (SAO), Cambridge, MA*, (1971).

Nerem, R.S., Lerch, F.J., Marshall, J.A., Pavlis, E.C., Putmey, B.H., Tapley, B.D., Eanes, R.J.,

Nerem, R.S., Lerch, F.J., Marshall, J.A., Pavlis, E.C., Putmey, B.H., Tapley, B.D., Eanes, R.J., Ries, J.C., Schutz, B.E., Shum, C.K., Watkins, M.M., Klosko, S.M., Chan, J.C., Luthcke, S.B., Patel, G.B., Pavlis, N.K., Williamson, R.G., Rapp, R.H., Biancale, R., Nouel, F.: Gravity Model Development for TOPEX/POSEIDON: Joint Gravity Models 1 and 2, *J.Geophys.Res.*, **99**, 24421-24447, (1994).

Sengoku, A., Cheng, M.K., Schutz, B.E.: Anisotropic Reflection Effect on Satellite, Ajisai, *Jour. Geod.*, **70**, 140-145, (1995).

NEW MAPPING FUNCTION OF THE TROPOSPHERIC REFRACTION IN SLR

Haojian YAN and Chugang FENG

Shanghai Observatory, 200030 Shanghai, P.R. China

Electronic Mail: yhj@center.shao.ac.cn

Abstract. Based on the generator function method proposed by Yan & Ping (1995), the mapping function of refractive delay at optical frequencies has been introduced in this paper. The improved frequency-related mapping function, associated with the effect of wavelength on the zenith delay, has theoretically achieved an accuracy better than $0.3cm$ at 5^o elevation for wide ground meteorological conditions and keeps convergent at an elevation angle near to horizon. Some related correction terms are also considered for high accurate laser ranging measurements at low elevation observations. The purpose of this research is mainly aimed to the low elevation objects and polychrome laser techniques in the future.

Key words: SLR - Tropospheric Refraction

1 Introduction

The accuracy of the Satellite Laser Range (SLR) has been greatly improved from decimeters to about one centimeter or better in recent decades. The correction formula of the tropospheric refraction nowadays hired in SLR has been used for more than twenty years since it was deduced by Marini and Murray (1973), meanwhile the change of the tropospheric refraction expression in Very Long Baseline Interferometry (VLBI) was made from Chao's (1970) to CfA2.2 (Davis et al. 1985) or those of Herring (1992). Recent developments of space techniques have led to a situation of that their main errors are in some extent related to the influence of atmospheric refraction. In the case of VLBI or GPS (Global Positioning System) measurement differencing, the signals received at two separated stations are differentiated. But SLR is used to precisely and directly measure the distance from a receiver point on the Earth to satellite on orbit. The laser beams suffer the effects of refraction and scattering when through atmosphere near the Earth. Atmospheric refraction increases the optical path length, which is considered as the direct results of radio wave distance measurement, by a magnitude of about two to decades meters that depends mainly on the elevation of observation. It was proved both practically and theoretically that Marini-Murray formula keeps the accuracy about centimeters at elevation above 10^o, and the accuracies become worse seriously when the elevations are down below 10^o. Developing a formula of SLR refraction correction below 10^o might have a potential interest in future development of space techniques.

If the accuracy of millimeters is considered, some corrections, which are neglected in the nowadays used formula, may become significant especially for lower height spacecrafts at low elevation. The dispersive characteristic of optical signal of SLR is the first factor to be considered in the improved continued fraction mapping function proposed by Yan & Ping (1995).

The extra correction terms involve the influencies coming from the height and latitude of site, the height of spacecraft.

2 Atmospheric Refraction Correction

The tropospheric refractive delay $\Delta\sigma$ of the optical signal through atmosphere is defined as the difference between the optical and geometric distances from laser site P to satellite S:

$$\Delta\sigma = \int_P^S n_g d\ell - \int_P^S dx \ , \tag{1}$$

where ℓ is the path of signal and x the straight line connecting site and satellite, n_g is the group refractive index of atmosphere which has relation with the group refractivity N_g (Marini & Murray 1973; Gardner & Rowlett 1976):

$$10^6(n_g - 1) = N_g = 82.4148 f(\lambda)\frac{P}{T} - 11.268\frac{e}{T} \ , \tag{2}$$

in which λ is the wavelength of radiation in microns, P is the total atmospheric pressure in millibars, T is the temperature in Kelvin, e is the partial pressure of water vapor in millibars, and:

$$f(\lambda) = 0.94075 + \frac{0.01598}{\lambda^2} + \frac{0.0002224}{\lambda^4} \ , \tag{3}$$

here for YAG laser with the relation

$$f(0.5320) = 1 \ .$$

3 Expressions of Refractive Delay

The tropospheric delay $\Delta\sigma$ is written as (Yan & Ping 1995):

$$\Delta\sigma = \Delta\sigma_z \cdot m \ , \tag{4}$$

where $\Delta\sigma_z$ is the zenith delay and m is defined the mapping function. Using the perfect gas law, the law of partial pressure, and the hydrostatic equation, it is not difficult to write the zenith delay as:

$$\begin{aligned} \Delta\sigma_z &= \Delta\sigma_z^{YAG} f(\lambda) \\ &= \frac{f(\lambda)}{W(\phi,h_0)}(0.0024178 P_0 + 0.00014586 e_0) \ , \end{aligned} \tag{5}$$

in which P_0 is the atmospheric pressure in millibars taken at the laser site, e_0 is the water vapor partial pressure in millibars at the laser site, h_0 is the elevation of the station in kilometers, ϕ is the latitude of station. The term

$$W(\phi, h_0) = 1 - 0.00266\cos 2\phi - 0.00028 h_0 \tag{6}$$

is the correction of the zenith delay related to the latitude and height of the station (Saastamoinen 1972).

The water vapor partial pressure e_0 can be calculated from the relative humidity R_h (in percent) by Magnus experimental formula

$$e = \frac{R_h}{100}(6.11)10^{\frac{7.5(T-273.15)}{237.3+(T-273.15)}} . \tag{7}$$

In research of refraction correction, the mapping function has gotten more attention than the zenith delay. The expression of the mapping function nowadays adopted in laser ranging techniques was based on expansion of integrand in atmospheric refraction integral (Marini & Murray 1973). It was proved that the formula obtained by expansion method of integrand could not be available for observation elevation lower than 10^o even if troublesome correction terms were included. The quadratic atmospheric profile hired in Marini & Murray formula could introduce some error in the mapping function. From the generator function theory of atmospheric refraction integration, a new continued fraction form of the mapping function was proposed, which was deduced from the expansion of the complementary error function (Yan & Ping 1995). This form of the mapping function can get higher accuracy and wider elevation coverage than those previous used. We take the atmospheric pressure, temperature and humidity as the required meteorological parameters in our presentation. Some other geophysical and meteorological parameters are usually not available in normal SLR observation data and so as to be taken constants: the tropospheric temperature lapse rate $\beta = -6.^o5K\ km^{-1}$, the height of the tropopause $h_t = 11.132km$. Another important fact in laser techniques is the dispersion of air at optical frequencies, a frequency-relative mapping function is therefore appropriate for SLR technique.

The new mapping function is then generally written as:

$$m(E_0) = \cfrac{1}{\sin E_0 + \cfrac{D_1}{l^2 \csc E_0 + \cfrac{D_2}{\sin E_0 + \cfrac{D_3}{l^2 \csc E_0 + D_4}}}} , \tag{8}$$

in which

$$E_0 = 90^o - \xi_0$$

is defined the *proper elevation* of observation which is coincident with the true elevation for an object at infinity, r_0 is the radius of the Earth, and the effective height of atmosphere H can be written as a vertical integral of the refractivity N:

$$H = \frac{1}{N_{g0}} \int_{h_0}^{\infty} N_g(h)\, dh , \tag{9}$$

where N_{g0} is the value of the refractive obtained on the ground, and the parameter

$$l = \sqrt{\frac{r_0}{2H}} \tan E_0 \tag{10}$$

is named the *normalized effective zenith argument*.

If the standard atmosphere model (Davis et al. 1985) is used, which is proved nearer to the true atmosphere (Allen 1973) than the quadratic profile used by Marini & Murray (1973), the coefficients D_i in Eq.(8) are listed:

$$
\begin{aligned}
D_1 &= 0.463184 + 3.019 \times 10^{-5}(P_o - 1013.25) \\
&\quad -1.222 \times 10^{-4}(T_o - 15) + 1.1 \times 10^{-6}(T_o - 15)^2 \\
&\quad -9.122 \times 10^{-3}(\lambda - 0.532) + 2.74 \times 10^{-2}(\lambda - 0.532)^2 \\
\\
D_2 &= 0.828752 + 1.905 \times 10^{-5}(P_o - 1013.25) \\
&\quad +5.203 \times 10^{-4}(T_o - 15) + 0.6 \times 10^{-6}(T_o - 15)^2 \\
&\quad -5.887 \times 10^{-3}(\lambda - 0.532) + 1.82 \times 10^{-2}(\lambda - 0.532)^2 \\
\\
D_3 &= 2.53662 + 0.9095 \times 10^{-4}(P_o - 1013.25) \\
&\quad +3.869 \times 10^{-3}(T_o - 15) + 0.3 \times 10^{-6}(T_o - 15)^2 \\
&\quad -2.787 \times 10^{-2}(\lambda - 0.532) + 8.76 \times 10^{-2}(\lambda - 0.532)^2 \\
\\
D_4 &= 47.1584 + 1.377 \times 10^{-3}(P_o - 1013.25) \\
&\quad -3.584 \times 10^{-2}(T_o - 15) + 1.1 \times 10^{-4}(T_o - 15)^2 \\
&\quad -4.291 \times 10^{-1}(\lambda - 0.532) + 1.34 \times (\lambda - 0.532)^2 \ ,
\end{aligned}
\tag{11}
$$

in which P_o in millibars, e_o in millibars, and T_o in Celsius are the corresponding values on ground, λ the wavelength in micron. Because the permanent dipole term of the refractivity is no longer significant in optical wavelength, the influences of the wet partial on the coefficients D_i of the mapping function have been greatly weakened and we can ignore their influences in above expression only introducing a negligible error to our results.

In comparison with the integrals along the path of signals the theoretical accuracy of the new model is proved better than $0.1cm$ above 10^o elevation and $0.3cm$ above 5^o elevation for wide meteorological conditions.

4 Correction of Finite Distance Object

In Fig.1, $\vec{SP}$ is the direction pointed from satellite S to observer P, $\vec{SQ}$ is the direction along the tangent to the light trajectory of the path of signal between S and P, and Q is the intersection point with the vertical Z-axis, which is named the *equivalent point* of observation. We call $\vec{QS}$ the *proper direction*, and $\vec{PS}$ the *true direction* which can accurately calculated from satellite ephemeris and the geophysical parameters. We can further define ξ_0 the *proper zenith distance*, and $\angle ZPS$ the *true zenith distance*, respectively. From above sections, it is found that the angular argument in the mapping function is physically the proper zenith distance. Only for the observation of an infinite object, the proper direction coincides with the true direction. If the heights of the satellites with laser reflectors cover from several hundreds to thousand kilometers, it might be reasonable to consider a distance correction for lower height satellites (Marini 1972), which comes from the difference between the true and the proper zenith distances.

For a spherically symmetrical atmospheric model Snell's law holds (Woolard and Clemence 1966):

$$
n \cdot r \cdot \sin z = n_0 \cdot r_0 \cdot \sin z_0 = r_s \sin z_s \ , \tag{12}
$$

where r is the geocentric distance, z the arrival zenith taken on the path of light, r_0 and z_0 are the corresponding values taken at station, r_s and z_s the values at the field point taken on the orbit of satellite, and here it is assumed that

$$n(r_s) = 1 \ .$$

From Eq.(12), see Fig.1, the *equivalent height* QP (Murray 1973) or the *vertical proper displacement of the atmospheric refraction* (simply called the *proper displacement*) for the observer at P is obtained (Yan et al. 1992); (Yan, 1996):

$$QP = \left(\frac{n_0 \sin z_0}{\sin \xi_0} - 1 \right) r_0 \ . \tag{13}$$

The angle between the proper direction and the true direction $\Delta\theta$ is readily represented by:

$$\Delta\theta = \frac{QP \sin \xi_0}{x} = \frac{r_0}{x}(n_0 \sin z_0 - \sin z_0 - \cos z_0 \ \Delta z_0) \ . \tag{14}$$

In above equation, the astronomical refraction for a finite distance object Δz_0 is further related to the proper zenith distance ξ_0 and the mapping function of the astronomical refraction m^* (Yan & Ping 1995):

$$\Delta z_0 = 10^{-6} N_{g0} \sin \xi_0 m^*(\xi_0) \ , \tag{15}$$

where m^* can also be formulated by an improved continued fraction form:

$$m^*(\xi_0) = \cfrac{1}{\cos \xi_0 + \cfrac{0.578710}{I^2 \sec \xi_0 + \cfrac{1.30248}{\cos \xi_0 + \cfrac{13.2497}{I^2 \sec \xi_0 + 173.423}}}} \ . \tag{16}$$

In order to get an accurate proper zenith distance ξ_0, an iteration algorithm can be used. Then the proper zenith distance is readily obtained by Fig.1

$$\xi_0 = (90^o - E) + \Delta\theta \ , \tag{17}$$

here the true elevation E of object can be accurately calculated from the ephemeris and the geophysical parameters.

5 Discussion

The numerical comparisons between the tropospheric delays of the model presented in this paper and that of (Marini & Murray 1973) have been made. Fig.2 gives the differences between these two model for different meteorological conditions.

After summerizing above sections we have following conclusions:

a. The atmospheric profile of SLR refraction correction used in our model has been renewed from the quadratic refractivity (Marini & Murray 1973; Gardner & Rowlett 1976) to the standard model (Allen 1973; Davis et al. 1985).

b. The generator function method of atmospheric refractive integral (Yan and Ping 1995) and the improved continued fraction form of the mapping function is applied to facility at optical

frequency in this paper. In such a way we offer a possibility to calculate the refraction correction of SLR observations with high accuracy at elevations of few degrees. The new mapping function has an unit when the observation is made in the zenith direction. The simulative computation results show the fact that Marini-Murray's formulas have several millimeters discrepancies above 10^o elevation and becomes worse very rapidly when the elevation is keeping decreasing.

c. The angle argument in our mapping function is related to the proper elevation of observation for a finite distance object. The object distance correction of the mapping function is represented as the difference between the proper and the true elevations of object. This term might be considerable for satellites with height of several hundreds kilometers or less and to be observed at lower elevation angles. Fig.3 shows the range corrections of the objects with the heights of $960km$, $425km$ and $5900km$, respectively.

d. At optical frequencies, the operation frequency is most important factor in the parameters of the mapping function. Fig.4 represents the influences of laser beam frequency on the mapping function. This term will be of interest in multi-frequencies observation consideration of laser ranging.

References

Allen, C.W. 1973: *Astrophysical Quantities*, 3d ed., The Athlone Press, Chap.6, 114-120.

Chao, C.C., 1970: A preliminary estimation of tropospheric influence on the range and range rate data during the closest approach of the MM71 Mars Mission. *JPL Tech. Memo 391-129.*

Davis, J.L., T.A. Herring, I.I. Shapiro, A.E.E. Rogers and G. Elgered, 1985: Geodesy by radio interferometry: effects of atmospheric modeling errors on estimates of baseline length. *Radio Science,* **20**, 1593-1607.

Gardner, C.S. and J.R. Rowlett, 1976: Atmospheric refraction errors in laser ranging system. *RRL Pub. No.477,* University Illinois, Urbana, Illinois.

Herring, T.A.; 1992. Modeling Atmospheric Delay in the Analysis of Space Geodetic Data, in "Refraction of Transatmospheric Signals in Geodesy", Proc. of the Symp. Hague, May 19-22, Netherlands Geodetic Commission Publications on Geodesy, New Series No36.

Marini, J.W., 1972: Correction of satellite tracking data for an arbitrary tropospheric profile. *Radio Science,* **7**, 223-231.

Marini, J.W. and C.W. Murray, 1973: Correction of laser range tracking data for atmospheric refraction at elevation above 10 degrees. *NASA Tech. Rep. X-591-73-351.*

Murray, C.A., 1983: *Vectorial Astrometry*, Adam Hilger Ltd, Chap.7.

Owens, J.C., 1967: Optical refractive index of air: dependence on pressure, temperature and composition. *Appl. Opt.,* 6, 51-58.

Saastamoinen, J., 1972a, 1972b, 1973: contributions to the theory of atmospheric refraction. *Bull. Geod.,* **V105-107**, 279-298, 383-397, 13-34.

Woolard, E.W. and G.M. Clemence, 1966: *Spherical Astronomy*, Academic Press, Landon and New York, Chap.5.

Yan, H.J., K. Sauermann and E. Groten, 1992: The ray bending corrections in tropospheric refraction. in *"6th International Geodetic Symposium on Satellite Positioning"*, March 17-20, 1992, The Ohio State University, Columbus, Vol.1, 291-301.

Yan, H.J. and J.S. Ping, 1995: The generator function method of the tropospheric refraction corrections. *A.J.* 110, 934-939.

Yan, H.J., 1996: A new expression for astronomical refraction, A.J. 112, 1312-1316.

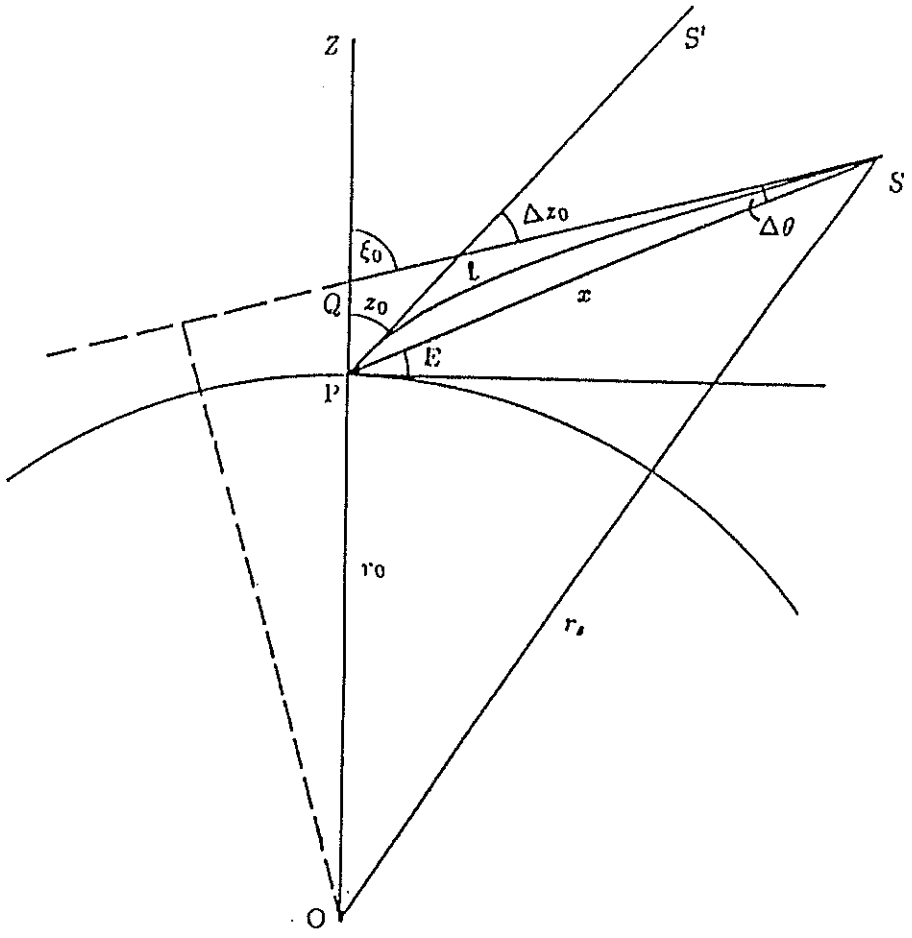

Fig.1 Geometry of a finite distance object

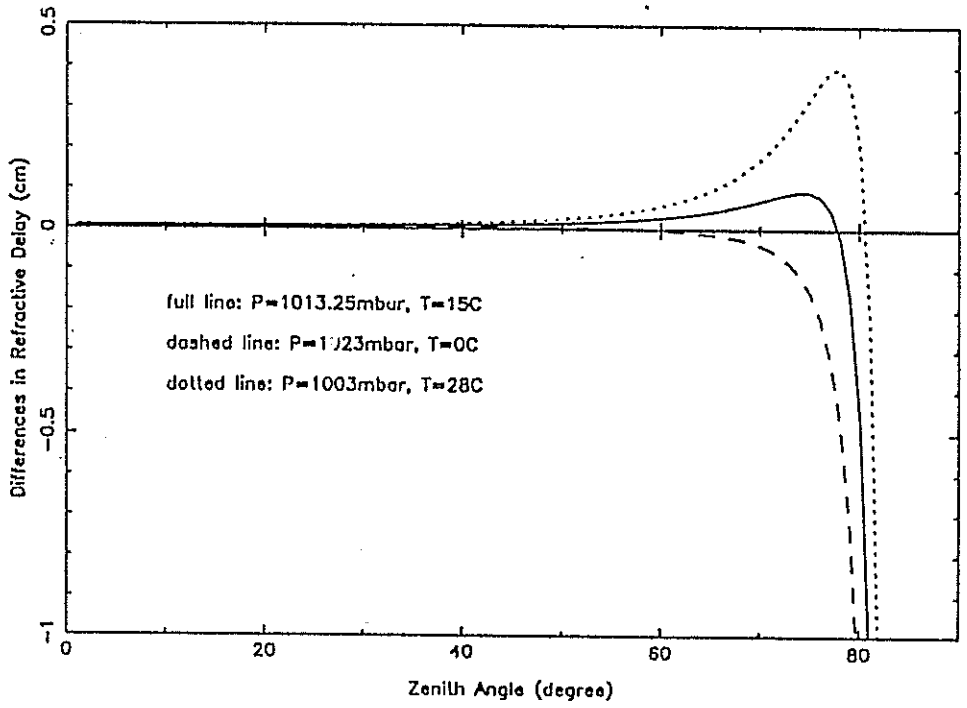

Fig.2 Comparison between new and Marini-Murray models

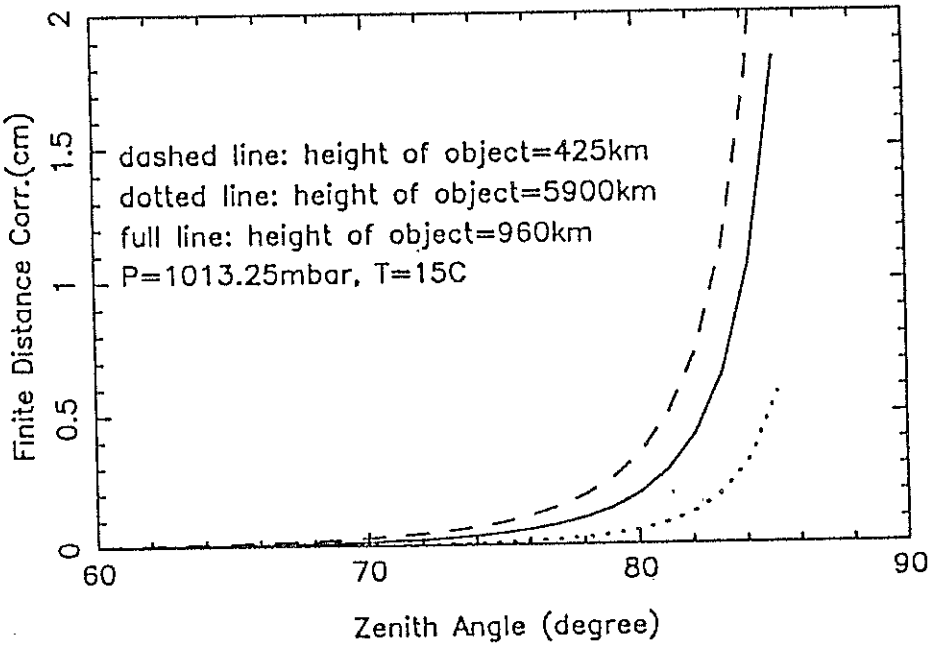

Fig.3 Corrections of finite distance objects

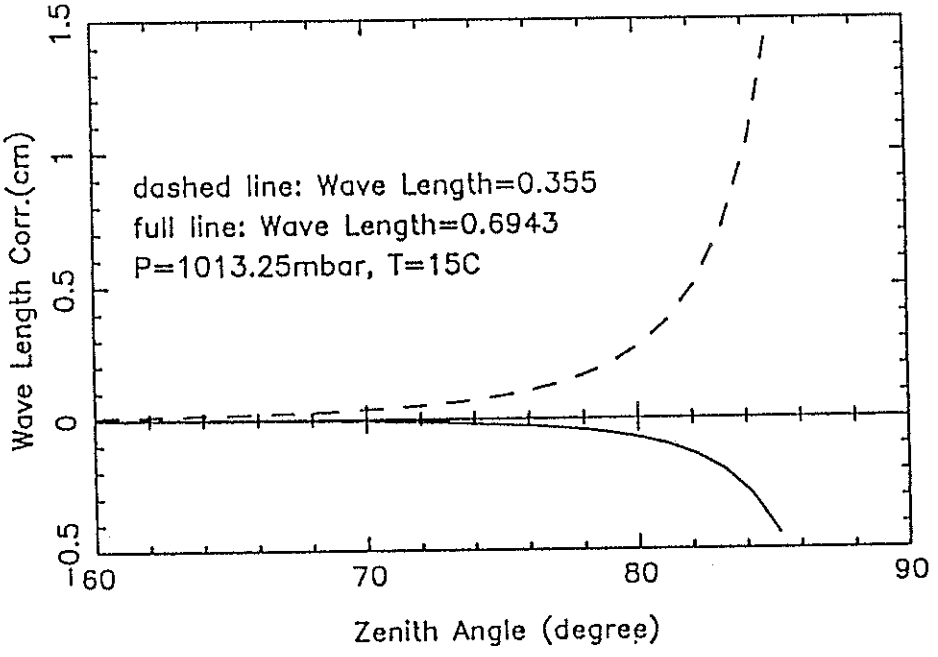

Fig.4 Frequency corrections in mapping function

The Question of SLR Measuring Error Distribution

Wu jie
National University of Defense Technology, China
wj@at.nudt.edu.cn

Li Zhengxin, Zhang Zhongping, Yang Fumin, Tan Detong
Shanghai Observatory, Academia Sinica

Abstract

The actual distribution of SLR measuring error is discussed in this paper. Through the analysis of 22 pass SLR data of Shanghai Observatory, it appeals that the standard model of error distribution (Normal distribution) is not always suitable for SLR measuring error. Instead of the conventional normal distribution, p-norm distribution is put in use, and adaptive least p-norm (ALp) estimation is put forward for SLR data preprocessing. The preliminary result shows that the ALp estimation is more reliable and efficient than the classical least square estimation.

1. Introduction

Each observation unavoidably include error in it. Measuring error obey Normal distribution, this is the simple hypothesis which we generally make in practice. But the hypothesis is not always suitable. In the case of SLR, because of highly automatic data collection and unavoidable external effect, there will be amount of gross errors (noise) in measuring data. It is then unsuitable to use only Normal distribution to describe SLR measuring errors. If the gross errors be deleted, will the measuring errors of remained observations obey Normal distribution ? No, they will not. Neubert, etc. (1995) indicate that: the distribution of SLR measuring error is related to laser pulse width, response function of satellite reflectors, and detector, the distribution density function is very complicated. The purpose of Neubert's research is to find out a 'reference point', and to calculate the center of mass correction. But the problem of how to get reliable estimation of real measuring error from practical measuring data (especially the data including amount of gross errors), is not researched. It is suggested in this paper that: to describe SLR measuring error with p-norm distribution family, and to estimate parameters in data preprocessing with ALp method. Preliminary result indicate that p-norm distribution family is suitable for SLR measuring error, ALp estimation of parameters are more precise and reliable than least square estimation.

2. P-norm distribution and SLR error statistics

2.1 P-norm distribution

The density function of p-norm distribution is (Sun Haiyan 1993)

$$f(x) = \frac{1}{\sqrt{2}\Gamma(1/p)b} \cdot \exp\{-(\frac{\sqrt{2}}{p}\frac{|x|}{b})^p\} \quad .....(1)$$

where x is the value of random variable, Γ() means gama function, p,b are parameters of the distribution. P-norm distribution family (with different p) include Laplace distribution (p=1), Normal distribution (p=2), uniform distribution (p=∞) and so on.

2.2 SLR error statistics

Let's research the distribution of SLR measuring error with the example of a SLR data pass of Shanghai Observatory. regarding the difference between laser ranging and calculated distance as a new observation, and then conducting polynomial imitation (with iteration of gross error rejecting), the imitation parameters and residuals of all observations are obtained at last. These residuals are regarded as the real value of SLR measuring errors, and to be researched. Figure 2 gives out the histograms, p-norm distribution density curves, and Normal distribution curves of the residuals at different steps of gross error rejecting.

Summary

(1) SLR measuring errors as a whole obey Laplace distribution (p=1), not Normal distribution.

(2) After each step of gross error rejecting, p-norm distribution (with different p) is always suitable to describe SLR measuring errors (p-norm curves approach histograms), but Normal distribution is suitable only in special case (fig.2 (22-5,6)).

(3) The p of p-norm distribution will continually increase if so called 'gross errors' are continually rejected. the p will tend to be infinite when 'gross errors' are over rejected. In this case, the remained residuals obviously will not represent the normal SLR measuring error. We suggest that:

Stop gross error rejection if p just greater than 1, and then regard the remained residuals as 'normal' SLR measuring errors.

Table 1 gives out p-norm distribution parameter values of 'normal' SLR measuring errors of 22 pass at shanghai Observatory.

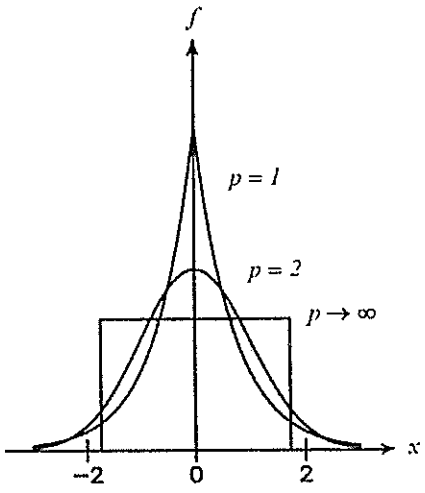

Fig.1 p-norm distribution density function

Tab.1 'normal' SLR measuring errors statistics

No.	n/n_0	p	σ(m)©
1	0.20	1.4	0.09
2	0.32	1.3	0.05
3	0.44	1.2	0.05
4	0.43	1.3	0.04
5	0.42	1.4	0.06
6	0.49	1.2	0.07
7	0.51	1.3	0.05
8	0.45	1.7	0.06
9	0.55	1.6	0.05
10	0.48	1.0	0.07
11	0.24	1.3	0.06
12	0.33	1.4	0.06
13	0.49	1.7	0.03
14	0.83	1.8	0.04
15	0.71	1.5	0.04
16	0.53	2.1	0.04
17	0.51	1.6	0.04
18	0.83	1.8	0.05
19	0.74	1.3	0.06
20	0.83	1.9	0.05
21	0.73	1.5	0.05
22	0.57	2.0	0.04

annotations: p means the parameter of p-norm distribution, σ indicates precision, n/n_0 means the ratio of remained residuals number to total.

Tab.2 Statistics of the remained residuals (3.0 σ rejection)

No.	ALp method				LS method		
	n/n_0	p	σ(m)	IT	n/n_0	σ(m)	IT
1	0.20	1.6	0.079	8	0.99	99.530	1
2	0.32	1.3	0.056	3	0.31	0.049	12
3	0.43	1.1	0.044	3	0.44	0.047	6
4	0.45	1.3	0.041	3	0.45	0.040	6
5	0.43	1.8	0.066	3	0.43	0.069	6
6	0.46	1.4	0.056	3	0.47	0.059	9
7	0.52	1.2	0.054	3	0.53	0.059	8
8	0.46	1.2	0.060	3	0.79	0.782	2
9	0.55	1.4	0.049	2	0.78	0.492	3
10	0.47	1.2	0.069	4	0.68	0.501	7
11	0.24	1.3	0.058	6	0.45	0.900	12
12	0.34	1.2	0.064	3	0.57	0.746	7
13	0.49	1.4	0.035	2	0.49	0.036	11
14	0.83	1.7	0.045	1	0.83	0.043	3
15	0.72	1.1	0.050	1	0.71	0.043	3
16	0.53	2.0	0.037	2	0.54	0.040	4
17	0.52	1.9	0.038	3	0.44	0.046	10
18	0.83	1.8	0.048	1	0.82	0.046	3
19	0.71	1.9	0.048	2	0.73	0.055	7
20	0.84	1.5	0.050	1	0.83	0.046	4
21	0.73	1.6	0.045	1	0.73	0.048	3
22	0.57	1.9	0.039	2	0.58	0.045	3

annotations: n/n_0 means the ratio of remained observation number to the total, p means adaptive p (distribution parameter), σ the precision of residuals, IT means iteration number of gross error rejection.

3. ALp estimation and SLR data preprocessing

Adaptive least p-norm (ALp) estimation is the most probable estimation of parameters when measuring error obey p-norm distribution with p unknown (Wu Jie 1995,1996).

3.1 ALp estimation principle

ALp estimation of parameters X are the solution of equations as below

$$\begin{cases} \begin{cases} \Sigma|v_i|^p = \min \\ V = AX - l \end{cases} \\ \Phi = \ln f(v_i, p, b) = \max \end{cases} \quad \text{..... (2)}$$

where { means a body of iteration, V a vector of observation residuals, v_i the i'th element of V, A a constant matrix, X the unknown parameter vector to be estimated, f( ), p, b as in equation

(1), p also to be called as adaptive p. Wu Jie (1996) put forward a method to find the solution of equation (2) in detail. ALp estimation has the main properties (Wu Jie 1995,1996):

(1) Robustness. When there are amount of gross errors in the data, adaptive p will tend to be 1, ALp estimation becomes L1 estimation(least the sum of absolute residuals). L1 estimation is robust (Huber 1981). so be ALp estimation.
(2) Most probability (asymptotic efficiency). ALp estimation is derived with the condition under which probability function be maximal. So that ALp estimation is the most probable estimation, and asymptotic efficient too.

3.2 Preprocessing of SLR data

Since SLR measuring error obey p-norm distribution with p unknown, then ALp method should be used so as to obtain the most efficient parameter estimation. Observations of the 22 pass in table 1 are preprocessed again with ALp and LS (least square) method , and without screen edition. In the preprocessing, gross errors be treated with 3.0σ rejection (σ means the precision of remained residuals), and the rejection stop when adaptive p>1 in ALp, or every residuals beneath the 3.0σ boundary in LS. Observation equation is as below

$$r_i = a_0 + a_1\dot{\rho}_i + a_2 t_i + \ldots\ldots + a_N t_i^{N-1} \qquad \ldots\ldots (3)$$

where r_i (the difference between laser ranging and calculated distance) means the new observation at epoch time t_i, $\dot{\rho}_i$ means the velocity at radial direction, t_i the observing epoch time, $a_0, \ldots\ldots, a_N$ means imitation parameters to be estimated. In this equation, a_0, a_1 are estimated at the same time with $a_2, \ldots\ldots, a_N$ together, the purpose is to reduce the model error of observation equation. If $\dot{\rho}_i$ item and t_i item are strongly related, the equation should be adapted as below

$$r_i = a_0 + a_1 t_i + \ldots\ldots + a_N t_i^N \qquad \ldots\ldots (4)$$

The preprocessing results are displayed in table 2 and figure 3.

Summary:

(1) ALp estimation of imitate parameters is reliable, LS estimation is not (fig.3(1b) ,LS imitate curve be out of the plot boundary). ALp estimation is theoretically robust, LS unrobust , so that there must be the result.
(2) If screen edition be made (initially delete gross errors),LS estimation will generally be correct, but still different from ALp estimation. Such as showed in figure 3 (3b), LS curve and ALp curve (V=0, unplotted) have difference of 1-2 centimeters, while ALp curve is more reliable at first look.
(3) When parameter estimation are correct, the iteration number of gross error rejecting (IT) in ALp method is much less than LS method (2nd, 3rd,.. in table 2, and (2a),(3a) in figure 3). This result is also because of the robustness of ALp estimation.

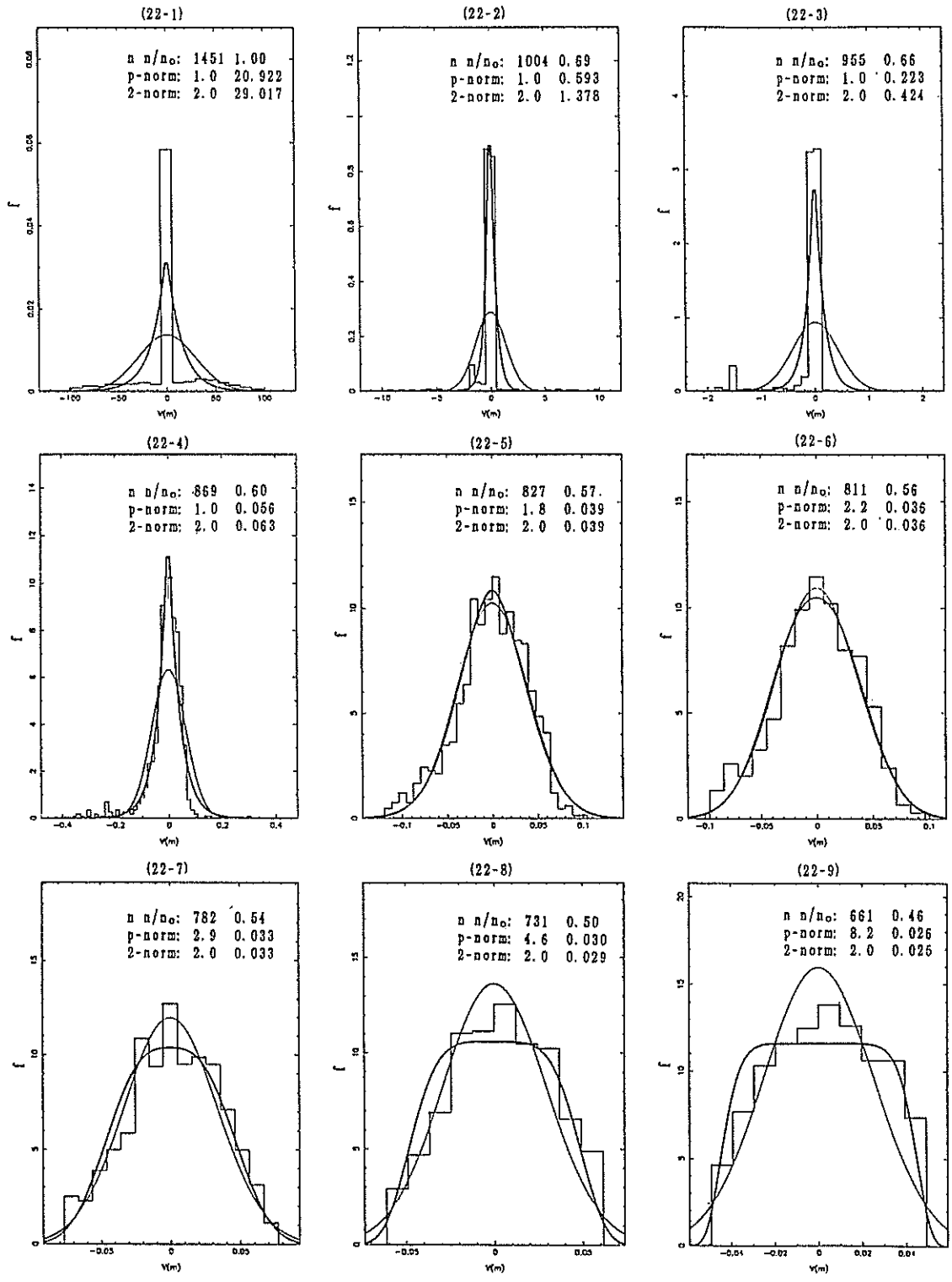

Fig.2 residual statistics of a SLR data pass

annotations:

[1] n means the number of remained residuals, n_0 the total, p-norm: p σ, p means p-norm distribution parameter, σ means precision.

[2] stress line means p-norm distribution density curve, light line the Normal, ladder-shaped line the histogram.

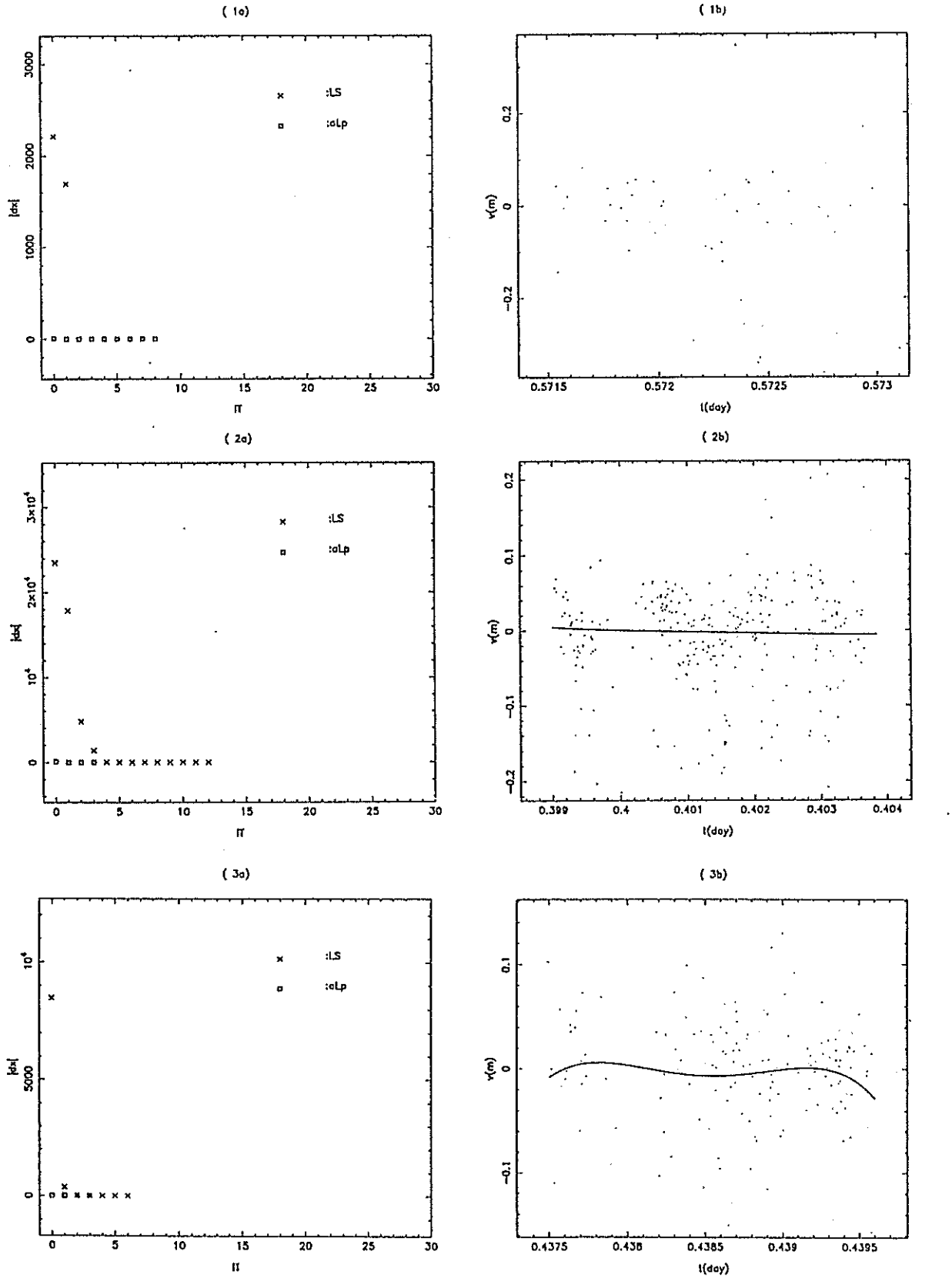

Fig.3 SLR preprocessing result (3.0 rejection)

annotations:

(1) (ia),(ib) means the result of i'th pass, i=1,2,3.

(2) in plot (ia), IT means the iteration number of gross error rejection, |dx| means the modulus of parameter error vector (ALp estimation as the real).

(3) in plot (ib), t means the observing time, V means the residuals in ALp method, dot '.' stand for observation. ALp imitation curve is just horizontal axis (v=0, unplotted), LS imitation curve be plotted.

4. Conclusions

(1) SLR measuring error in whole obey Laplace distribution(including amount of gross errors).
(2) When gross errors are not deleted completely (such as in screening), the remained SLR measuring errors obey p-norm distribution with different p values. If so called 'gross errors' be over deleted, the adaptive p will tend to be ∞ . We suggest that:
Stop gross error rejecting just when adaptive p>1, and regard each remained observation as a normal one.
(3) In SLR preprocessing, ALp method is more efficient and reliable than LS method.
(4) Most of normal observations are remained in ALp method. The ' normal point' data derived from imitation parameters correspond to the mean of normal SLR measuring errors, and then the 'center of mass' correction will be constant, for example 242.7 mm for Lageos (summary 1995). The 'normal point' data in LS method with tight gross error rejection (2.0σ or 1.0σ) will correspond to the distribution peak of normal SLR measuring errors (summary 1995). This method perhaps has defects as below:
   (a) Observations be over deleted, useful information is not utilized completely.
   (b) The center of mass correction is not constant, for example 7 mm variation for Lageos.

5. Subject for research

The p-norm distribution should be asymmetriclized, so as to fit in with SLR measuring error in practice more favorably, and then to get estimation of imitation parameters more efficiently and reliably.

References

[1] Huber, P.J., Robust Statistics, John Willey&Sons, 1981.
[2] Neubert, R., Satellite signature model: Application to Lageos and Topex, Proceedings of Annual Eurolas Meeting, Munich, March 1995.
[3] Sinclair, A.T., Data screening and peak location, same as [2].
[4] Summary of technical session on 'Satellite signatures and Centre-of Mass Corrections', same as [2].
[5] Sun Haiyan, Unified model of error distribution, Journal of Wuhan Surveying Technology university, China, Vol.18, No.3, p.49-56, 1993.
[6] Wu Jie, Li Zhengxin, etc., Adaptive Lp estimation and its applying in photographic astrometry, ACTA ASTRONOMIC SINICA, Vol.37, No.2, p.132-139, 1996.
[7] Wu Jie, Adaptive Least p-norm estimation and its application in astronomy and geodesy, doctor thesis of Shanghai Observatory of Academia Sinica, 1996.
[8] Yang Fumin, etc., Space geodesy, press of Chinese geological University, 1990.

Full-rate vs. Normal points: two ways of managing SLR data

R.Devoti, M.Fermi, V.Luceri, P.Rutigliano and C.Sciarretta
nuova telespazio s.p.a. CGS-Matera, Roma

G.Bianco
Centro di Geodesia Spaziale, Matera

Introduction

The huge quantity of SLR data became, at the beginning of the eighties, an urgent problem to avoid highly expensive analyses. The use of compression procedures that aggregate the data avoiding redundancy without losing information was willingly accepted by the scientific community; almost all analyses were performed, since then on, using the so-called normal points instead of full-rate data.
The decision, taken in December 1996 at the CSTG/Eurolas meeting in Berne, to cease also the archiving of the SLR full-rate data for all satellites raised the necessity to test once again the assumption that the normal points, or better the field generated normal points (FGNP), are completely equivalent to the full-rate data in terms of achievable results and information content.
For the result comparison, a set of tests has been addressed to check if the normal points can reproduce a satellite orbit obtained using the full-rate data. The attention has been focused on the orbit of the satellites because its precise determination permits to establish an accurate reference frame for the estimation of geodetic parameters. This kind of tests, already performed in the past on Lageos normal points, have been extended to other satellites with different orbital and physical characteristics.
The check on the respective information content has been directed toward the statistical analysis of the pass residuals going into the details of their distribution.

Orbit comparison

These tests consist in the comparison of the satellite orbits determined processing full-rate and normal points separately, with the same force model and arc structure, for all 1993; for all the arcs the set of station position has been kept fixed.
Among the geodetic satellites of the available constellation, we have chosen three satellites at different altitudes and with different sizes: Starlette, Ajisai and Lageos. Their physical characteristics, some information on their orbit and the analysis setup are shown in fig.1.
For each of them, the comparison of the orbits is performed by comparing the state vectors, estimated using GeodynII, at the beginning of each arc looking at the semi-major axis and at the relative satellite positions in the radial, cross-track and along-track directions.
In the first set of tests, the orbit determination is done weighting the data at 1, both for full-rate and normal points, as we were used to do for Lageos. The results of the comparison of the satellite positions in the radial and cross-track directions show that there is no significant difference in the estimates using the two types of data and this is valid for all the three satellites; in the case of the semi-major axis and the along-track component of the difference vectors, the results differ from satellite to satellite.

Satellite info		Analysis setup
LAGEOS - I		**15 days arc**
Diameter	0.6 m	**No estimation of global parameters**
Mean height	5900 Km	Estimated arc parameters :
Orbit inclination	109.84°	- ephemerides at the begin of each arc
CCR	426	- solar reflectivity coefficient
		- constant along track acceleration
		- once-per-rev acceleration
AJISAI		**10 days arc**
Diameter	2.15 m	**No estimation of global parameters**
Mean height	1500 Km	Estimated arc parameters :
Orbit inclination	50°	- ephemerides at the begin of each arc
CCR	1436	- solar reflectivity coefficient
Mirrors	318	- daily CD coefficient
		- once-per-rev acceleration
STARLETTE		**5 days arc**
Diameter	0.36 m	**No estimation of global parameters**
Mean height	960 Km	Estimated arc parameters :
Orbit inclination	49.83°	- ephemerides at the begin of each arc
CCR	60	- solar reflectivity coefficient
		- daily CD coefficient
		- once-per-rev acceleration

Fig. 1

For Lageos, the weighted mean of the differences is very low and always within the associated sigma (0.1±0.0 mm for s.m.a., 1.8±1.4 cm for the along-track); for Starlette, nothing significant for the semi-major axis but a 6 cm weighted mean for the along-track component (fig.3: bullets); for Ajisai, the differences in the semi-major axis (fig.2: bullets) point out a bias of about 5 mm, the NP estimates longer than the FR one, and those in the along-track component (fig.3: bullets) a large bias of 20 cm.

Further analysis has been performed to understand the meaning of the results and the way to manage the data to avoid discrepancies.

One possible explanation has been found in the use of the same unitary weight for the normal points that alters the network balance defined by the full-rate data; substituting the FR with the NP with equal weights, we change the contribution of each station to the solution and also the influence of the range biases often present in their data. The situation is critical for Ajisai because many stations have higher biases in the data acquired from this satellite.

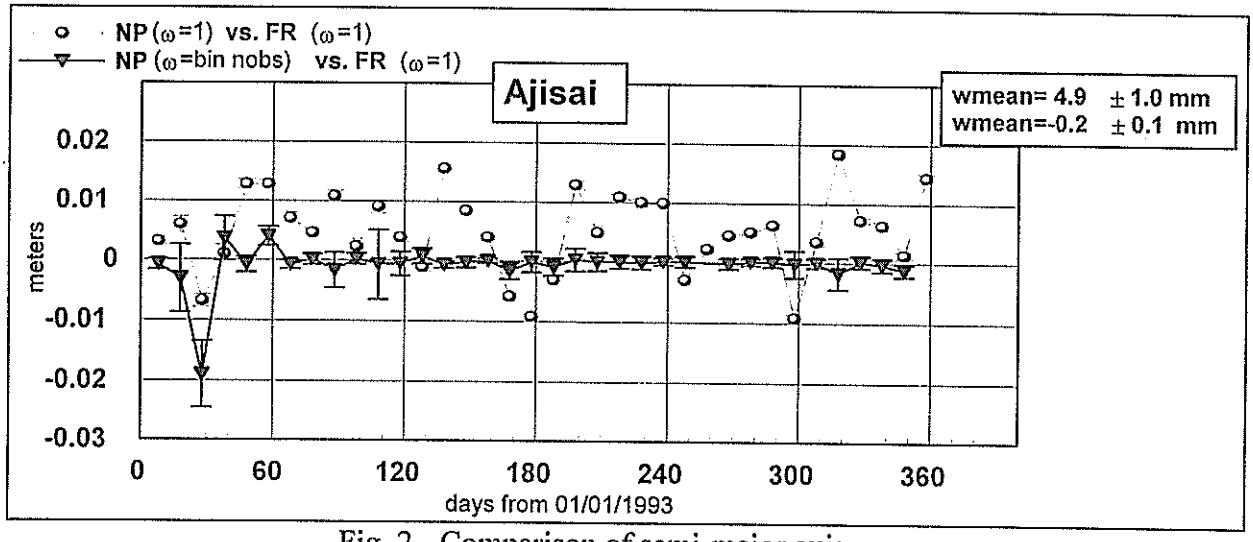

Fig. 2 - Comparison of semi-major axis

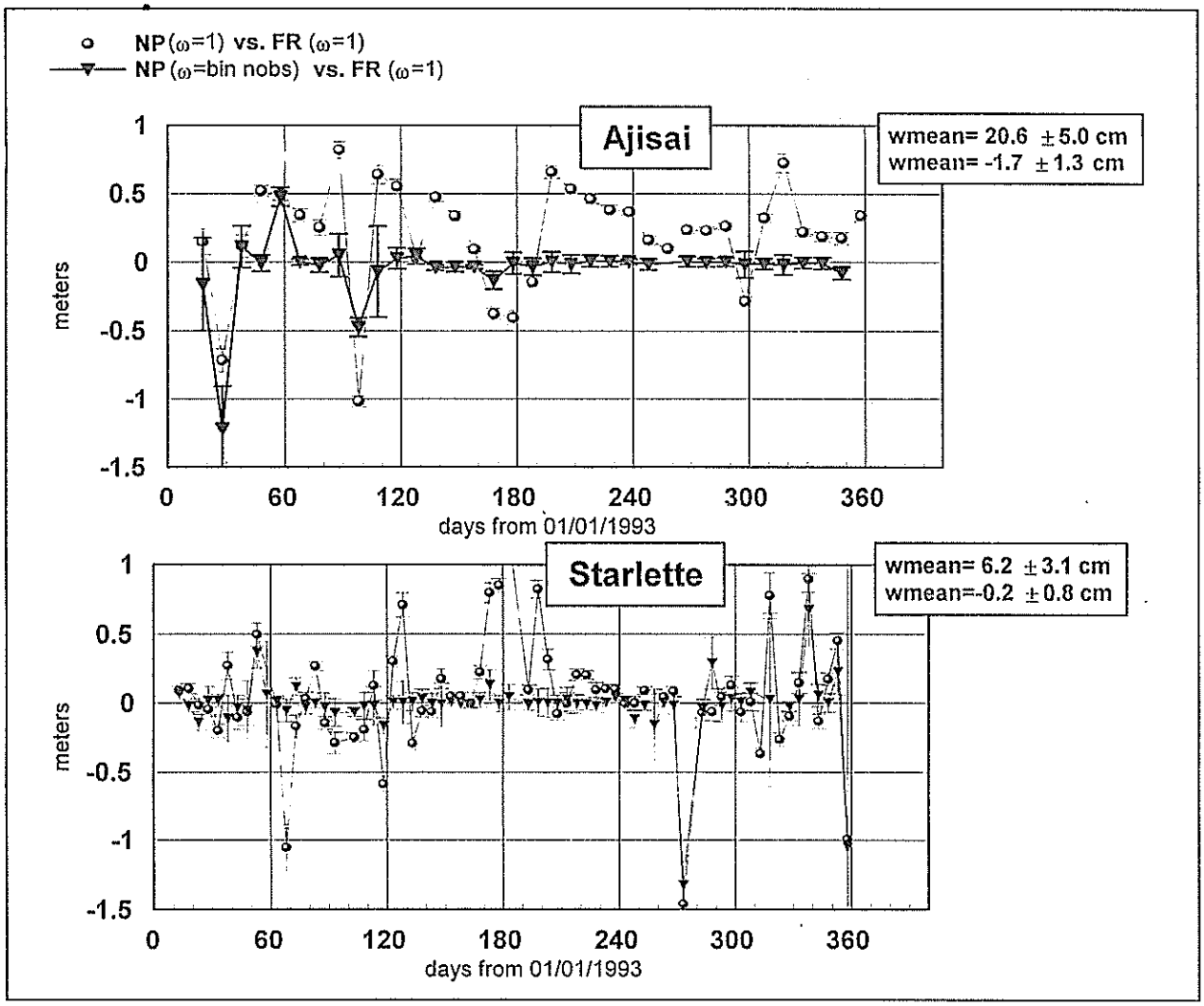

Fig.3 - Comparison of along-track components

For this reason, in the second set of tests, the NP have been weighted at n , where n is the number of observations in each bin, to reproduce the real situation and the results (fig.2, fig.3: triangles) clearly show that the biases disappear. More or less similar results are obtained when weighting the data at *1/bin variance* or, better, *n/bin variance* which is the best weight to give each normal point information on the number of the observations in a bin and on the dispersion of the bin residuals.
Future tests will check if the estimation of the station biases, during the orbit determination process, can overcome the problem.

Residual analysis

During the orbit determination process, the range residuals were computed and the analysis we are going to describe is based on the investigation of the distribution of these measurements residuals.
The procedure of normal points construction assumes that the range residuals have a gaussian distribution and this is true for most passes of Lageos; we have seen that this is not valid for Ajisai and Starlette.

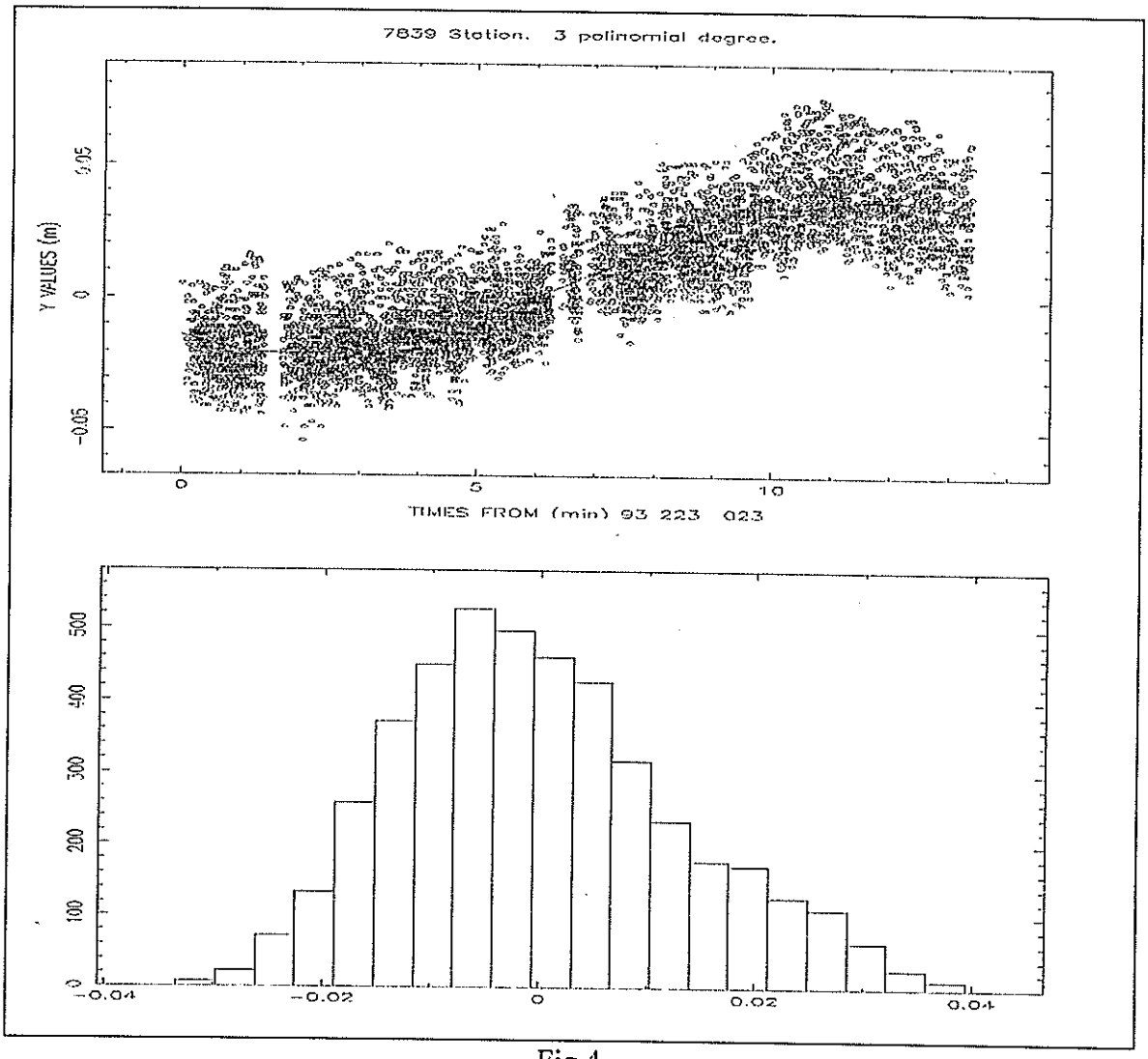

Fig.4

A typical Ajisai pass is shown in fig.4; the top of the figure is the plot of the orbit residuals with their fitting polynomial, the bottom is the histogram of the fit residuals. In the residual plot, the cloud of points along the pass, above the denser cluster below, indicates that the range of a large number of observations is longer than the real one. This situation is clearly pointed out in the residuals distributions. As you can see, it shows a strong tail (positive skewness: skewness is zero in a gaussian distribution) and the consequence is that the residuals is moved away from the peak of the distribution toward the tail itself.
The figure refers to an entire pass but we have checked that the bins of a skewed pass, when the number of observations is sufficiently high to permit this check, have a similar distribution. Since each normal point is computed using the mean of the residuals not the peak, in case of skewed passes we compute biased normal points and the bias is not recoverable without the full-rate data.
The value of the skewness depends on the satellite and station characteristics; the single-photon stations have a very high number of skewed passes, above all for Ajisai, probably due also to a target depth signature in the collected data.

Fig. 5 shows a pass analysis for Graz. For each pass we have computed the values of skewness and kurtosis, normalizing them with their sigmas, and performed the gaussianity test. The value of the normalized skewness and kurtosis is significative when it is higher than 3 (real value greater than 3σ) and we have found a value of about 10 in the case of Graz. The gaussianity test, which includes tests on the kurtosis, reveals that the percentage of non-gaussian passes is almost 90%. For some stations the situation is much better, for others worse.
In any case useful information coming out from the analysis of the data distribution is lost within the normal points.

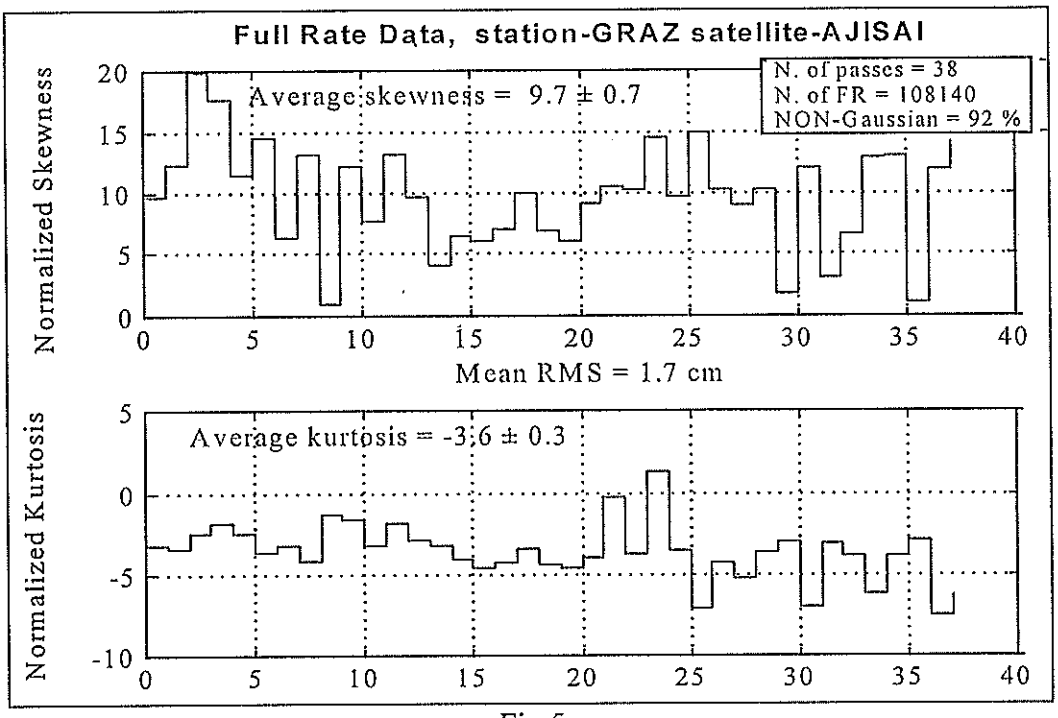

Fig.5

Conclusions

The SLR normal points are fundamental for the scientific analysis permitting to save computer and time resources but they cannot always be analysed as they were full-rate data, they need to be carefully used to achieve the same results.
The normal points will continue to be the primary type of data for analyses, however, on the other hand, the discontinuation of the full-rate archiving could be the source of future worries.
Some problems may have origin in the normal point construction phase:
- the passes with skewness could generate biased NP
- some information (e.g. pass distribution) could be lost
- future possible changes in the NP construction could not be applied to old data

others in the analysis phase:
- present and future analysis areas could need FR data
- different SLR analysis approaches (e.g. geometrical or semi-dynamical) could be compromised.

This decision is a point of no return, the risk is high and we hope that each station will continue to archive its own data anyway.

Fast computing the spherical harmonic perturbation on artificial satellite and the recurrence relations of the coefficients of the Earth's gravity[1]

Lin Qinchang

(Guangzhou Satellite Station,
Chinese Academy of Sciences,
Guangzhou 510640, China)

Lin Yuan

(Computer Sciences Department,
Zhongshan University,
Guangzhou 510275, China)

Abstract

A new method of fast computing the spherical harmonic perturbation on artificial satellite and the recurrence relations of the coefficients of the Earth's gravity is given in this paper. The method increases the computation speed in comparison with Cunningham's method and other existing methods, and has no overflow in operation occurs even the order and degree of the Earth's spherical harmonic are extended to 100×100 or more. The method satisfies for the accurate application of the SLR, GPS and LLR.

This method has been programmed and used in practice. For all computations of perturbations, it needs only 10 seconds in 486/66 for 1440 steps of numerical integration.

1. Introduction

The Earth's gravitational potential can be expressed as

$$V = \sum_{n=0}^{\infty} \sum_{m=0}^{n} \frac{R_{\oplus}^{n} P_n^m(\sin\phi)}{r^{n+1}} (C_{n,m} \cos m\lambda + S_{n,m} \sin m\lambda), \tag{1}$$

where $R_{\oplus}$ is the equatorial radius of the Earth; $C_{n,m}$ and $S_{n,m}$ are Earth's spherical harmonic coefficients; P_n^m is associated Legendre polynomial; and r, ϕ and λ are, the satellite's geocentric distance, the geocentric latitude and the longitude measured eastward from the meridian of Greenwich, respectively.

Up till now, among the numerical methods to compute the spherical harmonic perturbation on artificial satellite, the computation speed of Cunningham's method is the fastest. On theory, his method can be used to compute any number of zonal and tesseral terms in the Earth's gravitational potential. However, during running programs based on this method, it is easy for overflow to occur. For example, Cunningham used following equations. Define

$$V_{n,m} = \frac{P_n^m(\sin\phi)(\cos m\lambda + i \sin m\lambda)}{r^{n+1}}, \tag{2}$$

then the Earth's gravitational potential can be transformed into

[1] Project supported by the National Natural Science Foundation of China and the Natural Science Foundation of Guangdong Province.

$$V = Re\left(\sum_{n=0}^{\infty}\sum_{m=0}^{n} R_{\oplus}^{n}(C_{n,m} - iS_{n,m})V_{n,m}\right), \tag{3}$$

where $i = \sqrt{-1}$ is the imaginary number unit; Re expresses to take the real part.

The recurrence relations among the Earth's gravitational potential $V_{n,m}$ were given in Cunningham's method. The computation of the perturbations of various orders and degrees is convenient and fast. However, the main disadvantage of his method is that the coefficients of $V_{n,n}$ rapidly increase as n increases. And other $V_{n,m}$ must be determined with $V_{n,n}$. From

$$V_{0,0} = \frac{1}{r} \tag{4}$$

derive out

$$V_{n,n} = (2n-1)\frac{(x+iy)}{r^2}V_{n-1,n-1} \tag{5}$$

Some of $V_{n,n}$ are listed as following.

$$\cdots\cdots\cdots\cdots\cdots\cdots\cdots\cdots\cdots\cdots\cdots\cdots$$
$$r^{57}V_{28,28} = 8.7\times10^{36}(x+iy)^{28},$$
$$r^{59}V_{29,29} = 8.7\times10^{38}(x+iy)^{29},$$
$$\cdots\cdots\cdots\cdots\cdots\cdots\cdots\cdots\cdots\cdots\cdots\cdots$$
$$r^{121}V_{60,60} = 7.0\times10^{98}(x+iy)^{60},$$
$$r^{123}V_{61,61} = 8.4\times10^{100}(x+iy)^{61},$$
$$r^{125}V_{62,62} = 1.0\times10^{103}(x+iy)^{62},$$

where x, y and z in Equation (11) are the satellite's rectangular coordinates.

$$\begin{aligned} x &= r\cos\phi\cos\lambda, \\ y &= r\cos\phi\sin\lambda, \\ z &= r\sin\phi. \end{aligned} \tag{6}$$

It can be found out that the tendency of the coefficients of $V_{n,n}$ increases more and more rapidly as n increases. With improvement of the observational accuracy of the satellite, higher order and degree perturbation of the Earth's spherical harmonic must be considered. But for example, the coefficient of $V_{29,29}$ reaches 5.0×10^{38}. Further, the coefficient of $V_{62,62}$ has exceeded 1.0×10^{103}.

In order to prevent from the overflow, in practice on computation with computer, normalized P_n^m have been adopted to replace the p_n^m by many people.

$$\overline{P_n^m}(\mu) = \frac{P_n^m(\mu)}{N_n^m},$$

$$N_n^m = \frac{1}{\sqrt{(2n+1)\dfrac{(n-m)!}{(n+m)!}\delta}}. \qquad \delta = \begin{cases} 1 & m = 0, \\ 2 & m \neq 0. \end{cases} \tag{7}$$

And the all coefficients of $C_{n,m}$ and $S_{n,m}$ are multiplied by the module N_n^m. However, when the n and m increase, (n+m)! also rapidly increases. As a sample, when n=m=35, (n+m)! is larger than 10^{100}. If the Equation (5) is directly used to compute, the opportunity of overflow in operation is even more than with $V_{n,n}$. When that method is programmed, it is possible to avoid the overflow in operation with the great effort. But there is no doubt that, using the normalized method, the operational machine time will increase further.

2. The Earth's gravitational potential

For both to prevent from the overflow in operation and to save the machine time at the same time, the fast computing the spherical harmonic perturbation on artificial satellite and the recurrence relations of the coefficients of the Earth's gravity would given in this paper. Let

$$L_{0,0} = V_{0,0}, \qquad L_{n,m} = \frac{(n-m)!}{(2n-1)!!} V_{n,m}, \tag{8}$$

where, (2n-1)!!=1 · 3 · 5 · · (2n-1). From

$$L_{0,0} = \frac{1}{r}, \tag{9}$$

we get

$$L_{n+1,n+1} = \frac{x+iy}{r^2} L_{n,n}. \tag{10}$$

And using Equation (10), we get

$$L_{n+1,m} = \frac{zL_{n,m}}{r^2}, \qquad n = m,$$

$$L_{n+1,m} = \frac{zL_{n,m}}{r^2} - \frac{n^2-m^2}{4n^2-1}\frac{L_{n-1,m}}{r^2}, \quad n > m. \tag{11}$$

3. Derivatives

In practice of our method on computer, following equations would be adopted. Define

$$G_{n,m} = \frac{(2n+1)!!}{2(n-m)!} C_{n,m}, \qquad H_{n,m} = \frac{(2n+1)!!}{2(n-m)!} S_{n,m}, \qquad m > 0,$$
$$G_{n,0} = \frac{(2n+1)!!}{n!} C_{n,0}, \tag{12}$$

where, $G_{n,m}$ and $H_{n,m}$ are the program constants to replace spherical harmonic coefficients $C_{n,m}$ and $S_{n,m}$. Then Equation (3) can be transformed into

$$V = \mathrm{Re}\left(\sum_{n=0}^{\infty}\sum_{m=0}^{n} R_{\oplus}^{n}(G_{n,m} - iH_{n,m})U_{n,m}\right). \tag{13}$$

The derivatives of $U_{n,m}$ are

$$\begin{aligned}
&\frac{\partial U_{n,m}}{\partial x} = -L_{n+1,m+1} + L_{n+1,m-1}, \quad m > 0; \qquad \frac{\partial U_{n,0}}{\partial x} = \mathrm{Re}(-L_{n+1,1});\\
&\frac{\partial U_{n,m}}{\partial y} = i(L_{n+1,m+1} + L_{n+1,m-1}), \quad m > 0; \qquad \frac{\partial U_{n,0}}{\partial y} = I_m(-L_{n+1,1});\\
&\frac{\partial U_{n,m}}{\partial z} = -2L_{n+1,m}, \qquad\qquad m > 0; \qquad \frac{\partial U_{n,0}}{\partial z} = -L_{n+1,0};
\end{aligned} \tag{14}$$

where, I_m expresses to take the image part.

4. The recurrence relations, using $C_{n,m}$ and $S_{n,m}$

If we only have $C_{n,m}$ and $S_{n,m}$, let the ratio $K_{n,m}$ as following:

$$K_{n,m} = \frac{G_{n,m}}{C_{n,m}} = \frac{H_{n,m}}{S_{n,m}} = \frac{(2n+1)!!}{\delta(n-m)!}. \tag{15}$$

1) The recurrence relations of zonal terms coefficients

When m=0, δ =1, it corresponds computation of zonal terms coefficients.

$$K_{n,0} = \frac{(2n+1)!!}{n!}. \tag{16}$$

From

$$K_{0,0} = 1,$$

derive out

$$K_{n,0} = \frac{2n+1}{n} K_{n-1,0}, \qquad n > 1. \tag{17}$$

2) The recurrence relations of tesseral terms coefficients

When m>0, δ =2, it corresponds computation of tesseral terms coefficients. From

$$K_{1,1} = 1.5, \tag{18}$$

derive out

$$K_{n,1} = \frac{2n+1}{n-1} K_{n-1,1}, \qquad n > 1, \tag{19}$$

and

$$K_{n,m} = \frac{n-m+1}{n-m} K_{n,m-1}, \qquad m > 2. \tag{20}$$

5. The recurrence relations, using $\bar{C}_{n,m}$ and $\bar{S}_{n,m}$

Sometimes, the spherical harmonic coefficients of the Earth would be normalized. In the case, following recurrence relations would be used. The definitions of normalized $\bar{C}_{n,m}$ and $\bar{S}_{n,m}$ are:

$$\bar{C}_{n,m} = C_{n,m} N_n^m, \qquad \bar{S}_{n,m} = S_{n,m} N_n^m, \tag{21}$$

where, the definition of N_n^m is in Equation (7). We get the ratio

$$K_{n,m} = \frac{G_{n,m}}{\bar{C}_{n,m}} = \frac{H_{n,m}}{\bar{S}_{n,m}} = \frac{(2n+1)!!}{\delta(n-m)!}. \tag{22}$$

Thus,

$$K_{n,m} = (2n+1)!! \sqrt{\frac{2n+1}{\delta(n-m)!(n+m)!}}. \tag{23}$$

1) The recurrence relations of zonal terms coefficients

When m=0, δ =1, it corresponds computation of zonal terms coefficients.

$$K_{n,0} = \frac{(2n+1)!!}{n!} \sqrt{2n+1}. \tag{24}$$

From

$$K_{0,0} = 1, \tag{25}$$

derive out

$$K_{n,0} = \frac{2n+1}{n} \sqrt{\frac{2n+1}{2n-1}} K_{n-1,0}, \qquad n > 1. \tag{26}$$

2) The recurrence relations of tesseral terms coefficients

When m>0, δ =2, it corresponds computation of tesseral terms coefficients. From

$$K_{1,1} = 1.5\sqrt{3} \tag{27}$$

derive out

$$K_{n,1} = (2n+1)\sqrt{\frac{2n+1}{(n^2-1)(2n-1)}}K_{n-1,1}, \qquad n>1, \tag{28}$$

and

$$K_{n,m} = \sqrt{\frac{n-m+1}{n+m}}K_{n,m-1}, \qquad m>2. \tag{29}$$

6. Practice on computer

In practical computations, the values of $G_{n,m}$ and $H_{n,m}$ are independent of the satellite's coordinates, and they are the same for all satellites. Therefore, Equations (15) to (29) only need to compute once. Derived the ratio $K_{n,m}$ and $\overline{K}_{n,m}$, $G_{n,m}$ and $H_{n,m}$ are derived at once. As a constant file, $G_{n,m}$ and $H_{n,m}$ are stored in the computer and can be used to any Earth's satellites. The another feature of $G_{n,m}$ and $H_{n,m}$ is that their variable spans are much less than $V_{n,m}$. The reason is that as n increases, (2n+1)!! increases, but the values of $C_{n,m}$ and $S_{n,m}$ decrease. In fact, every value of $G_{n,m}$ or $H_{n,m}$ is a big figure multiplied a small one. Therefore, the possibility of the overflow becomes much less on the computer. The method satisfies for the accurate application of the SLR, GPS and LLR.

The gravitational potential and its derivatives have been programmed. For computing the order and degree of the Earth's spherical harmonic perturbation to 20×20, including all other computations of perturbations, it needs only 10 seconds in 486/66 for 1440 steps of numerical integration. Thus, the accuracy to compute the spherical harmonic perturbation on artificial satellite is improved, and machine time is saved.

Work organization and some results of the data analysis on satellite laser location at Russian Mission Control Center

Glotov V.D. , Mitrikas V.V., Poliakov V.S., Pochukaev V.N.
Russian Mission Control Center, Moscow, Russia.

Abstract.

This paper describes briefly the work organization and some activity results of the Laser Operational-Analytical Center at Russian Mission Control Center (MCC). In particular, there are some examples of the SLR data quality analysis results for the Shanghai and Changchun stations and comparison of this results with other data analysis centers.

1. Laser Operational-Analytical Center "LOAC" was created at MCC in 1991 on the basis of ballistic service of Earth Artificial Satellite (EAS) orbit determination and has passed some stages in its development. Originally, the LOAC goals consisted of the ephemeride support of the domestic network' s laser stations, acquisition of measurement data from these stations at location by them of 2-3 specialized spacecraft (SC), data preprocessing and transferring to the international centers of the measurements analysis within the framework of work on introduction of Russian stations into world laser subsystem.
For period 1991-1994 yr. the methodical and software-mathematical means of the acquisition, storage and high-precision analysis of laser measurements were developed in MCC, LOAC hardware instrumentation is conducted by means of electronic communication and computer data processing, principles of interface with stations and Centers of a world laser network are fulfilled. Now LOAC (besides functions on maintenance of regular work of a domestic network of stations at location of 14-16 specialized EAS within the framework of realization of the international programs of ephemeride support, acquisition, storage, processing and transferring of the measurement information) is one of the four world operative centers of the laser data analysis, ensuring high-precision determination of Earth Rotation Parameters and the analysis of stations work quality in a mode of a regular service.

2. The software (SW) -mathematical support of the LOAC, intended for processing of laser measurements, is realized on personal computers within the framework of operating system MS-DOS. Developed in MSS , the SW provides both as the solution of problems of technological and operative character : formation of normal points, express - analysis of data, storage of the information, preparation of the reports ,etc. `, and realization of the precision analysis of measurements of whole world network's stations at solution of multiparametrical problems of the parameter estimation . Both as the models, recommended by the international standards and by the agreements (IERS Standards), and own original techniques of calculation realization - were used at SW development .
In particular, the accounting of a gravitational field of the Earth in various models , gravitational effect of planets, Sun and Moon, tides in solid Earth , oceanic tides, indirect influence of the Earth oblateness, direct solar pressure, nonmodelled empirical acceleration ,etc - is admitted in motion model. The lithosherical plates motion , coordinates displacement due to the pole motion, tides in solid Earth, deformation of rotation because of tides - is taken into account in model of ground stations

coordinates. Mentioned SW provides the opportunities of EAS orbits determination with residual errors within the level of units of centimeters, parameters of orientation of the Earth, coordinates and velocities of ground stations in earth coordinate frame , etc.

3. The fact, that LOAC, being in structure of a laser stations domestic network, has strongly come into the structure of a world laser subsystem and works successfully within the framework of world cooperation at realization of the Russian and international programs of a specialized EAS location and scientific analysis of received results - can be referred to main results of the LOAC work for period since 1991. Constant quality surveillance of measurements of the station's domestic network and analysis of available errors character, realized in LOAC, promoted to increase the measuring data accuracy and high stability of stations work during the realization of the programs of SC tracking, located by the world network , total - about 20 EAS.
Results of operative determination of parameters of the Earth orientation: pole coordinates and day duration , received by LOAC in mode of a regular service during the data processing of a laser ranging of the SC "LAGEOS-1" and "LAGEOS-2" by world network's stations (total about 50 stations), are sent in Central (Paris) and Operative (Washington) Bureau of the International Earth Rotation Service. Thus , the accuracy of received in 1996 results of Earth Rotation Parameters corresponds to the best world level, achieved by similar international centers of the data analysis: Texas and Delft Universities with average errors of pole coordinates determination , being equal to 1-3 centimeters on Earth surface .
Moreover , the series of scientific and applied researches on precision data processing on Satellite Laser Ranging , is conducted, as a result of which at 1996, in particular , the "Glonass-63" and "Glonass-67" high -precision orbit on semi-annual interval of tracking for these SC by world network's laser stations and model of EAS motion of the given class, ensuring the accuracy increase of SC orbit determination and forecasting in 3-8 times in comparison with similar regular model - was constructed .

GLOBAL LASER RANGING STATISTICS

January-October, 1996

SC	Maidanak (1864)	Komsomolsk (1868)	Mendeleevo (1870)	Katzively (1893)
GFZ-1	20	-	2	-
ERS-1	54	6	37	11
ERS-2	154	19	86	13
ADEOS	1	-	1	-
TOPEX	104	66	90	7
AJISAI	-	-	-	5
RALPH	10	-	-	-
NORTON	8	-	-	-
LAGEOS-1	141	54	-	31
LAGEOS-2	111	53	-	15
GPS-35	10	1	-	-
GPS-36	8	8	-	-
GLO-63	52	18	-	2
GLO-67	63	14	-	12
ETALON-1	37	10	-	3
ETALON-2	58	14	-	3
TOTAL	831	263	216	102

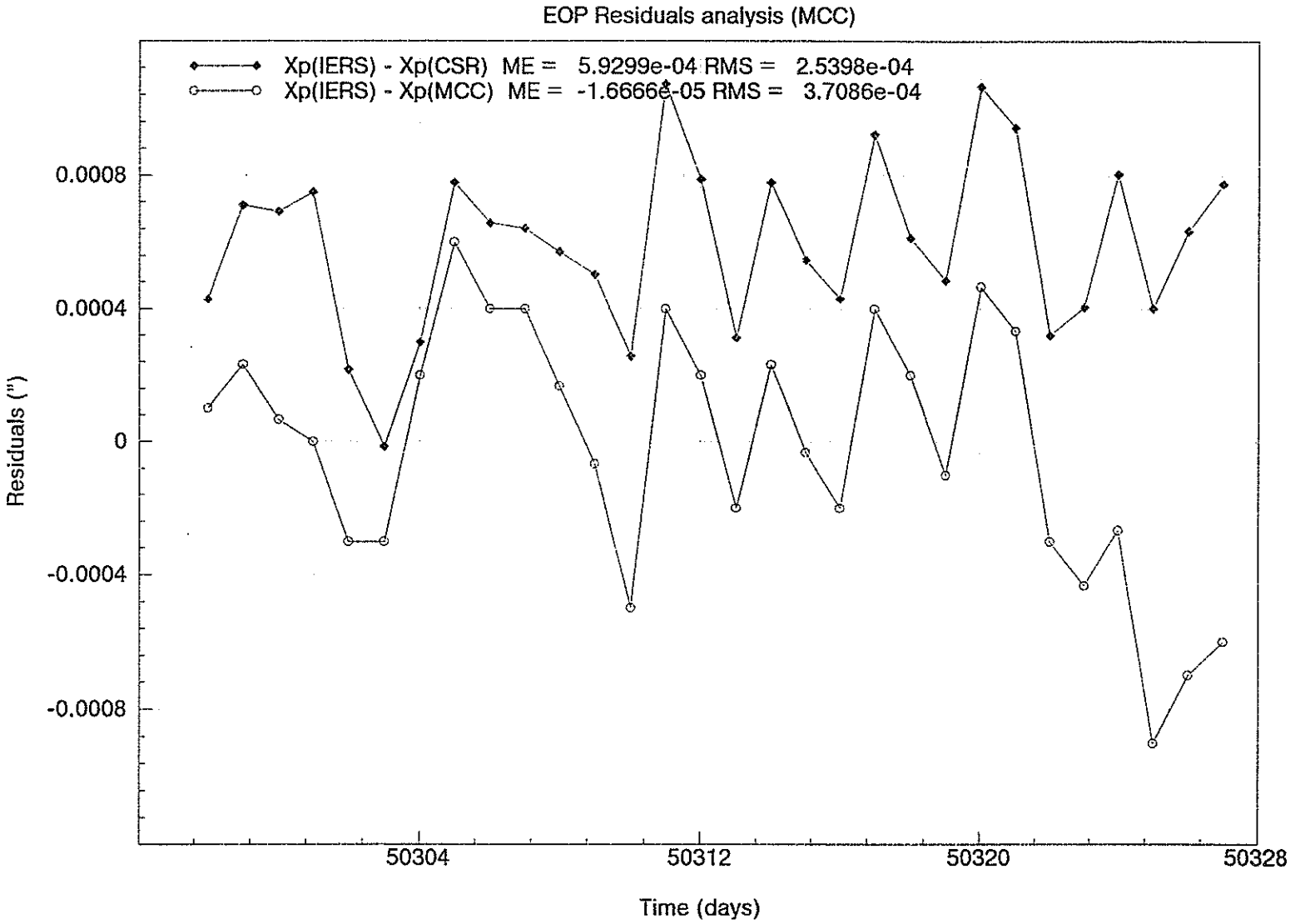
EOP Residuals analysis (MCC)
Xp(IERS) - Xp(CSR) ME = 5.9299e-04 RMS = 2.5398e-04
Xp(IERS) - Xp(MCC) ME = -1.6666e-05 RMS = 3.7086e-04
0.0008
0.0004
0
-0.0004
-0.0008
Residuals (")
50304
50312
50320
50328
Time (days)

Cutting out Quicklook Residual Analysis Report (CSR)

STA ID	AVG PASS TIME YY/MM/DD HH:MM	SAT	GOOD OBS	RAW RMS (MM)	PREC EST (MM)	RANGE BIAS (MM)	TIME BIAS (US)	PASS DUR (MIN)	EDITED OBS	CALIB+ MEAN (MM)	CALIB SDEV (MM)	CALIB++ SHIFT (MM)	STPASS RMS (MM)
> (7837) Shanghai													
7837	96/10/02 13:37	L2	13	332	147	-64	-126	29	0 ALT	8127 E	45	0 P	30
> (7237) Changchun													
7237	96/10/04 10:18	L2	3	263	247	-90	0	3	0 ALT	22912 E	45	0 P	25
7237	96/10/09 12:32	L2	23	141	39	138	22	56	0 ALT	22946 E	45	0 P	64

Cutting out Quicklook Residual Analysis Report (MCC)

Shanghai (7837 NP)

DATA	T ini	T fin	SC	TTL	INC	ME mm	RMS mm	ORMS mm	ELEV deg	T C	P mm	H %	CALIB mm	TB us	RB mm	PRMS mm	
02.10.96	13:21	13:50	L2	13	13	70	342	349	027-060	23	763	87	8127	-128	-20	318	(*)
02.10.96	13:21	13:50	L2	13	11	-31	10	34	027-060	23	763	87	8127	7	-27	8	

Changchun (7237 NP)

DATA	T ini	T fin	SC	TTL	INC	ME mm	RMS mm	ORMS mm	ELEV deg	T C	P mm	H %	CALIB mm	TB us	RB mm	PRMS mm
04.10.96	10:17	10:20	L2	03	02	50	26	75	029-034	10	737	74	22911	0	50	26
09.10.96	12:09	13:04	L2	23	17	29	48	58	017-084	4	742	90	22946	32	52	29

(*) - no edited

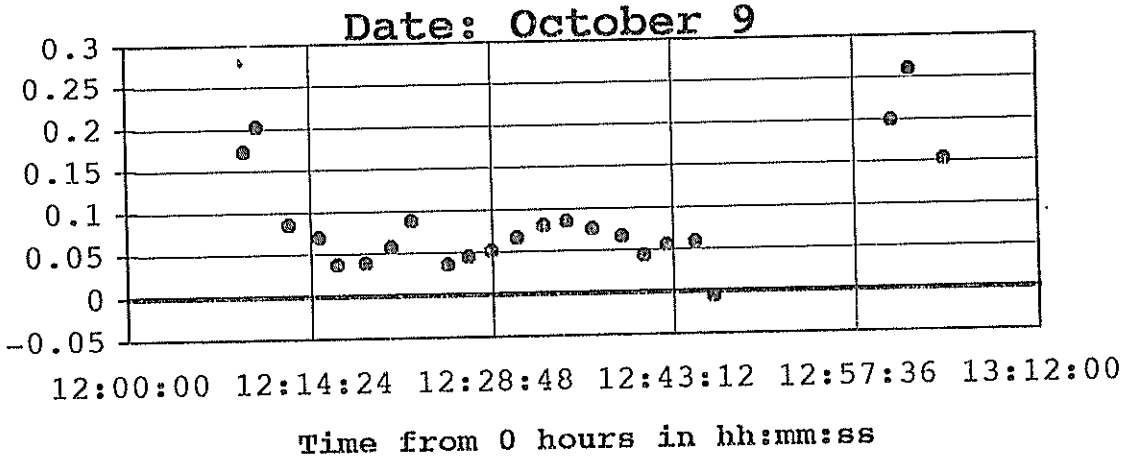
Changchun Laser Station (7237)
Residuals from the orbit in meters
Date: October 9
0.3
0.25
0.2
0.15
0.1
0.05
0
-0.05
12:00:00 12:14:24 12:28:48 12:43:12 12:57:36 13:12:00
Time from 0 hours in hh:mm:ss

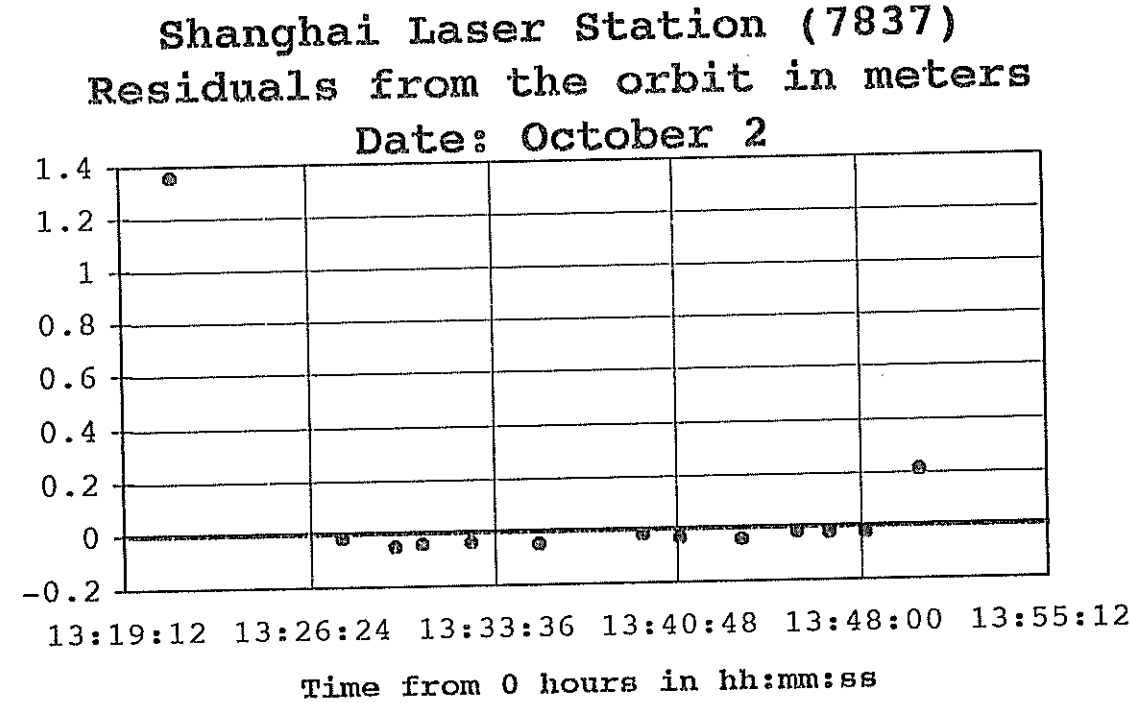
Shanghai Laser Station (7837)
Residuals from the orbit in meters
Date: October 2
1.4
1.2
1
0.8
0.6
0.4
0.2
0
-0.2
13:19:12 13:26:24 13:33:36 13:40:48 13:48:00 13:55:12
Time from 0 hours in hh:mm:ss

Russian Mission Control Center

Residual Analysis Report
Shanghai (7837 NP)

DATA	T ini	T fin	SC	TTL	INC	ME	RMS	ORMS	ELEV	T	P	H	CALIB	TB	RB	PRMS
						mm	mm	mm	deg	C	mm	%	mm	us	mm	mm
02.10.96	13:21	13:50	L2	13	11	-31	10	34	27-60	23	763	87	8127	7	-27	8
02.10.96	16:07	16:23	L1	09	09	-18	7	21	31-42	22	763	85	8127	-3	-17	7
02.10.96	17:45	18:18	L2	18	18	-29	20	35	34-56	22	763	83	8127	5	-29	18
02.10.96	19:33	19:50	L1	10	10	-81	12	85	48-60	21	763	81	8125	-10	-80	8
04.10.96	13:45	14:24	L2	21	19	-25	18	32	19-56	21	764	80	8141	16	-34	7
04.10.96	13:45	14:24	L2	21	21	-25	18	32	19-56	21	764	80	8141	10	-30	12
04.10.96	16:45	17:12	L1	15	15	-21	17	28	34-57	20	764	84	8140	-10	-20	8
04.10.96	16:45	17:12	L1	15	15	-21	17	28	34-57	20	764	84	8140	-10	-20	8
04.10.96	17:57	18:32	L2	19	19	-22	22	33	32-61	20	764	84	8140	17	-21	7
04.10.96	17:57	18:32	L2	19	19	-22	22	33	32-61	20	764	84	8140	17	-21	7
09.10.96	12:37	12:50	L2	07	05	639	61	716	30-57	17	767	83	8122	239	186	29
18.10.96	15:39	15:58	L2	11	11	21	32	38	42-52	20	767	90	8259	-17	24	28
19.10.96	13:25	13:50	L2	14	14	52	14	57	28-47	18	770	73	8182	14	64	8
19.10.96	14:12	14:24	L1	07	07	60	14	68	22-28	18	770	75	8182	-10	68	12
19.10.96	17:17	17:32	L1	09	09	-14	12	20	25-65	16	770	81	8182	17	21	8
19.10.96	17:41	17:52	L2	07	07	21	8	24	37-65	16	760	81	8183	-14	-3	6
22.10.96	16:48	17:04	L1	10	10	-58	28	68	34-76	20	768	99	8259	21	-28	21

Discussion over Orbit Determination of Satellite Ajisai

Jiang Hu Feng Chugang
Shanghai Observatory, the Chinese Academy of Sciences

Abstract

When we make researches on near-Earth satellite orbit determination, it is inevitable that we should be subject to meeting with some atmospheric models, such as exponential atmospheric model, DTM, CIRA86, J77,and so forth. As a noted, comparatively later established atmospheric model, J77 seems so conspicuous that it is usually taken into full considerations as far as air drag perturbation is concerned.

Here we are involved in a puzzle of calculation divergence resulting from introduction of J77 as an atmospheric model to deal with the precision orbit determination of the near-Earth satellite Ajisai, if a computer operating system named VAX3800 is utilized. Based on many simulating calculations and postanalyses we suppose that the essence of calculation divergence may be brought about by improperly adopting a default value of parameter ε in our software SHORDE for researches on satellite orbit determination and dynamical geodesy. Calculation shows that this parameter is dependent of, but not just equal to, the significant value of a specific computer operating system. After adjusting the parameter ε, we recalculate its orbital elements and find the results convergent. Finally we compare the results with those produced by some other atmospheric models, and comparisons indicate that our adjustment of parameter ε is rational, necessary and effective.

1. Introduction

J77 is one of the currently noted atmospheric models; it was presented by L.G., Jacchia with SAO (1977). His other similarly patterned models are J65, J70, and J71(Jacchia,1965,1970,1971a,1971b). Those models constitute a family of Jacchia's.

J77 includes the basic static models and a set of formulae; the former offers temperature and density profiles for the relevant atmospheric constituents for specified exospheric temperature; the latter is used to calculate the exospheric temperature and the expected deviations from the static models as a result of all the recongnized kinds of thermospheric models. Like any other atmospheric models, J77 is by no means perfect. So far it has been proved that there is much to be desired in J77 (Tang, 1995).

2. Problem arising

when we do researched on atmospheric drag in order to further our study of precision orbit deterniation of near Earth satellite Ajisai, it happens that RMS for observational data seems beyond explicitly reasonable explanation since the batch-moded calculation fails to work. Debuging the calculation process finds that divergence appears in certain integration phase of satellite motion equations. However the essentially original key cause lies elsewhere as is expected to be expounded in the coming section.